SCINTILLATION COUNTERS APPLIED TO THE STUDY OF ENERGY LEVELS OF Be^8.

by

Alan John Fraser Boyle, B.Sc.

A Thesis submitted for the
degree of Doctor of Philosophy,
Australian National University.

May, 1957.

PREFACE

This dissertation deals with a number of experiments that were performed in an attempt to clarify the experimental situation pertaining to the level structure of Be^8 at low excitation energies.

This nucleus offers an unambiguous interpretation on any simple nuclear model and the only levels predicted below an energy of about 10 MeV are a 0^+ ground level and a 2^+ level at about 3 MeV. However, evidence accumulated from a number of experiments, suggesting a more complicated level structure. Since these results could not be explained by any modification of the existing theories it was considered essential to verify and extend these earlier results.

The work described in Chapter 1. was carried out at the University of Melbourne during 1952 in collaboration with Dr. J.G. Campbell. The experiment began as an attempt to examine the spectrum of gamma-radiation from the $Li^7(p,\gamma)$ reaction for evidence of transitions to reported levels in Be^8 other than the ground and first excited states. However, the means of detection chosen, the scintillation counter, proved to be inadequate. Since little was known, at the time, about the characteristics

of scintillation counters when used for gamma ray detection, an investigation was undertaken to explain the poor results obtained with the high energy radiation from this reaction. No particular section of this work was contributed by either Dr. Campbell or myself.

The remainder of the work described was carried out at the Australian National University over the period 1953-5. The experiment described in Chapter 4, Part A, was performed in collaboration with Dr. E.K. Inall. I had little to do with the initial design of this experiment, but helped in much of the experimental work. The remaining experiments described were performed independently.

I would like to express my sincere thanks to Professor E.W. Titterton C.M.G., who provided many of the initial ideas, and by his continual drive and enthusiasm has made this work possible.

I would also like to acknowledge the encouragement given by Professor Sir Leslie Martin F.R.S. during my year at the University of Melbourne.

Thanks are also due to my many colleagues at both the Australian National University and the University of Melbourne for their encouragement and assistance and also to members of the workshop staffs for their patient aid in the construction of apparatus.

Scholarships provided by the Dunlop Rubber Company and the Australian National University enabled me to undertake this research.

CONTENTS

SECTION A

SCINTILLATION COUNTERS FOR GAMMA-RAY AND ALPHA-PARTICLE DETECTION.

CHAPTER 1

THE RESPONSE OF A SODIUM IODIDE SCINTILLATION COUNTER TO HIGH ENERGY GAMMA-RAYS.

1.1 Introduction.

It had recently been shown that the historical method of detecting radiation by the light it produced in certain materials had gained a new significance with the development of the high gain photomultiplier tube and the discovery of many new types of scintillating material.

Gamma-rays are detected by means of the secondary electrons produced throughout the volume of the scintillator by the various absorption processes. To serve as an efficient gamma-ray detector the scintillator must therefore be of high atomic weight and be obtainable in large clear crystals. Sodium iodide activated with thallium, which has a high luminescent conversion efficiency, proved to be the most useful of the new materials for gamma-ray spectroscopy.

Figure 1. shows the variation with energy of the linear absorption coefficient of gamma-rays in sodium iodide. The values for the partial coefficients for each of the three absorption processes were obtained from the data given by Davisson and Evans[1].

---

1. Davisson, C.M., and Evans, R.D., Rev.Mod.Phys. 24: 79, 1952.

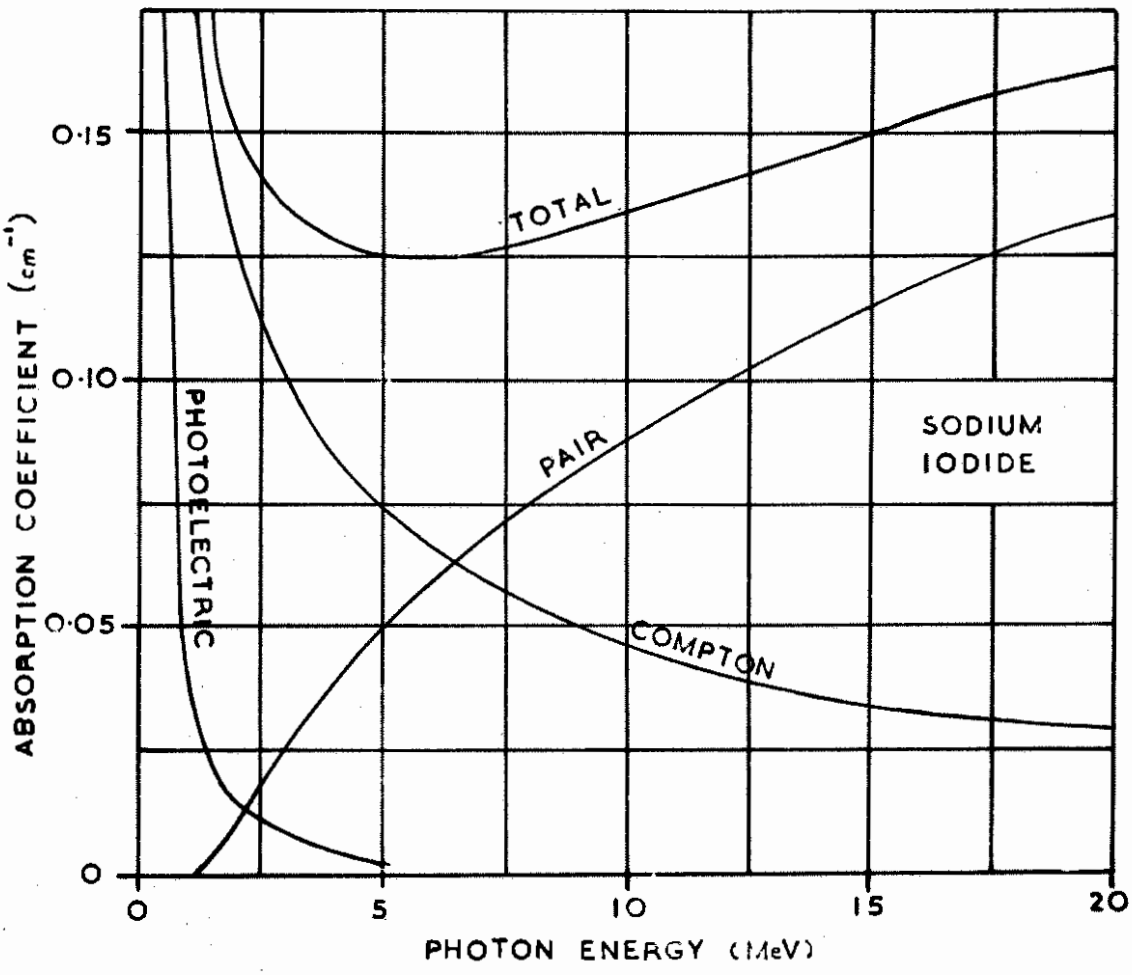

FIGURE 1. ABSORPTION COEFFICIENTS OF GAMMA-RAYS IN SODIUM IODIDE.

Hofstadter and McIntyre[2,3] showed that for energies of the order of 1 MeV, the pulse height distributions obtained from a scintillation counter using a thallium-activated sodium iodide crystal could be interpreted in terms of the energy distributions of secondary electrons from the gamma-capture processes of photoelectric effect, Compton scattering and pair production.

Maeder and Wintersteiger[4,5] showed the further effect of capture of degraded Compton-scattered quanta in the crystal.

It was suggested by Hofstadter and McIntyre[3] that the complexity of the spectrum could be reduced, with subsequent loss of efficiency, by using two or three crystals in coincidence. In the first method, which is useful for energies below the pair production threshold, the second crystal is set at a large angle (140°) to the incident gamma-ray beam. Thus, only those events are recorded in the main crystal for which a Compton-scattered quanta is detected in the second crystal. Above

---

2. Hofstadter,R., and McIntyre,J.A., Phys.Rev. 79: 389, 1950.
3. Hofstadter,R., and McIntyre,J.A., Phys.Rev. 80: 631, 1950.
4. Maeder,D., and Wintersteiger,V., Phys.Rev. 87: 537, 1952.
5. Maeder,D., and Wintersteiger,V., Helv.Phys.Acta 25: 465,1952

the pair production threshold the second method can be used to isolate those pulses due to events in which a positron is annihilated in the main crystal and both annihilation quanta escape from it[6,7]. For single gamma-rays of low energy both these methods result in a pulse height spectrum consisting of a single peak.

The results of these early workers suggested that it would be possible to examine the gamma-ray spectrum from a reaction such as $Li^7(p,\gamma)Be^8$ with a high degree of resolution. This spectrum was known to possess two components, 17.6 MeV and 14.8 MeV.[8] However, the pulse height distribution which is shown in Figure 2 was considerably broader than could be accounted for by the above mentioned processes alone. In view of this it was decided to undertake a more complete investigation of the factors affecting the shape of the pulse height distribution obtained with a sodium iodide scintillation counter for high energy gamma-rays.

---

6. Johannson, S.A.E., Nature 166: 794, 1950.

7. Bair, J.K. and Maienschein, F.C., Rev. Sci. Instrum. 22: 243, 1951.

8. Walker, R.L., and McDaniel, B.D., Phys. Rev. 74: 315, 1948.

1.2 Experimental determination of the shape of the pulse height distributions for gamma-rays up to 18 MeV.

The experiment was performed with thallium activated sodium iodide crystals of two different sizes. These were polished with successively finer grades of abrasive paper and finally with a cloth, while being kept wet with Nujol.

The smaller crystal (2.5 cm. long by 2.5 cm. diameter) was covered with aluminium foil and immersed in Nujol in a small glass beaker. This was mounted directly on the photocathode of a EMI Type 5311 photomultiplier. Nujol was used to optically couple the two glass surfaces.

The larger crystal (7.5 cm. long by 3.8 cm. diameter) was a composite one consisting of three separate crystals, each 2.5 cm. long by 3.8 cm. diameter, placed together on one axis. This was sealed into a perspex block which served as a light pipe. The crystal lay on the axis of the photomultiplier 4 in. from the photocathode, and the crystal axis made a right angle with the photomultiplier axis.

The gamma-radiation was obtained by bombarding thick fluorine, boron, and lithium targets with protons from a 700 kV electrostatic generator. The targets were deposited on copper backings by evaporating lead fluoride, by pressing amorphous boron, and by evaporating lithium hydroxide, respectively. The bombarding energy used on all three targets was 510 KeV.

since at this energy the thick target spectrum is known in each case. The main components and their relative intensities are shown in Table 1. The gamma-radiation entered the 1 in. crystal 9 in. from the target, and the 3 in. crystal 5 in. from the target.

TABLE 1.

REACTION	COMPONENT	RELATIVE INTENSITY
$F^{19}(p,\alpha\gamma)O^{16}$ [9.]	6.1 MeV	96%
	7 MeV	4%
$B^{11}(p,\gamma)C^{12}$ [10.]	4.4 MeV	45%
	11.8 MeV	45%
$Li^{7}(p,\gamma)Be^{8}$ [8.]	16.3 MeV	10%
	14.8 MeV	33%
	17.6 MeV	67%

The output pulses from the photomultiplier were fed, after amplification to a single channel analyser.

The experimental pulse height distributions so obtained are shown as histograms in Fig.2. Because of the greater distance of the 3 in. crystal from the photocathode and the intervening thickness of perspex, the light collection efficiency from it was much less than from the 1 in. crystal. A higher

9. Hornyak,W.F., Lauritsen,T., Morrison,P. and Fowler,W.A., Rev.Mod.Phys. 22: 291,1950.

10. Walker,R.L., Phys.Rev. 79: 172, 1950.

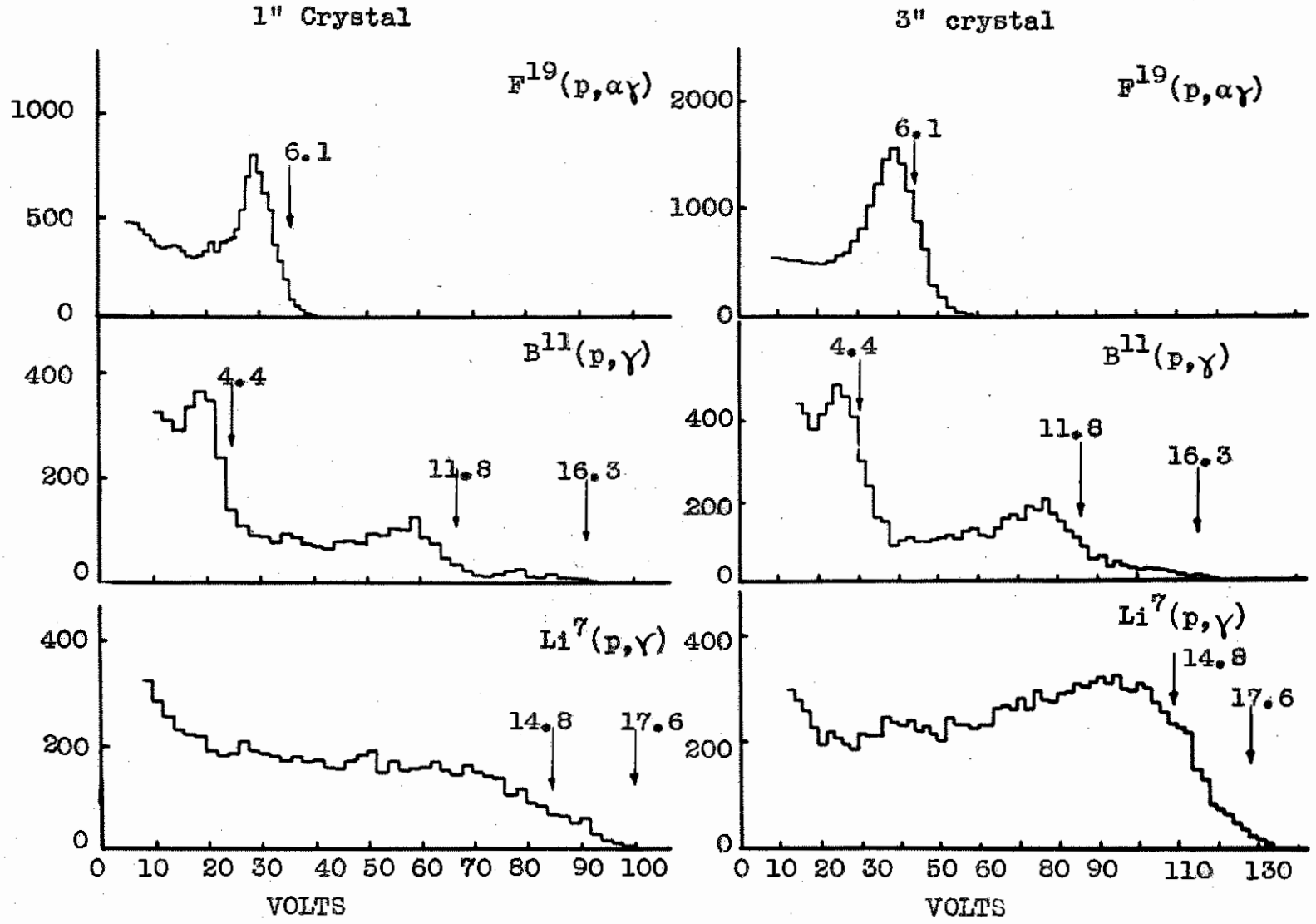

FIGURE 2. EXPERIMENTAL PULSE HEIGHT DISTRIBUTIONS.

photomultiplier voltage was needed with the 3 in. crystal to bring the pulse heights into the same voltage range as for the 1 in. crystal.

Since the response of sodium iodide to electrons is linear[11], the calibration of the pulse height scale in terms of gamma-ray energy could be deduced from the positions of the peaks in the distributions for gamma-radiation from the fluorine reaction. A 6.1 MeV gamma-ray is absorbed approximately equally by the Compton and pair production processes (Figure 1.) and since the pulse height distribution of the secondary electrons from Compton scattering is inherently broad, the peak in the fluorine distribution must be the result of pair production. The energy corresponding to the peak depends however, on the proportion of events in which one or both of the annihilation quanta are absorbed in the crystal.

Since the probability of annihilation of a positron before coming to rest is small[12], it was assumed that the two annihilation quanta are emitted in opposite directions along a line randomly orientated in space. The length of this line was taken to be equal to the mean diameter of the

---

11. Taylor, C.J., Jentschke, W.K., Remley, M.E., Eby, F.S., and Kruger, P.G., Phys.Rev. 84: 1034, 1951.

12. Heitler, W., "The Quantum Theory of Radiation" Oxford University Press, 1936.

crystal and was divided into intervals of 0.25 cm. The probable energy loss of a quantum originally 0.5 MeV, was obtained for each successive interval from the known absorption coefficients and energy distributions of Compton electrons.[12] Energy was considered in discrete steps of 0.1 MeV. From these results the probability distributions shown as histograms in Figure 3. were obtained for the energy loss of pairs of annihilation quanta whose points of origin were spread uniformly throughout the crystal. The peaks at 0, 0.5 and 1.0 MeV correspond to absorption of none, one or both of the quanta.

The fluorine peak in the 1 in. crystal was thus due to those events in which neither annihilation quantum was absorbed and therefore corresponds to an energy of 5.1 MeV. The slight bump on the high energy side of the peak was produced by those events in which one of the quanta was absorbed. The broader peak in the 3 in. crystal must be interpreted as arising from the unresolved contributions of the two events in which either none or one of the two quanta was absorbed. Using this calibration the positions at which lines of the full gamma-ray energy would occur are marked on Figure 2.

It is immediately apparent that serious deterioration of the spectral shape occurs with

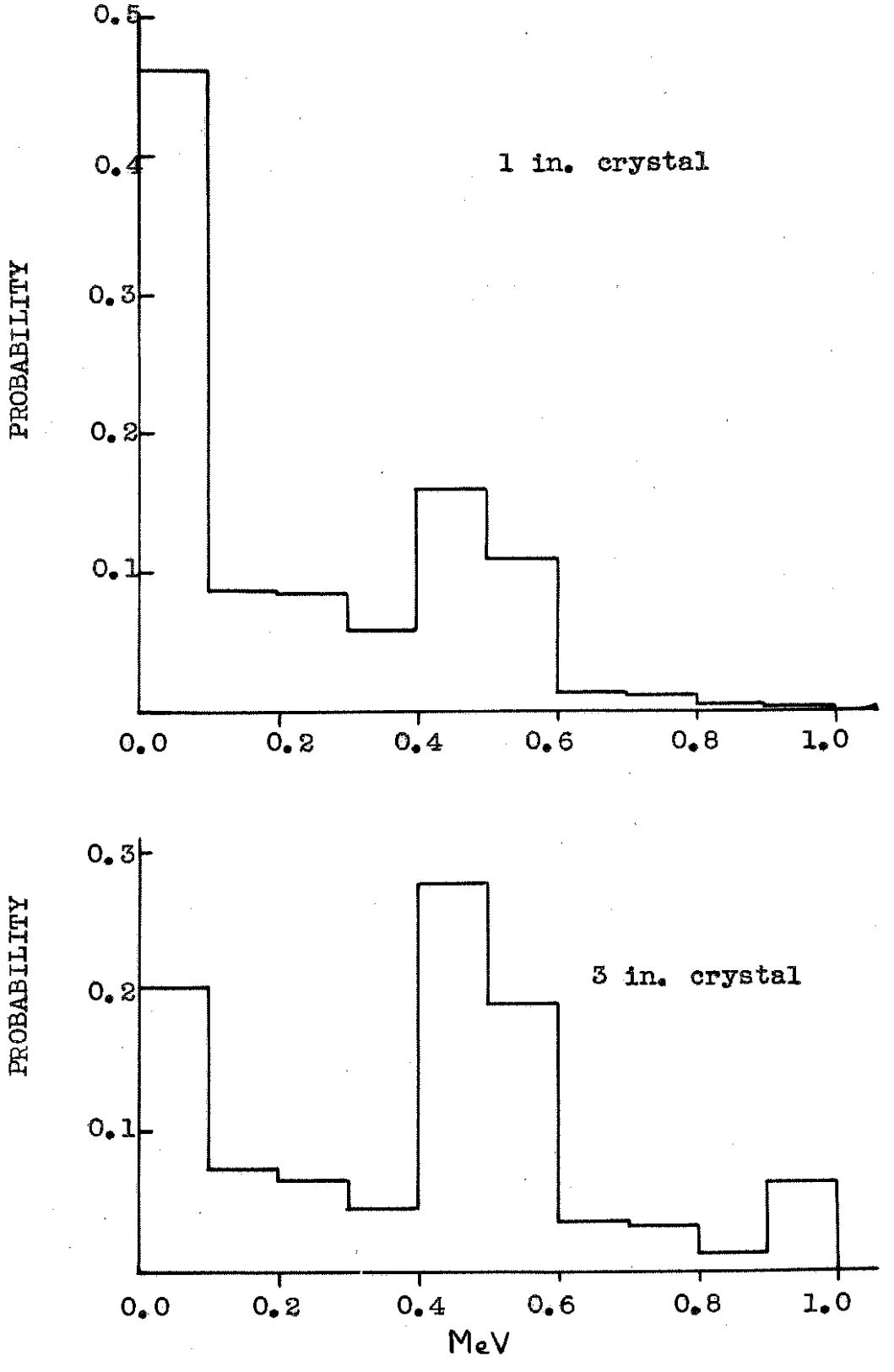

FIGURE 3. DISTRIBUTIONS OF IONIZATION ENERGY FROM ANNIHILATION QUANTA.

increasing gamma-ray energy. This is more marked in the smaller crystal. Factors which affect the distribution in the case of low energy gamma-rays, such as crystal characteristics and light collection efficiency, could not account for this deterioration. On the contrary, the larger light output from the higher energy event should in itself result in improved resolution.

With the increase in gamma-ray energy there will be a corresponding increase in the range of the secondary electrons. This could lead to a broadening of the distribution if a significant fraction of the incident energy was lost as a result of the escape of electrons from the crystal. The mean range of the secondary electrons from an 18 MeV gamma-ray was found to be about 0.3".[13] Thus the fraction of events in which energy is lost in this way is about 30% for the 1" crystal and 10% for the 3 in. crystal. Although this would have a noticeable effect in the smaller crystal, it is not sufficient to account for the distributions in Figure 2.

Another factor which only becomes important at higher energies is bremsstrahlung of the secondary electrons. The energy lost with the escape of these photons from the crystal might account for the effects

---

13. Wilson,R.R., Phys.Rev. 84: 100, 1951.

observed.

An attempt is made below to explain the experimental pulse height distributions in terms of this partial shower process which takes place when each quantum is absorbed.

1.3. Operation of the scintillation counter.

The use of a scintillation counter as a gamma-ray spectrometer depends on the approximate proportionality which exists between the output pulse height and the energy of the incident photons. By breaking down the operation of the counter into consecutive stages it is possible to see where significant departures from strict proportionality can arise. Considering only homogeneous gamma-rays of energy E, possible sources of variation of pulse height are:

(i) The energy I given up by ionization in the crystal. $f(I,E)dI$ will denote the probability that a quantum loses energy between I and I + dI.

(ii) The number of light photons emitted per unit energy of ionization in the crystal. In sodium iodide this number is independent of I for electrons above 1 KeV[11], and any variation in fluorescence efficiency through the crystal will be neglected. Since, furthermore, the number is large, purely statistical variation is small, and so it will be assumed that the number of photons emitted is

proportional to I.

(iii) The fraction of the light photons which reach the photosensitive surface of the photomultiplier. The main variation in this arises from the dependence of the efficiency of light collection upon the position in the crystal from which the light emanates. This can be due to imperfections in the optical properties of the crystal[14], or to differences in the effective solid angle subtended by the photo-surface. For the purposes of the present work, this source of variation will also be neglected, and the number of photons reaching the photosensitive surface will be taken to be aI, where a is a constant.

(iv) The fraction of photons reaching the photosensitive surface which eject electrons, and

(v) The multiplication of electrons in the multiplier.

The last two factors have been considered in detail by various workers[14,15]. $g(p,aI)dp$ will denote the probability that aI photons reaching the photosensitive surface give rise to an output pulse between p and $p + dp$ in height.

---

14. Garlick, G.F.J., and Wright, G.T., Proc.Phys.Soc.Lond. B65: 415, 1952.

15. Seitz, F., and Mueller, D.W., Phys.Rev. 78: 605, 1950.

The probability that a gamma-ray of enerfy E absorbed in the crystal gives rise to an output pulse from the photomultiplier between p and p+dp is now h(p,E)dp, where $h(p,E) = \int_0^E g(p,aI).\ f(I,E)dI$

In the following section a method is described for finding the form of f(I,E) as a function of I. This was carried out for E = 18 MeV for a cylindrical sodium iodide crystal 2.5 cm. long by 2.5 cm. diameter.

The function g(p,aI), which includes the effect of statistical variation in the number of electrons ejected from the photosurface by equal flashes of light and in the multiplication of the tube, was assumed, for any value of aI, to be a Poisson distribution function of p with mean value proportional to aI. A later section describes a measurement of the ratio of the standard deviation to the mean of the distribution as a function of the mean value.

1.4 Calculation of f(I,E)

Only one case could be considered in detail because of the length of the calculations. That of a 18 MeV gamma-ray in a 1 in. crystal was chosen so that comparison could be made with the experimental distribution from the $Li^7(p,\gamma)Be^8$ reaction where the effect is most marked.

f(I,E) can be written as the sum of distributions resulting from each of the photon absorption processes.

$$f(I,E) = a_{pe}\, f_{pe}(I,E) + a_c\, f_c(I,E) + a_{pp}\, f_{pp}(I,E)$$

where a_{pe}, a_c and a_{pp} are the relative probabilities of absorption of an 18 MeV gamma-ray by the photoelectric, Compton scattering and pair production processes respectively. These values can be obtained from Figure 1. where it is seen that a_{pe} is effectively zero.

Each of the functions $f_c(I,E)$ and $f_{pp}(I,E)$ can now be expressed in terms of energy loss distributions of single electrons originating at any point in the crystal. For the purposes of the calculation which follows the length of the crystal was divided into 10 intervals each 0.25 cm. and the cross section into five concentric annuli of equal area. Energy was considered in increments of 0.5 MeV. Then $f(E_i, I'; d,n)$ denotes the probability that an electron of energy E_i MeV originating in the d^{th} interval and the n^{th} annulus lost energy I' MeV by ionization in the crystal. It is understood that $f(E_i, I'; d,n) = 0$ unless $0 \quad I' \quad E_i$.

When E = 18 MeV, $f_{pp}(I,E)$ can be written as

$$\sum_{I''=0}^{1} f(\overline{I + I''},\ 17) \cdot f(I'',1)$$

f(I,17) is the probability that a pair of electrons with a total energy of 17 MeV formed anywhere in the

crystal, lost energy I. f(I",1) is the probability that the two annihilation quanta, each 0.5 MeV lost energy I". f(I",1) is given in Figure 3.

f(I,17) can be further expressed as

$$\sum_{d=1}^{10} e^{-\mu(d-1)} \sum_{n=1}^{5} \sum_{E_i=0}^{8.5} P(E_i) \sum_{1'=0}^{I} f(E_i,I';d,n).f(\overline{17-E_i},\overline{I-I'};d,n) \text{---(1}$$

$P(E_i)$ is the probability that a pair of total energy 17 MeV has one electron of energy E_i. $P(E_i)$ was derived from Figure 11. of the paper of Rossi and Greisen[16]. The summation over E_i is taken only to 8.5 MeV because the function is symmetrical with respect to the two electrons. The flux of the gamma-ray beam was taken to be uniform over the cross section of the crystal in the summation over n. The attenuation of the gamma-ray beam in passing through the crystal is allowed for with the term $e^{-\mu(d-1)}$, where μ is the linear absorption coefficient for 18 MeV photons in NaI as given in Figure 1.

The expression for the ionization distribution resulting from the Compton scattering process was simplified by assuming that when a scattered photon was reabsorbed it lost all its energy in the crystal. Since the probability energy distribution for scattered photons is strongly peaked at low energies this was

---

16. Rossi,B., and Greisen, K. Rev.Mod.Phys. 13: 240, 1941.

generally justified. $f_c(I,E)$ then becomes -

$$\sum_{d=1}^{10} e^{-\mu(d-1)} \sum_{n=1}^{5} \sum_{E_i=0}^{18} C(E_i)(1-R_{dn}\overline{18-E_i})f(E_i,I';d,n)$$

$$+R_{dn}(18-E_i)f(E_i,\overline{I'+18-E_i};d,n) - - - - - - (2)$$

$R_{dn}(18-E_i)$ is the probability of reabsorption of the scattered photon of energy $(18-E_i)$ formed at d,n and was found using the photon absorption data of Figure 1. $C(E_i)$ is the relative probability of the production of a scattered electron of energy E_i by an 18 MeV gamma-ray and was derived from the Klein-Nishina formula[12].

The calculation of f(I,E) was thus reduced to the problem of evaluating the function $f(E_i, I'; d,n)$. This was done using the Monte Carlo technique which Wilson[17] has applied to the similar problem of shower production in lead. The technique was not applied directly to the incident photons because of the difficulty of assessing the multiple scattering effects for two electrons formed simultaneously in a pair production event.

The principle of the method is best illustrated by a trivial example. Consider the case of gamma-ray absorption in a certain thickness of material for which the absorption coefficient is known. The probability that a gamma-ray will be absorbed in passing

---

17. Wilson, R.R., Phys.Rev. 86: 261, 1952.

through the material can then be calculated. Assume that this probability is, say, 0.356. The fate of a gamma-ray passing through the material can then be decided by choosing a number from a table of three figure random numbers. If this number is less than 356, the gamma-ray has been absorbed, and if it is greater than 356 it has not been absorbed. Obviously if this process is repeated many times it will be found that within the statistical fluctuations, 35.6% of the gamma-rays will have been absorbed.

To apply the method, the crystal was first divided into 25 intervals of length each 0.1 cm. and a set of curves was drawn (Figure 4) representing the bremsstrahlung process for electrons in each interval. For a particular value of energy, the difference in ordinate between adjacent curves represents the probability of bremsstrahlung occurring per interval and giving photons of the stated energy. It was for this purpose that energy was "quantised" into increments of 0.5 MeV. Quanta of 0.25 MeV were allowed at this stage however, because although the energy content of each such photon is small they occur ffequently. The total ordinate of the figure represents unit probability per interval. The spacing of the curves in Figure 4 was derived from Figure 7 in the paper by Rossi and Greisen.[16]

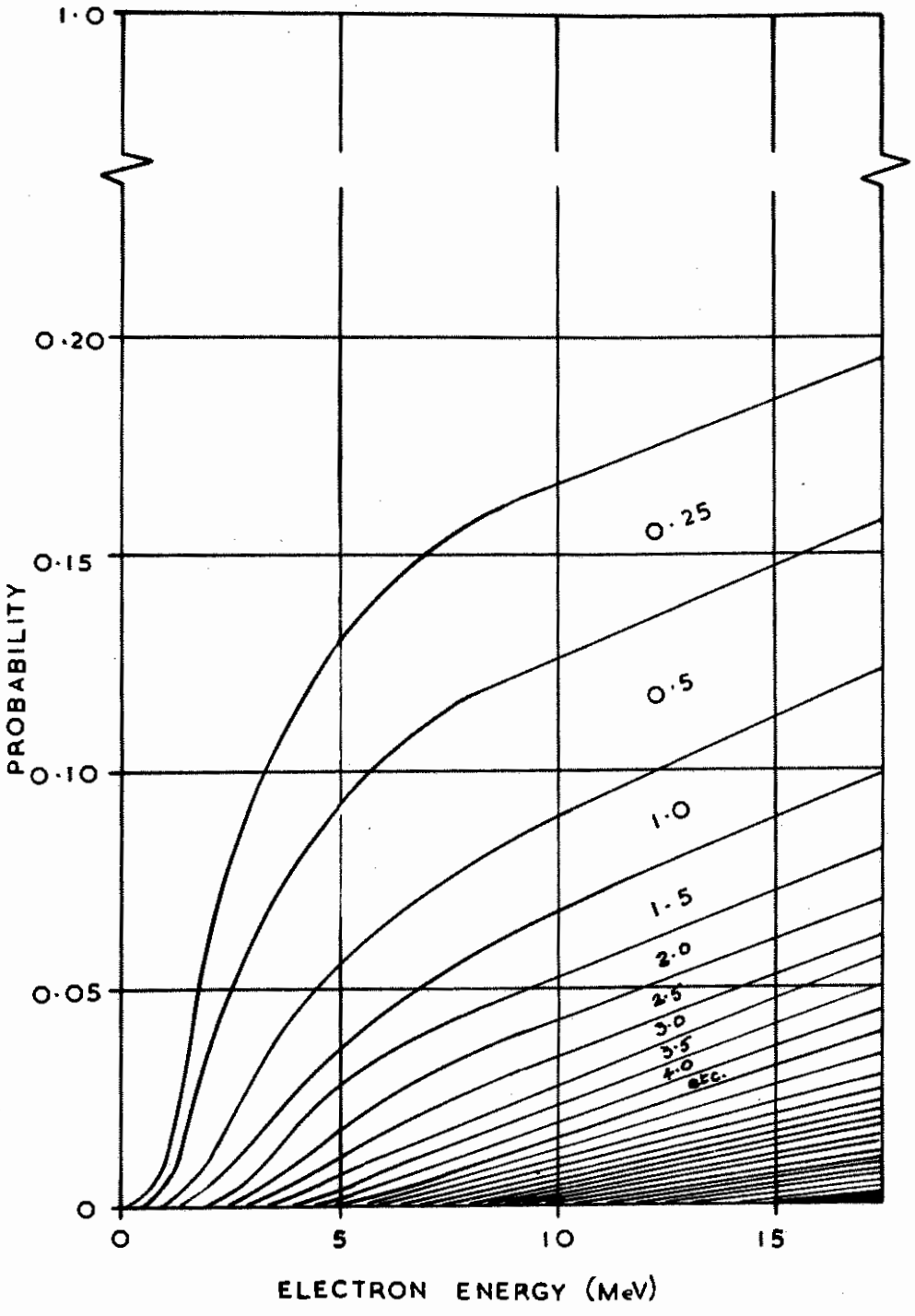

FIGURE 4. BREMSSTRAHLUNG PROBABILITY IN SODIUM IODIDE.

Throughout this work it has been assumed that the incident gamma-rays entered the crystal parallel to the axis and that all secondary electrons proceeded initially in the forward direction. For pair production by 18 MeV photons, the solid angle into which the positron and electron are emitted is of the order of 0.01 stererad. In Compton scattering, secondary electrons with high energy move off in the forward direction, whilst those which proceed in directions far removed from that of the incident photon are of low energy and are soon brought to rest. In all cases little error is introduced by the assumption of initial forward direction.

A set of life histories was compiled for individual secondary electrons, with each of the initial energies 3,6,9,12,15 and 18 MeV. The electrons, all beginning in the first interval, were followed through each section of the crystal in turn, assuming at this stage that their paths did not deviate. A random number taken from the tables [18,19] decided how much energy was lost by

---

18. Kendall,M.G., and Smith,B.B.-"Tables of Random Sampling Numbers" Tracts for Computers, No.24 (Cambridge Univ.Pres 1939.

19. Tippet,L.H.C.,-"Random Sampling Numbers" Tracts for Computers, No.15. (Cambridge Univ. Press). 1927.

radiation in each section and the process was continued until the electron came to rest or escaped across the end face of the crystal. To allow for ionization loss, 0.5 MeV was subtracted from the electron energy on crossing each 0.1 cm. interval. This value was derived from the data given by Sternheimer[20] and holds within 10% for electrons in the energy range 4-20 MeV.

The fate of each photon produced during the passage of the electron through the crystal was then decided from Figure 5 by drawing a single random number. This figure was derived from the published data of Dixon[21] on self absorption of large sources, together with the known photon absorption coefficients[22] for NaI.

To apply Dixon's results it was necessary to assume that the bremsstrahlung photons had a uniform distribution of origin throughout the volume of the crystal and, in addition, were emitted isotropically. Isotropy follows from the first assumption in conjunction with the directional spreading caused

---

20. Sternheimer,R.M., Phys.Rev. 88: 851, 1952.

21. Dixon,W.R., Nucleonics 8 (4): 68, 1951.

22. Campbell,J.G. and Boyle,A.J.F., Aust.J. Phys. 6: 171, 1953.

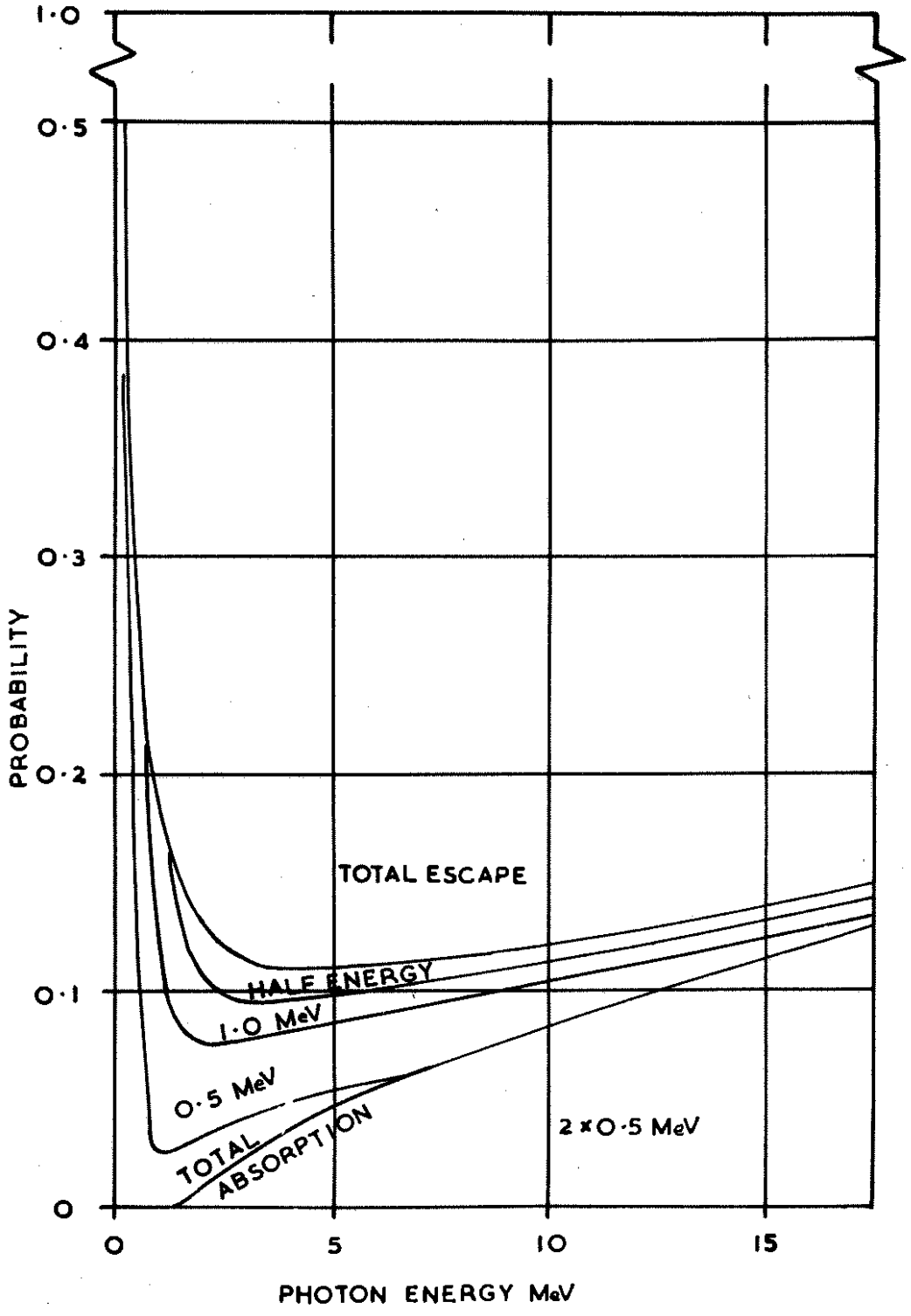

FIGURE 5. ABSORPTION PROBABILITY OF BREMSSTRAHLUNG IN THE 1 INCH CRYSTAL.

by multiple scattering. The energy of electrons resulting from reabsorption was assumed to be completely converted into ionization, being insufficient to produce further bremsstrahlung or to escape from the crystal.

The life histories for electrons formed in any interval of the crystal could be derived from the set of life histories obtained above for the case of electrons originating in the first interval. For example, the set for electrons formed in the second interval was obtained by removing the 25^{th} interval and all that occurred in it, from the original set. Similarly for electrons in other intervals.

To introduce sideways deflexion and the accompanying loss of energy caused by electrons escaping through the sides of the crystal, a formula given by Janossy[23] was used. This states that the mean square displacement of an electron passing through a homogeneous absorber of thickness Z is

$$x^2 = E_s^2 \int_0^z \frac{z'^2\, dz'}{E(z')^2}$$

---

23. Janossy, L. "Cosmic Rays" (Oxford University Press) 1948.

where $E(z^1)$ is its energy in MeV at depth $(z-z^1)$ and E_s is 21 MeV, distance being measured in radiation lengths. For the calculation, the electrons were assumed to start in each of the five annuli in turn. By a graphical method similar to one published later by Dickinson and Dodder[24], the fractions of electrons escaping through the side of the crystal were determined for each section of length, for each initial energy and each annulus of cross section. These results were applied to the life histories.

Upon resubdivision of the length of the crystal into 0.25 cm. sections, the function $f(E_i, I'; d,n)$ was completely determined for six values of E_i.

It was now necessary to find the function for all values of E_i from 0 to 19 MeV in steps of 0.5 MeV. To carry out this interpolation it was necessary to convert the distributions, which were in the form of histograms, into an analytical form. The form which was arrived at for the function $f(E_i I': d,n)$ was

$$A\delta(I'-I_i) + (1-A)E^{p-1}(E_i-I')^{q-1} / E_i^{p+q-1} B(p,q)$$

where $\delta(I'-I_i)$ is the delta function and $B(p,q)$ the beta function. The first term is the contribution of those electrons whose passage through the crystal had

---

24. Dickinson, W. C., and Dodder, D. C., Rev. Sci. Instrum. 24: 428, 1953.

been so far uneventful, so that they had all lost the same amount of energy I_i by ionization. The value of A was determined directly from the peak in each histogram. The second term is due to those electrons which in addition had emitted bremsstrahlung or had escaped through the side of the crystal. The parameters p and q were found from the first and second moments of each histogram after the peak had been removed. The form of this term, which is known as the beta distribution, was found in each case to approximate well to the shape of the Monte Carlo histogram. The ionization distributions for the six initial energies having thus been converted to analytical form, those for the intermediate energies were derived by linear interpolation of the three parameters A, p and q.

The functions $f(E_i, I' ; d,n)$ having been determined, the functions $f_{pp}(I,E)$ and $f_c(I,E)$ and hence $f(I,E)$, could be derived using equations (1) and (2) above. The calculation of the summation over I' in equation (1) was carried out on Hollerith punched-card equipment through the co-operation of the Commonwealth Bureau of Census and Statistics and the Australian Wool Realization Commission. Since the Compton process amounts to only 20% of the total absorption, this sum was only evaluated for representative values of n and d,

the remainder being found by interpolation.

1.5 Determination of $g(p,aI)$

In order to measure directly the broadening of the pulse-height distribution which is introduced by statistical effects in the tube, it was necessary to expose it to flashes of light of constant integrated intensity and to measure the spread in height of the resulting output pulses.

The experimental arrangement is shown in Figure 6. Short flashes were produced by a beam of light which was reflected from a rotating mirror and passed across the photocathode of the photomultiplier. The duration of the pulses for two different slits was 0.3 and 0.5 μsec. To ensure that the recorded voltage pulses did not depend on the shape of the light pulses, an integrating time constant of 4 μsec. was inserted at the collecting electrode of the photomultiplier. The same time constant had been used in the previous experiment with sodium iodide, which has a decay time of 0.25 μ sec. The photomultiplier, amplifier and pulse height analyser were also those used previously to determine the experimental pulse height distributions. A number of pulse height

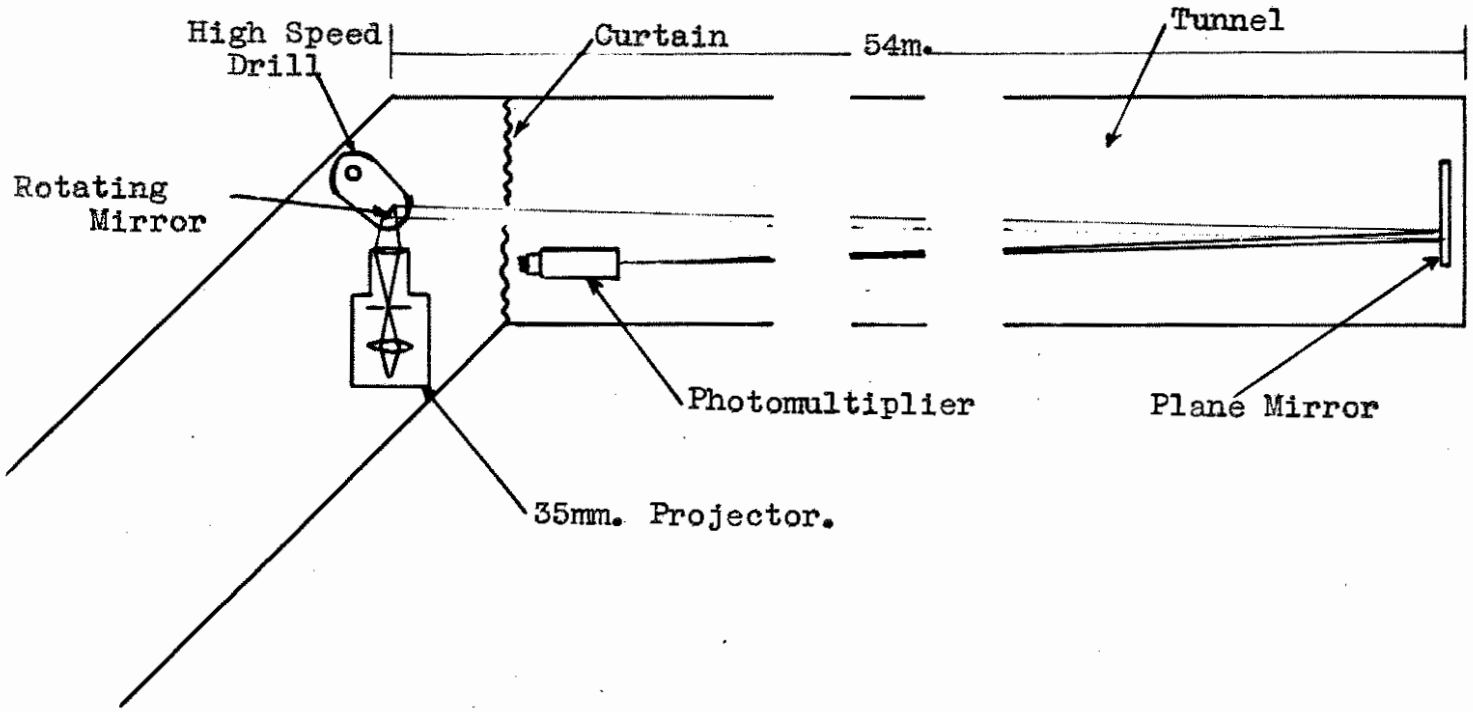

FIGURE 6. EXPERIMENTAL ARRANGEMENT FOR MEASUREMENT OF STATISTICAL SPREAD.

distributions were obtained for each of several lamp voltages with both slits, using total multiplier voltages of 930, 1040 and 1150 V. The two distributions shown in Figure 7 illustrate the spread obtained in the two extreme cases, for the least and for the greatest integrated light intensity per flash. It can be seen that these distributions are consistent in shape with the Poisson distribution shown as the full curves in the figure.

The mean value and standard deviation of the pulse-height distributions were calculated in each case, and the value of (standard deviation/mean) was plotted against $(\text{multiplier gain}/\text{pulse height at collector})^{1/2}$, the result being shown in Figure 8. The multiplier gain was measured relative to that at 930 V., and the pulse height at the collector was found by dividing the mean of the pulse-height distribution in volts by the measured amplifier gain. The fact that the points are well fitted by a straight line through the origin indicates that the fractional spread of the distribution is inversely proportional to the square root of the number of electrons entering the multiplier, and therefore that sources of spread in pulse heights from uniform light flashes other than statistical variations were unimportant. Furthermore, there is no great dependence of the

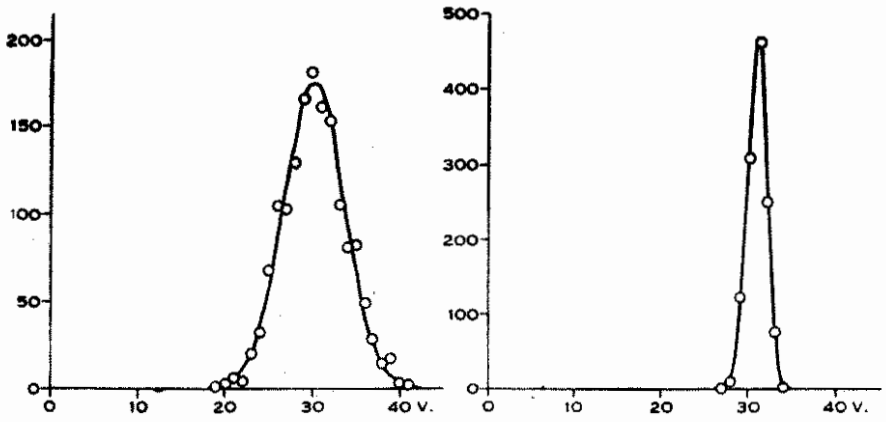

FIGURE 7. PULSE HEIGHT DISTRIBUTIONS FROM LIGHT FLASHES OF CONSTANT INTEGRATED INTENSITY.

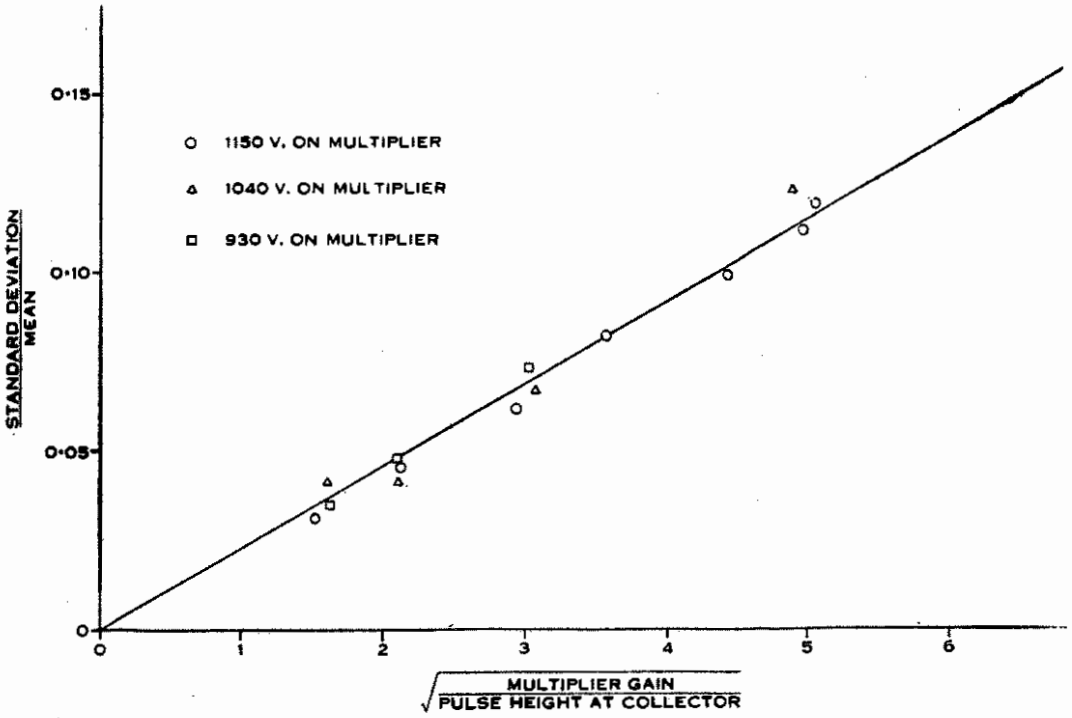

FIGURE 8. RESULTS OF DETERMINATIONS OF STATISTICAL SPREAD.

spread on a multiplier voltage in the range used.

Thus the function g(p,aI) was determined. Using it and the function f(p,aI) derived in the previous section, h(p,E) could be found by graphical integration.

1.6 Comparison with experiments.

The experimental pulse-height distribution found in section 1.2 for the gamma-rays from the reaction $Li^7(p,\gamma)Be^8$ is reproduced as the histogram in Figure 9. The arrows indicate the energy calibration arrived at using the $F^{19}(p,\alpha\gamma)$ radiation.

In determining the theoretical distribution for the $Li^7(p,\gamma)$ radiation, the component at 14.8 MeV was assumed to give a distribution of the same shape as the more intense one at 17.6 MeV, except that its high energy edge was spread by the natural line width of 2 MeV. The further spreading due to statistical effects in the photomultiplier was less than 2 per cent at the high energy end. The resulting theoretical distribution, scaled horizontally to fit the energy calibration and vertically to fit the histogram, is shown by the smooth continuous curve in the figure. The agreement is satisfactory apart from the usual divergence at low energies. This is the result of detection of degraded radiation from material around the target.

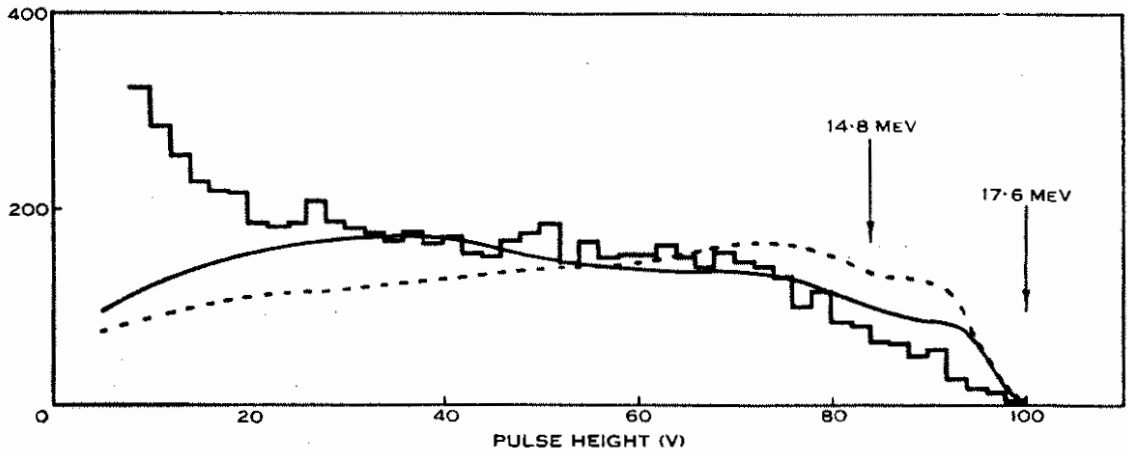

FIGURE 9. RESULTS FOR $^{7}Li(p,\gamma)$ RADIATION.

Histogram: experimental, uncollimated.

Continuous curve: theoretical, uncollimated.

Dotted curve: theoretical, collimated.

The effect of sideways loss of electrons by multiple scattering could be minimized by collimating the beam of gamma-radiation to a narrow pencil centred on the crystal axis. This would have little effect, however, on bremsstrahlung loss. The distribution to be expected in the case of a pencil 1.12 cm. in diameter, (corresponding to the centremost of the five annuli considered), is shown by the dotted line in Figure 9. This was not tested experimentally since the resolution is not significantly improved.

1.7 Discussion

It can now be seen that the broadening of the peaks in the pulse-height distributions for homogeneous radiation above about 6 MeV is explained as the effect of bremsstrahlung escaping from the crystal and taking with it an appreciable and variable fraction of the incident photon energy. The small improvement of the distribution with the 3 in. crystal implies that the probability of reabsorption of bremsstrahlung photons is only slightly increased above that for the 1 in. crystal.

Use of the three crystal spectrometer was mentioned in the introduction as a means of improving the pulse height distribution by selecting only that

part of the distribution contributed by pair production. Little would be gained by using this technique at 18 MeV since pair production accounts for 80 per cent of the primary processes and the only advantage would be the elimination of the spreading caused by reabsorption of annihilation quanta.

Albert[25] describes an anticoincidence spectrometer which might result in improved distributions at 18 MeV. This consists of a central crystal almost completely surrounded by many small crystals packed to a depth of about 4 in. The pulse height from the central crystal is recorded only when no event occurs in the surround. Thus the distribution would be a single peak corresponding to complete absorption of the incident gamma-ray within the crystal, provided that all energy escaping from the central crystal is detected in the surround. This method is obviously very useful for low energy gamma-rays, but for high energies, suffers from two disadvantages. Firstly, the number of events involving complete absorption in the main crystal is a very small fraction of the total, approximately 0.04% for a 1 in. crystal. Secondly, the surrounding crystal can not be completely efficient for absorption of escaping photons and many events will be recorded

---

25. Albert, R.D., Rev. Sci. Instrum. 24: 1096, 1953.

which correspond to less than the total energy.

The obvious way to overcome the limitations to the energy resolution of a single crystal counter, is to increase the size of the crystal so that the fraction of bremsstrahlung radiation that escapes is kept small. Thus while at low energies the minimum crystal size is determined by the necessity to ensure that electron ranges are small compared with crystal dimensions; above 10 MeV the crystal dimensions would need to be large compared with the mean free path of the bremsstrahlung photons. In sodium iodide, this is about 4 cm. for 1 MeV photons increasing to 8 cm. for 5 MeV, and then decreasing very slowly at higher energies. At the time this work was carried out, however, no crystals of this size were available. The improvement possible with larger crystals has since been shown by Foote and Koch[26], who have clearly resolved the two components of the $Li^7(p,\gamma)$ radiation using a crystal 8 in. long by 5 in. diameter.

---

26. Foote, R.S., and Koch, H.W., - Rev. Sci. Instrum. 25: 746, 1954.

CHAPTER 2

SCINTILLATION COUNTERS FOR ALPHA-PARTICLE DETECTION AND FOR USE WITH FAST COINCIDENCE CIRCUITS.

2.1. Introduction.

For many years zinc sulphide, activated with copper or silver, was widely used as an α-particle detector. The light flash resulting from a single α-particle is just detectable by the human eye, and a microscope enables counts to be made of a low flux of particles. However, with the development of the various types of gas counters this method became obsolete.

The gridded ionization chamber and the proportional counter both posses many advantages for work with α-particles, and it will be useful to summarize these here so that comparisons can be made later with the performance of the scintillation counter.

There is no limit to the efficiency of a gas counter and, in fact, 4π geometry is possible if the source is placed within the counter.

The energy response can be made linear over the whole range by using a noble gas in the chamber.

Theoretically, the energy resolution depends only on the number of electrons formed in each event and should therefore be better than 1%; however,

in practice, gas impurities increase this figure to approximately 5%. This resolution varies little for energies greater than a few hundred KeV.

Gamma-rays are detected in these counters only if the flux is so great that pile up occurs within the resolving time of the circuit.

The counting rate possible with any counter depends on the rise time of the pulse. For the proportional counter this is given by the time required for the positive ions to move away from the central wire. Since this time is less than 10^{-8} sec. the only limitation on the counting rate is imposed by the electronics.

The coincidence resolving time of these counters is limited by the fluctuations in the time required to produce the output pulse. In the gridded ionization chamber the variation in the time of arrival of the electrons is of the order of 1 μsec. In the proportional counter, the fluctuations in the time taken for the electrons to produce the avalanche are normally greater than 1 μ sec, because of the poorer electrode geometry in this case. Thus resolving times of better than 1 μsec. are difficult to achieve with a gas counter.

The advent of the high gain photomultiplier tube brought about a revival of zinc sulphide as an α-particle

detector. Zinc sulphide has the highest conversion coefficient (ionization energy to light energy) of any known phosphor, about 20%, but, unfortunately, can not be obtained in the form of large crystals. Only a very thin layer of powder can be used in order that as much light as possible reaches the photocathode from an event within the scintillator. Thus its use is limited almost entirely to the detection of α-particles. Since energy resolution depends on the uniformity of light collection from all parts of the scintillator as well as on the average total intensity from similar events, a zinc sulphide scintillator is virtually useless for energy discrimination. However, the use of a very thin layer has the advantage of almost complete insensitivity to gamma-radiation. α-particle counts can therefore be taken in the presence of a very high gamma-ray flux.

The choice of a phosphor to give good energy resolution with α-particles was restricted to sodium iodide or anthracene. The ratio of the pulse heights obtainable with these phosphors with α-particles of the same energy is approximately 9 : 1[27] and therefore the energy resolution obtainable with sodium iodide is three times better than with anthracene.

---

27. Birks, J.B. "Scintillation Counters" Pergamon Press Ltd. 1953.

All other phosphors available at the time give poorer results.

Although the resolution possible with sodium iodide is greater than with anthracene, its hygroscopic nature presented difficulties when it was to be used as an α-particle detector. Normally, for gamma-ray detection, the crystal is enclosed in an air tight case. This is not practicable when the crystal is to be used as an α-particle detector when, ideally, the crystal face should be exposed to the vacuum. Thus for some time, anthracene was preferred for work with α-particles.

At the present time crystals of cesium iodide are available which are only slightly hygroscopic. The conversion efficiency of cesium iodide is 80% that of sodium iodide and therefore these crystals are ideally suited to work with heavy charged particles.

Sections 2.2, 2.3. and 2.4 of this chapter describe the development and characteristics of the sodium iodide scintillation counter. The application of scintillation counters to work with fast coincidence circuits is discussed in section 2.5.

2.2 Linearity of response of Sodium Iodide.

Taylor et al[11] have shown that the response of sodium iodide to α-particles is not linear for energies below about 8 MeV. The conclusions could be checked from results obtained incidentally in the work described later in Chapters 4 and 5.

Figure 10. shows a plot of pulse height against energy for both protons and α-particles. The pointsmarked by a "x" were obtained with the apparatus described in Chapter 5; the protons arising from the $B^{10}(d,p)B^{11}$ and $C^{12}(d,p)C^{13}$ reactions, and the α-particles, from ThC+C' and the $B^{10}(d,\alpha)Be^{8}$ reaction. The energy corresponding to each of these points was not accurately defined owing to uncertainties in the thickness of foil between the source and the detector. The points marked by "•" were obtained with the apparatus described in Chapter 4, using a ThC+C' source. The range of energy values was obtained by altering the pressure of air in the target chamber. The ordinates of these points have been scaled to fit the other results.

Figure 10. is in general agreement with the results Taylor et al, showing linearity for protons and non linearity for α-particles below 8 MeV. The present work suggests, however, that the conversion

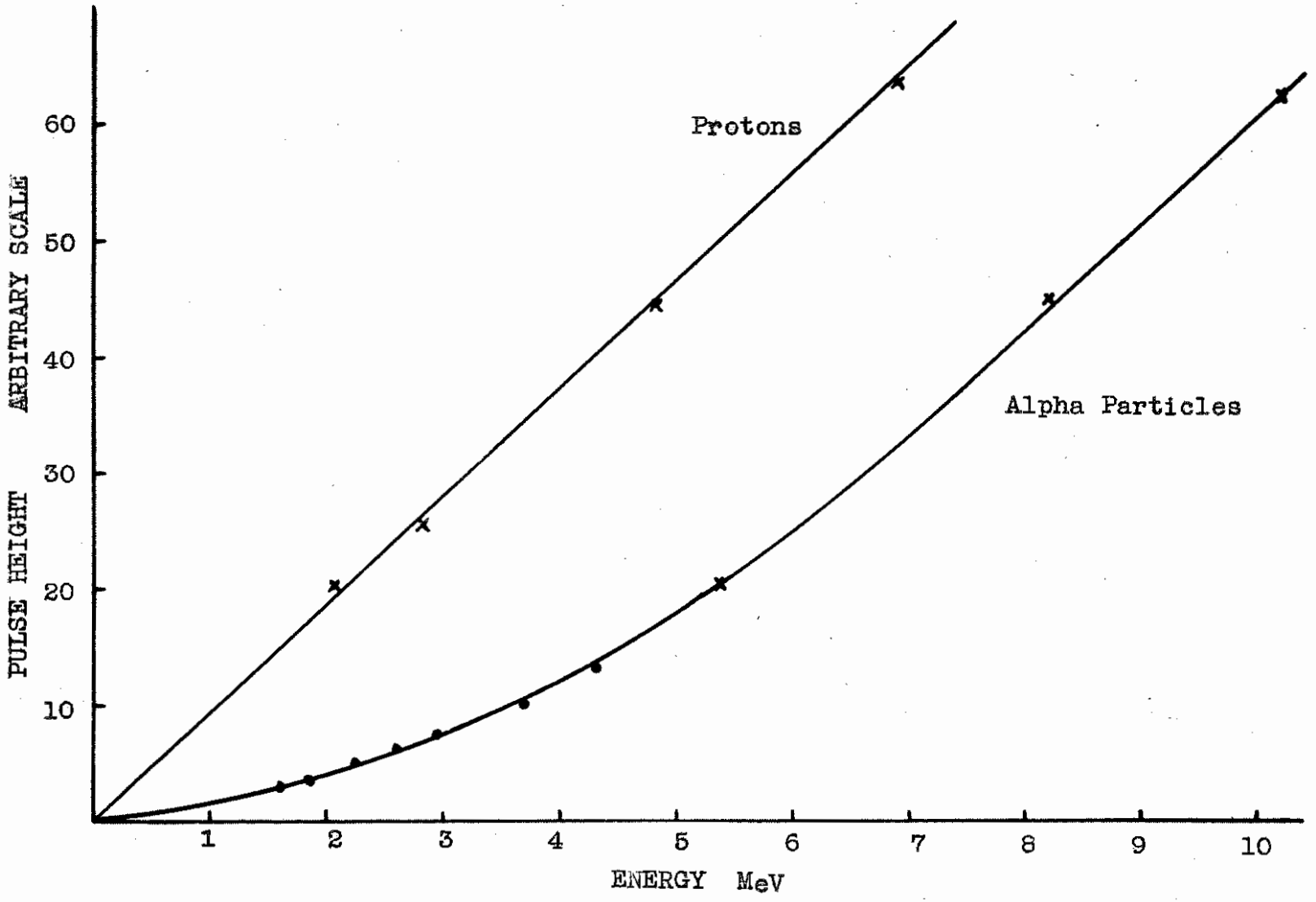

FIGURE 10. RESPONSE OF NaI TO PROTONS AND ALPHA PARTICLES.

efficiency for α-particles above 6 MeV is higher than the value indicated by Taylor et al.

This non-linear variation of pulse height with energy introduces little difficulty into the determination of the energy of a sharp α-particle group, provided an accurate calibration of the apparatus has been made. However, in cases where the spectrum is inherently broad and when a knowledge of the true shape of the spectrum is desired, this non-linearity is troublesome.

An α-particle pulse height distribution can be recorded with either a single - or multi-channel analyser, which produce a spectrum showing the number of α-particle pulses in a given voltage channel. In both cases the channel width is constant and independent of the channel height. However, the fact that the relation between channel height and energy is not linear implies that each channel covers a different range of energy, which decreases as the channel height increases. Thus the conversion of the voltage scale of the experimental spectrum to an energy scale involves multiplication of the ordinates by a factor depending on this energy range. The required factor $\frac{dV}{dE}$ can be found as a function of E by differentiating the calibration curve of channel height V, against α-particle energy, E. In an actual experiment[a] case, as in Chapter 5, this can not be

done very accurately and hence the final result is only approximate. This is an undesirable feature of sodium iodide when used for α-particle detection.

2.3 Energy Resolution.

The pulse height resolution that should be possible when sodium iodide crystals are used with α-particles can be estimated from the results of measurements with gamma-radiation. As mentioned in Chapter 1, the pulse height resolution depends almost entirely on the number of photoelectrons entering the multiplier. A high figure for the resolution of the 661 KeV gamma-ray line from Cs is 5% which corresponds to 500 electrons entering the multiplier per MeV of absorbed radiation. Since the response of sodium iodide to protons is the same as for electrons[11], this figure can be used in conjunction with Figure 10. Thus a 9 MeV α-particle should result in the production of approximately 2800 photoelectrons. If straggling effects associated in any way with the absorption of the α-particles can be neglected, the resolution for 9 MeV α-particles should be about 2%.

The general construction of the scintillation counters used for α-particle detection in the

experiments to be described in later Chapters, was as shown in Figure 11. In early versions of the counter the crystal A was about 1/16" thick and about 1" in diameter. This was polished in a dry box using fine carborundum on cloth wet with paraffin oil. The paraffin oil and any hydrated sodium iodide was removed by dipping the crystal, first into a 50:50 mixture of acetone and chloroform, and then into carbon tetrachloride. A final polish was given with dried cleansing tissues. The crystal was then attached with araldite to the glass plate B which had previously been stuck to the end of the perspex light pipe. This plate prevented moisture from the perspex from affecting the crystal. The crystal was covered with paraffin oil before it was removed from the dry box and this was quickly wiped off with dried cleansing tissues before the perspex was placed in position on the target chamber. This was evacuated immediately and the photomultiplier attached as shown. Highly viscous silicone oil was used to provide the optical coupling between the light pipe and the photomultiplier. The aluminium mask C defined the effective crystal area and eliminated possible edge effects.

Without the covering foil D, the resolution obtained for the 8.8 MeV α-particle from ThC' was 7%.

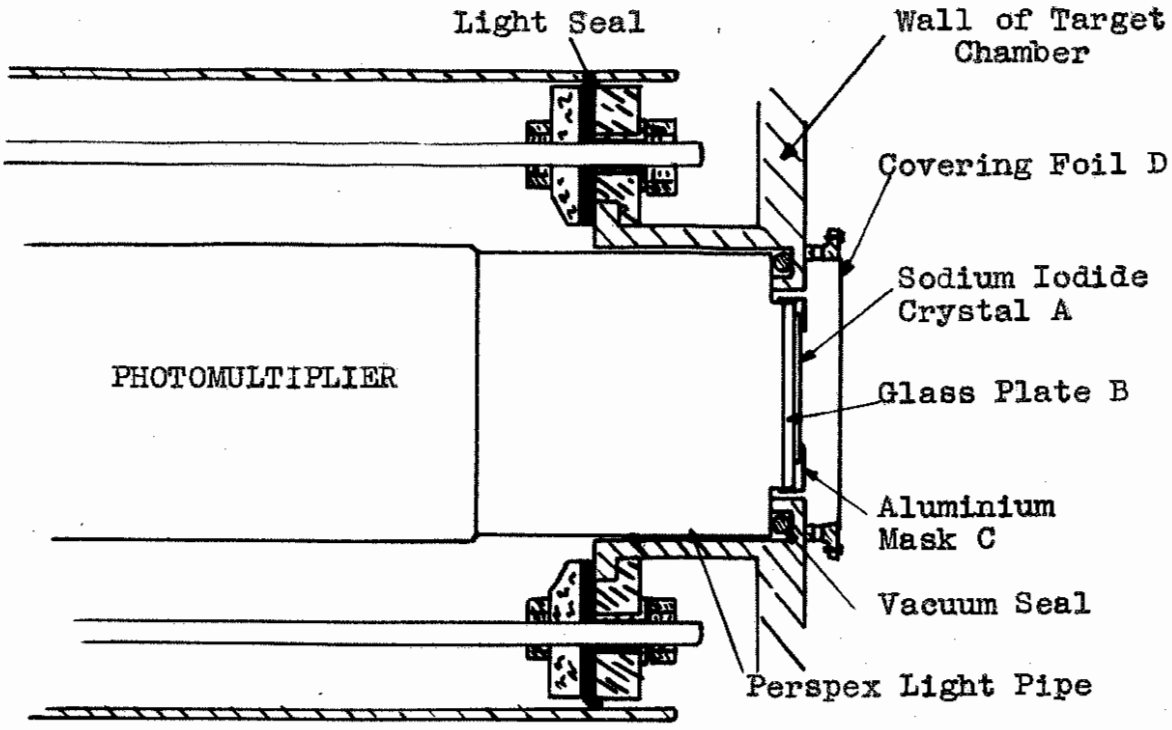

FIGURE 11. CONSTRUCTION OF NaI α-PARTICLE COUNTER.

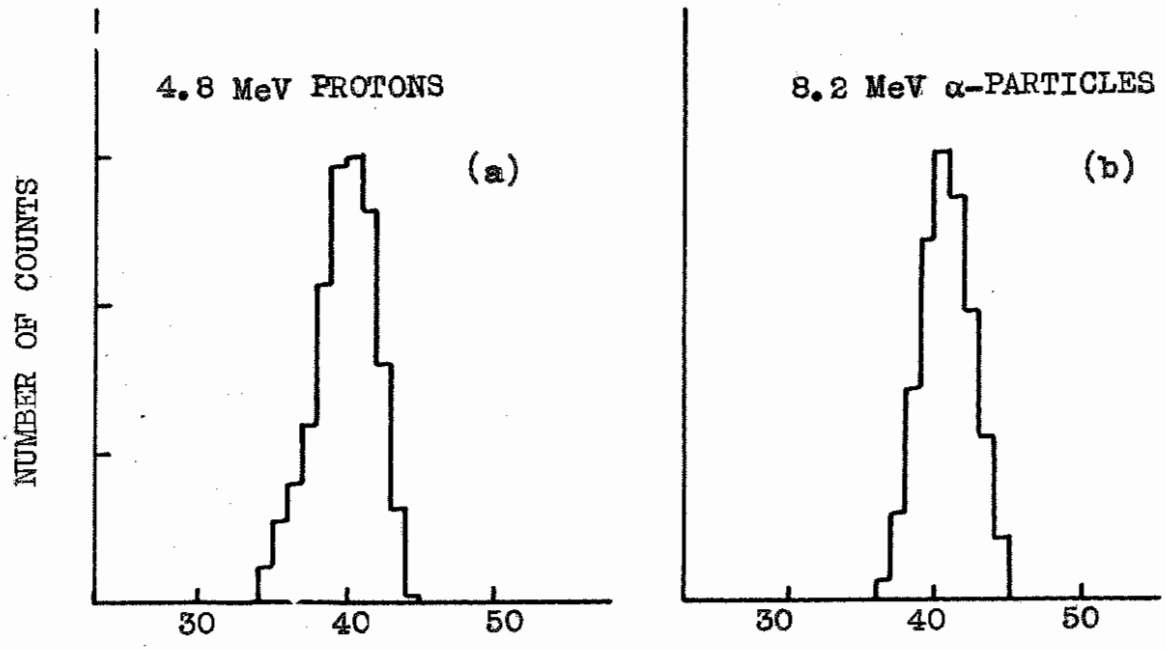

FIGURE 12. PULSE HEIGHT DISTRIBUTIONS FOR
(a) 4.8 MeV PROTONS (b) 8.2 MeV α-PARTICLES.

With a thin aluminium foil, 2mm. air equivalent, the pulse height was increased by a factor of 1.5 and the resolution improved to 6%. This was undoubtedly due to increased light collection.

The poor resolution compared to the expected figure of 2% was attributed at first to straggling effects in a thin surface layer of paraffin oil and hydrated sodium iodide. It was noticed that the surface of the crystal lost its polish and became slightly opaque when the chamber was first evacuated.

The technique of preparation and mounting was subsequently improved to eliminate this surface film. Wet polishing was avoided by cleaving the crystal in the dry box and then attaching it to the light pipe as described. The apparatus used for the experiments described in Chapter 5 enabled the crystal to be transferred from the dry box to its final position on the target chamber without exposing it to the air or to the vacuum until this was free of water vapour. In this way the freshly cleaved surface was preserved. The best resolution obtained under these conditions was 5.1/2% for 8.8 MeV α-particles.

The smallness of the improvement suggested that the poor resolution was not a result of surface straggling effects. This conclusion was checked by comparing the spectra of 8.3 MeV

α-particles and 4.8 MeV protons obtained with a slightly deteriorated crystal. These are shown together in Figure 12. Since the widths of the two distributions are roughly the same, surface straggling must be negligible as this would affect only the α-particle distribution.

Thus the resolution simply depends on the number of photoelectrons entering the multiplier and should be inversely proportional to the square root of the pulse height. This is confirmed by the results shown in Figure 13. which were derived from a series of pulse height spectra recorded for a range of α-particle energies. The poor resolution can only be attributed to inefficient light collection or to poor quality crystals. Surface deterioration of the crystals affects only the amount of light reaching the photocathode.

2.4. Discrimination of Gamma-Radiation.

In many applications, when an α-particle spectrum is to be recorded in the presence of z large gamma-ray flux, (e.g. in the $Li^7(p,\gamma\alpha)He^4$ experiment to be described in Chapter 4) the background of pulses resulting from the absorption

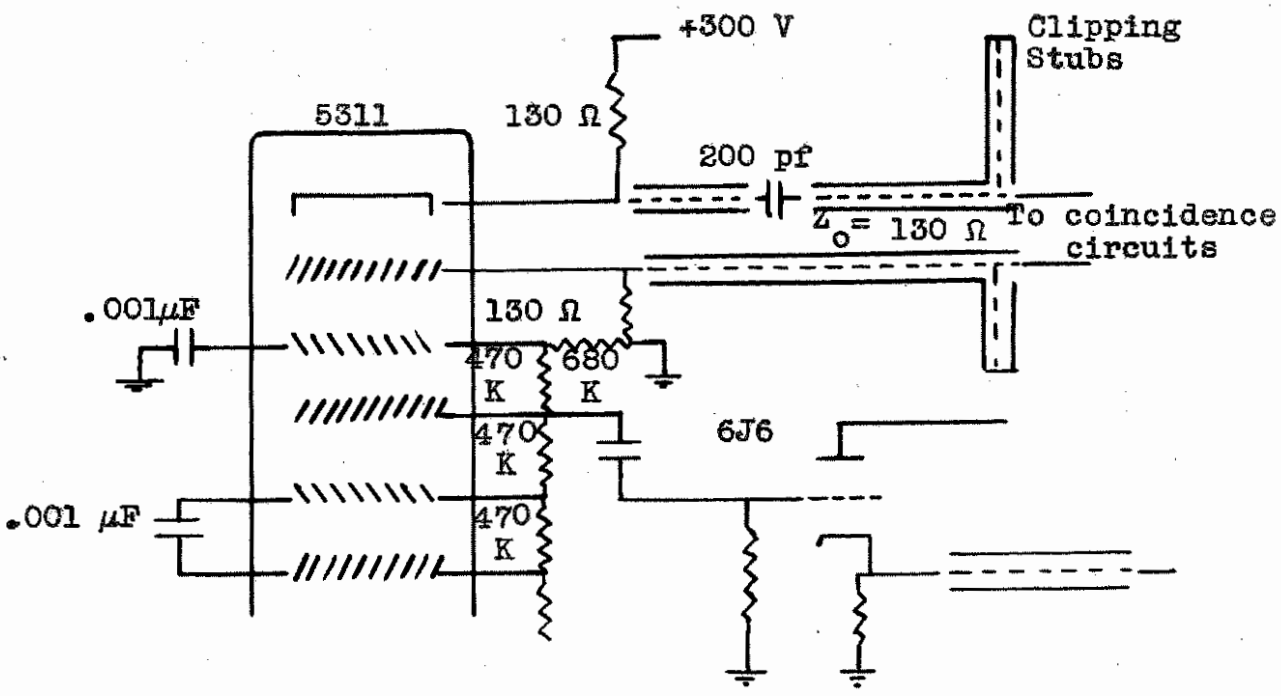

FIGURE 14. PHOTOMULTIPLIER CIRCUIT.

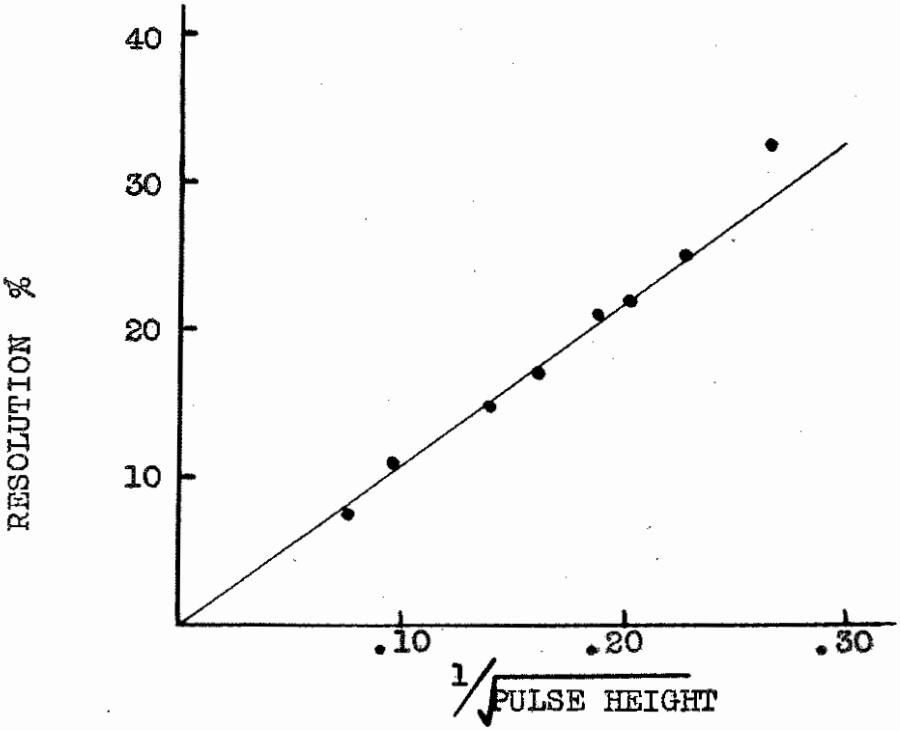

FIGURE 13. VERIFICATION OF STATISTICAL CHARACTERISTIC OF SCINTILLATION COUNTER.

of the gamma-radiation in the crystal is undesirable. With a crystal 1/16" thick the efficiency for gamma-ray detection is approximately 2% and the resultant pulse height distribution would extend over the range of α-particle energies up to about 3 MeV.

Cranberg[28] described a method by which the thickness of a sodium iodide crystal and hence the gamma-ray background can be reduced without affecting the response of the crystal to α-particles. Extending his method, it was possible to prepare crystals which were only .002" thick, which is sufficient to stop 17 MeV α-particles.

The perspex light pipe was placed in the chuck of a microtome and adjusted so that the glass surface was accurately parallel to the knife edge. A polished crystal, approximately 1/16" thick and 1" in diameter was then cemented to the glass face with araldite. Using a cut of 10μ, the thickness of the crystal was reduced to almost .002" (this being determined with a micrometer) and the final reduction was made with a cut of 1μ. The whole operation was carried out inside a dry box. The crystal was cleaned of shavings in paraffin oil and burnished with dried cleansing tissues.

The pulse height resolution of this crystal for

---

28. Cranberg, L. Rev. Sci. Instrum. 24: 328, 1953.

the 8.8 MeV α-particles from ThC' was 6%, which was identical to the value obtained with the thicker, polished crystal. Unfortunately, such a thin crystal deteriorated badly at the crystal-araldite surface after only one or two days under vacuum. Such crystals were used, therefore, only when insensitivity to gamma-radiation was essential.

It is obvious from the foregoing that on considerations of efficiency and linearity; and to a lesser extent, resolution and gamma-ray insensitivity, proportional counters are to be preferred to scintillation counters for α-particle detection. However, it is in the field of fast coincidence work that the scintillation counter is essential and this application is discussed in the following section.

2.5 Scintillation counters for use with fast coincidence Circuits.

It is often required to record coincidence events in the presence of an intense background of radiation from competing reactions. So that the number of chance coincidence events is small, the resolving time of the coincidence circuit must be short as possible. As discussed in section 2.1, the minimum resolving time obtainable with a gas counter

is about 1 μsec., whereas with scintillation counters, resolving time as short as 5×10^{-9} sec. can be achieved.

The time resolution of a scintillation counter is limited by two factors. These are the statistical variation in, firstly, the time taken for the photons produced in the crystal to release from the photo-cathode the number of electrons required to operate the coincidence circuit and, secondly, the time of arrival at the output, of the secondary electrons resulting from these primary electrons. As the incident radiation loses energy in the crystal, the intensity of the emitted light, I, rises to a maximum, I_o. This rise time is simply the time taken for the ionizing particle to come to rest, and since this is of the order of 10^{-11} sec. any variation in it can be ignored. From a maximum the intensity decays exponentially with the form $I = I_o e^{-t/\alpha}$, where α is the decay constant. If the total integrated light intensity (i.e. number of photons) from the event is denoted by L then $I_o = L/\alpha$. L depends on the energy lost in the crystal by the incoming radiation and the luminescent conversion efficiency of the phosphor which, in turn, depends on the type of radiation. If δ is the fraction of photons that reach the photocathode and K is the photoelectric conversion efficiency of the

photocathode, then the mean square deviation in time for the release of n electrons is $\frac{\alpha^2 n}{\delta^2 L^2 K^2}$.

The contribution from straggling effects in the multiplier can be expressed[29] by $\langle t^2 \rangle = \frac{\beta^2}{n}$ where β is the time dispersion introduced at each stage of multiplication. Assuming these two effects are additive then $\langle t^2 \rangle = \frac{\alpha^2 n}{\delta^2 L^2 K^2} + \frac{\beta^2}{n}$.

For the EMI type tubes used in these experiments β was approximately 4×10^{-9} sec.[30].

Some values of L and α are shown in Table 2. These are based on information given by Birks[27].

TABLE 2

L= No. of photons produced in Phosphor.

Phosphor	For 1 MeV Electron	For 2 MeV α-Particle	Decay constant $\alpha \times 10^9$ sec.
Anthracene	1.3×10^4	1×10^3	30
Stilbene	7.8×10^3	6.5×10^2	8
NaI (Tl)	2.6×10^4	1.2×10^4	250
NE 101[31]	$71. \times 10^3$	5×10^2	4

Typical values of the product δK can be obtained from estimates of the number of photoelectrons

29. Morton, G.A., Nucleonics, 10. No.3: 39, 1952.

30. Sommer, A., and Turk, W.E., J.Sci.Inst. 27: 113, 1950.

31. NE101 is a plastic scintillator produced by Nuclear Enterprises Ltd.

entering the multiplier in actual experimental arrangements. For a gamma-ray counter, this is roughly 500 photoelectrons/MeV, which gives $\delta K = .02$. For a typical α-counter, with a resolution of 6% for the 8.8 MeV ThC' α-particles, the corresponding value of δK is .003. Approximate values of $\frac{\alpha}{\delta LK}$ are given in Table 3, for three types of radiation.

TABLE 3

Phosphor	$\frac{\alpha}{\delta LK}$		
	15 MeV gamma-ray	2 MeV α-particle	100 MeV x-ray
Anthracene		9×10^{-9}	
Stilbene		4×10^{-9}	
NaI (Tl)	3×10^{-11}	7×10^{-9}	5×10^{-9}
NE 101			3×10^{-10}

For experiments involving 2 MeV α-particles, these approximate figures suggest that if the resolving time is to be kept in the region of 6×10^{-9} sec., then the coincidence circuit must be operated by one electron from the photocathode, almost irrespective of the phosphor used as the α-particle detector. Since the average measured capacity at the collector of the photomultiplier tubes used in later experiments was 15 pf, and

approximately 2 volts were required to operate the coincidence circuit, a gain of 2×10^{8} was therefore necessary in the multiplier. This was achieved with a voltage per stage of 220 volts and with 300 volts between the 11^{th} dynode and the collector. Under these conditions the current at the last few dynodes was limited to about 30 ma, by reason of the space charge effect[32], and the peak current at the 11^{th} dynode was determined solely by the collector voltage. With stilbene as the detector, the output pulse rose linearly to 1.2V in 3.3×10^{-9} sec. and reached a maximum of 1.8 V in 5×10^{-9} sec.

The fast coincidence circuit used for the experiments was similar to that described by Bay[33] and did not require pulses of accurately constant amplitude. The limiting achieved in the multiplier was sufficient. It was only necessary to clip the pulses to 6×10^{-9} sec. with a shorted transmission line. Portion of the photomultiplier circuit is shown in Figure 14. Pulses proportional to the energy dissipated in the crystal were obtained from the 9^{th} dynode where apace charge limiting effects were negligible.

---

32. Raffle, J.F., and Robbins, E.J., Proc. Phys. Soc. B65: 320, 1952.

33. Bay, Z., Rev. Sci. Inst. 22: 397, 1951.

Two limited outputs were required from each multiplier since two coincidence circuits were used in some of the experiments. One recorded the true plus chance coincidence events and the other, with one input pulse delayed artifically, only the chance events.

The figures in Table 3. suggest that for the detection of α-particles, stilbene is slightly preferable when short resolving times are essential. In experiments where it is necessary to have the best possible energy resolution in addition to good time resolution, sodium iodide is to be preferred to all other phosphors. Although cesium iodide is more convenient to handle and gives energy resolution approaching that of sodium iodide, its long decay time of more than 1 μsec. limits its use in fast coincidence work.

SECTION B

ENERGY LEVELS OF Be^8.

CHAPTER 3

THEORETICAL CONSIDERATIONS AND PREVIOUS EXPERIMENTAL EVIDENCE

The first theoretical approach to the problem of describing the energy level schemes of light nuclei was made in terms of the central model[34]. This is analogous to the Hartree model which had been applied successfully in the case of atomic phenomena. In the nuclear case it is assumed that the interaction of a single nucleon with the rest of the nucleus can be represented by an average central field.

On the basis of the central model, and on the assumption of LS coupling, several workers[35,36] have derived values for the spacings of the low lying levels in the nuclei between He^4 and O^{16}.

On this scheme the first three levels of Be^8 arising from the lowest configuration, $(1s)^4(1p)^4$ are the ^1S, ^1D and ^1G levels. The ratio of the spacing $(^1G - ^1S)$ to that of $(^1D - ^1S)$ was found

---

34. Wigner,E., Phys.Rev. 51: 106, 1937.

35. Freenberg,E., znd Wigner,E. Phys.Rev. 51: 95, 1937.

36. Feenberg,E., and Phillips,M. Phys.Rev. 51: 597, 1937.

to be 10 : 3 [36], and from estimates of the range and depth of the potential, the spacing ($^1D - {}^1S$) was calculated to be approximately 3 MeV.

At the time, the only information regarding the level structure of Be^8 came from the $B^{11}(p,\alpha)Be^8$ reaction and from the β decay of Li^8. Both of these reactions indicated a broad level in Be^8 at about 3 MeV. No evidence existed for a level at 10 MeV, and there was no information concerning the spin of the 3 MeV level. Since, however, this level decayed by emission of an α-particle, its parity must be even.

Wheeler [37] later found that the apparently anomolous results obtained in α-α scattering experiments of several workers [38,39] could be interpreted in terms of a broad (0.8 MeV) level at 3 MeV in the compound nucleus Be^8. However, a description of the Be^8 nucleus in terms of a central potential implies that, on the average, any group of nucleons does not retain its identity during the life time of the compound nucleus Be^8.

---

37. Wheeler, J.A., Phys.Rev. 59: 16, 1941.

38. Mohr, C.B.O., and Pringle, G.B., Proc.Roy.Soc. A160: 193, 1939.

39. Devons, S., Proc.Roy.Soc. A172: 564, 1939.

Therefore, since an α-particle must be reformed before it can be emitted, states derived from this assumption must be long lived and consequently very narrow.

Wheeler [40,41] suggested that at low energies, light nuclei spend a large part of their time in resonating particle groups. In the case of Be^8 these groups would be α-particles. The ground state of Be^8 is unstable by only 100 KeV against dissociation into two α-particles and since the binding energy of an α-particle is 28 MeV, a description of the Be^8 nucleus in terms of two α-particles seemed plausible. A weak interaction between the α-particles would be sufficient to give the nucleus a short life. The α-particle model does not imply permanent groups of the same nucleons, but only that the life of one particular grouping is longer than the period of rotation of the nucleus.

On the assumption of a simple harmonic interaction between the α-particles, the Be^8 nucleus would resemble a diatomic molecule and would therefore possess rotational and vibrational levels. Wheeler

---

40. Wheeler, J.A., Phys.Rev. 52: 1088, 1107, 1937.

41. Wheeler, J.A., and Teller, E., Phys.Rev. 53: 778, 1938.

stated however, that owing to the stability of Be^8 only the lowest vibrational level could have a life long enough to be observable, and also that rotational levels above J=4 would be too much widened by dissociation to be observed.

On an analogy with the molecular case, the energy values of the rotational levels would then be given by $E_J = \frac{\hbar^2}{2I_o} J(J+1)$, where J is the rotational quantum number and I_o is the moment of inertia of the nucleus. Since α-particles obey Bose statistics only even values of J are permitted. The first three levels are thus J = 0, 2 and 4 and the ratio $E_4 : E_2$ is 10:3, as was also found for the central model and LS coupling. The essential difference between the results of these two approaches lies in the breadth of the levels.

Haefner[42] has also applied the α-particle model to Be^8. He chose a potential which represents a strongly repulsive force for very small distance between the particles, an attractive force for intermediate ranges and the coulomb force beyond the range of nuclear forces. With a radius of Be^8 of 5.1×10^{-13} cm., this gives a value of

---

42. Haefner, R.R., Rev.Mod.Phys. 23: 228, 1951.

2.9 MeV for the energy of the D state, and if extended to higher energies predicts a G state at 10 MeV.

After the success of the jj coupling version of the central model in the region of heavy nuclei, attempts were made to extend the method to light nuclei. For Be^8 the configuration would be $(1s_{1/2})^4 (1p_{3/2})^4$ for the low lying levels. This also gives rise to states with J = 0,2,4 in that order. Kurath,[43] using Wheeler's results for the specific nuclear interaction and estimating the magnitude of the spin - orbit coupling, again finds a value of approximately 10:3 for the ratio of $E_4 : E_2$.

Since in the region of the p shell neither pure LS coupling or pure jj coupling could predict the positions and properties of all the energy levels, Inglis[44] attempted a description of these nuclei in terms of an intermediate coupling model analogous to that used to describe the Paschen-Back effect in the atomic case. In the case of Be^8 the order of the low lying levels is not altered and Inglis by choosing the energy scale to fit the first T = 1 state (which was then known[45] to occur

---

43. Kurath,

44. Inglis, D.R., Rev. Mod. Phys. 25: 412, 1953.

45. Wilkins, J.J., and Goward, F.K., Proc. Phys. Soc. 64A: 1056, 1951.

at 16.9 MeV) found the positions of the S, D and G levels, values of 0, 3 and 10 MeV.

The fact that the level found experimentally at approximately 3 MeV was very broad, suggested to Inglis that this level was probably a mixture of central model and α-model wave functions, since such a state of the α-model is above the coulomb + centrifugal barrier and would be expected to be extremely short lived and probably too broad to be recognized as a level at all. It is reasonable to assume also that since the next rotational state is a G state there would also be an admixture of this state with that derived on the central model.

From the foregoing it is evident that irrespective of the model chosen to represent the Be^8 nucleus only two excited levels are predicted below an energy of approximately 10 MeV. Green and Gibson[46], examining the spectrum of neutrons from the $Li^7(d,n)Be^8$ reaction, with photographic plates, found groups corresponding not only to the ground state and the level at approximately 3 MeV, but also suggested that groups also existed corresponding to states at 4.0 and 4.9 MeV. The statistical accuracy of this experiment was rather

---

46. Green, L.L., and Gibson, W.M., Proc. Phys. Soc. 62: 407, 1949.

poor in that only 70 counts were recorded at the 2.9 MeV peak. The levels claimed at 4.0 and 4.9 MeV had a width of approximately 0.5 MeV and an intensity of approximately 10% of the broad group at 2.8 MeV. Trumpy et al[47] also using this reaction reported levels at 2.2, 2.9, 4.1, and 5.0 MeV. The level at 4.1 had a width of 0.5 MeV and an intensity of approximately 20% that of the 2.9 MeV group. Sixty five events were recorded at the 2.9 MeV peak.

Brinkworth and Titterton[48] using the $B^{10}(\gamma,\alpha)Be^{8}$ reaction found events with photographic plates corresponding to levels in Be^{8} at 4.1, 7.5 and 9.8 MeV. Calcraft and Titterton[49], using the reaction $B^{11}(\gamma,t)Be^{8}$, again found events corresponding to a level at 4.1, and also to one at 5.5 MeV. In these experiments only six events were recorded in each case at the peak corresponding to the 3 MeV level. Erdös et al[50] also using these reactions, and Glattli and Stoll[51]

---

47. Trumpy, Grotdal and Graue, Nature 170: 1118, 1952.

48. Brinkworth, M.J., and Herton, E.W., Phil. Mag. 42: 952, 1951.

49. Calcraft, M.E., and Titterton, E.W., Phil. Mag. 42: 666, 1951.

50. Erdös, P, Scherrer, P, and Stoll. P., Helva. Phys. Acta. 26: 207, 1953.

51. Glattli, H., and Stoll, P., Helv. Phys. Acta. 26: 428, 1953.

using the $B^{11}(p,\alpha)Be^{8}$ reaction, have both reported levels in Be^{8} at 2.2, 2.9, 3.4, 4.0, 4.9, 6.8 MeV. In each case the number of events was very small, thirty at the 2.9 MeV peak.

The well-known level of Be^{8} at 17.63 MeV, which will be discussed later in Chapter 6, is formed by the resonance capture of 441 KeV protons in Li^{7} and decays by gamma-ray emission.

The gamma-ray spectrum was examined by Walker and McDaniel with a magnetic pair spectrometer and groups were found at 17.6 and 14.8 MeV corresponding to transitions to the ground state and to a level at 3 MeV. Several workers examined the photodisintegration of C^{12} [52,53] and Li^{7} [54], produced by this radiation and have reported evidence of a component in the gamma-ray spectrum at approximately 12.5 MeV with an intensity of about 10% that of the 17.6 MeV component. In all cases the number of events observed were small. Such a group would not have been observed by Walker and McDaniel as the efficiency of their spectrometer decreased rapidly with energy.

---

52. Nabholz,H., Stoll,P., and Waffler,H. Phys.Rev. 82: 963, 1951.

53. Goward,F.K., and Wilkins,J.J., A.E.R.E. G/M.127:

54. Titterton,E.W., Aust.J.Sci. 15: 174, 1953.

From the results of α-α scattering experiments, Steigert and Sampson[55] have proposed the existence of an S level at 7.5 MeV and a broad G level at 10.8 MeV. This was the first definite evidence for the existence of the expected G state at this energy.

All these experimental results suggested that besides the ground state and the broad levels at about 3 MeV and 10 MeV, there also existed in Be^8 levels at approximately 2.2, 3.4, 4.0, 5.5 MeV and 7.5 MeV. None of these levels can be explained by either the α-particle model or the independent particle model as they have been described above.

Inglis[44] has discussed the possibility that the state at 5.5 MeV could arise from the jj model excitation from $p_{3/2} \rightarrow d_{5/2}$. However, this configuration would imply odd parity for this state and as it has been observed in transitions involving the break-up of Be^8 into two α-particles, this explanation would not be plausible.

In an attempt to explain their results, Erdös et al[50] proposed a rotation-vibration scheme of the α-particle model of Be^8. The energy values are given by an expression of the form

$$E_{J,K} = A.J(J + 1) + BK$$

---

55. Steigert, F.B., and Sampson, M.B., Phys.Rev. 92: 660, 1953.

where J and K are the rotational and vibrational quantum numbers respectively and A and B were chosen to fit the experimental results. However, no assignment of A and B is successful in explaining all the levels. As mentioned above, levels predicted by an α-particle model alone would be expected to be very broad because of the low barrier against break-up into two α-particles. Since none of the experimentally observed levels has a width greater than about 0.5 MeV an interpretation in terms of an α-particle model therefore seems doubtful.

Since the statistical uncertainties in most of the experimental data were very great and because the level at 3 MeV was expected to be very broad, more accurate knowledge was required to confirm the existence of these other levels. The succeeding chapters describe some attempts to provide this information.

CHAPTER 4

THE ALPHA-PARTICLE SPECTRUM FROM THE REACTION $Li^7(p,\gamma)Be^8(\alpha)He^4$.

4.1. Introduction.

As mentioned in Chapter 3, the gamma-ray spectrum from this reaction has been examined by Walker and McDaniel using a magnetic pair spectrometer and by other workers using the gamma-radiation for photodisintegration studies.

Attempts to examine the spectrum with a sodium iodide scintillation counter with the crystal sizes available at the time proved fruitless for the reasons outlined in Chapter 1.

The α-particle spectrum from this reaction has been examined up to 2.2 MeV by Burcham and Freeman[56] using a magnetic spectrometer and their results showed only a broad α-particle group corresponding to the 3 MeV level in Be^8 apart from the narrow ground state group. In this experiment the direction of the gamma-ray was not defined and consequently the energy of the α-particles resulting from the break-up of Be^8 with a fixed energy was not homogeneous, but

---

56. Burcham, W.E., and Freeman, J.M., Phil.Mag. 41: 921, 1950.

was spread by the Doppler effect of the recoiling Be^8 nucleus. This introduces a spread of approximately $\pm$ 0.2 MeV in the α-particle energy which might be sufficient to obscure any low intensity lines in the α-particle spectrum.

The direction of gamma-ray emission could be defined by detecting the gamma-rays at a fixed angle to the α-particle detector and measuring the α-particle energy only when a coincidence event was recorded between the two counters. This method has the added advantage of preventing the detection of the products of any competing reactions, such as $Li^7(p,\alpha)He^4$ and $Li^6(p,He^3)He^4$.

Since the yield from these reactions is very great, it was necessary to make the resolving time of the coincidence circuit as short as possible to reduce the number of random coincidences. The advantages of scintillation counters for such work have been mentioned in Chapter 2, and it was decided to use these for the present experiments.

Since the technique of preparing thin sodium iodide crystals had not been developed at this stage, thin evaporated layers of stilbene were used for the α-particle detectors in the experiment to be described in the first part of this chapter. As the pulse height resolution obtainable with such a detector was very poor,

an alternative means of energy discrimination was used. Absorber foils of various thicknesses were used to define the α-particle energy and the stilbene was used simply as a detector. In this way an integral spectrum of the α-particle energies was obtained.

In the later sections of the Chapter similar experiments are described using thin sodium iodide crystals in place of the stilbene screens. Since reasonable resolution was possible with sodium iodide, the differential spectrum of α-particle energies could be obtained directly.

In these ways it was possible to examine the α-particle spectrum over a wider range of energies than had been done by Burcham and Freeman.

PART A. INTEGRATED SPECTRUM WITH STILBENE.

4.2. Apparatus.

The target chamber and counters were arranged as shown to scale in Figure 15. The target chamber itself was a brass tube 2" in diameter. The α-particles were detected by a scintillation counter in which the scintillator was a layer of stilbene, 6 mg/cm^2 thick, evaporated on to a glass slide. This was attached to the end window of the photomultiplier tube which itself formed the vacuum wall across the tube B. Aluminium foil of 1 mgm/cm^2 prevented light from the target and low energy radiation from entering the crystal. The solid angle of acceptance of the counter was $4\pi/138$ sterad, the crystal being 4.4 cm. from the centre of the target. This introduced a spread of less than 100 KeV in the energy of the α-particles.

The scintillator in the gamma-ray counter was a sodium iodide crystal 1 cm. thick by 2 cm. square placed with its centre 4 cm. from the target in the plane of the beam and the α-counter. Aluminium absorber foils of graded thickness were mounted on frames D, supported from the two plungers A and C, which could move into the end of the target chamber through Wilson seals. These foils could be interposed between the target and the α-counter,

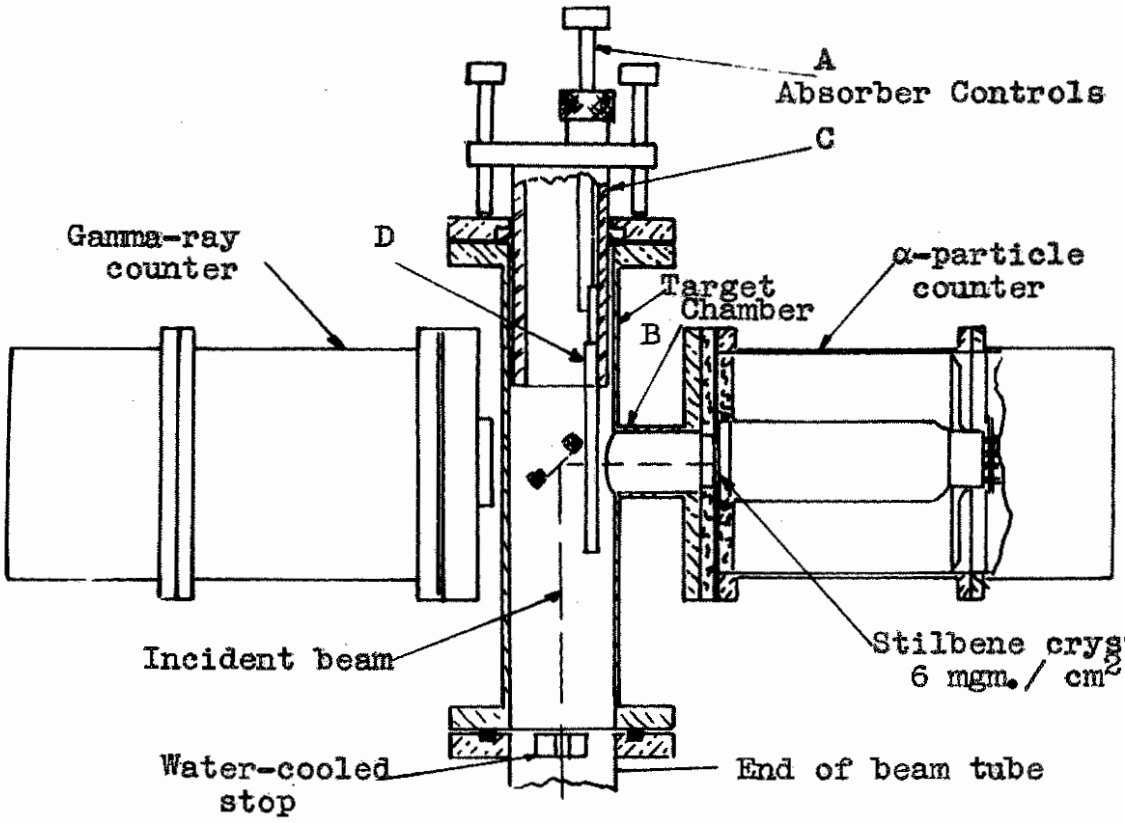

FIGURE 15. ARRANGEMENT OF TARGET CHAMBER AND COUNTERS.

so that the air equivalent of the total thickness of absorber between the target and counter could be varied from 0.66 cm. to 7 cm. in steps of about 0.1 cm. The straggling in energy introduced by 1 cm. air equivalent of aluminium is approximately 100 KeV.

A block diagram of the recording equipment is shown in Figure 16. Details of the photomultiplier circuits have been given above. The pulse amplitude selector and triple coincidence unit were included so that coincidences could be recorded only when the pulse heights proportional to the energy of the coincident events were greater than a preset value or between preset limits.

4.3. Experiment.

Separated Li^7 targets of 350 $\mu g/cm^2$ superficial weight deposited on a silver backing were bombarded with protons from a 1 MeV Phillips generator. Separated targets were desirable to eliminate the $Li^6(p,\alpha)He^3$ reaction which gives α-particles of 1.7 MeV and He^3 nuclei of 2.3 MeV. Although these would be detected only as chance coincidences the large yield of this reaction from natural lithium targets would introduce some uncertainties in interpretation.

The gamma-ray yield per microcoulomb of charge on

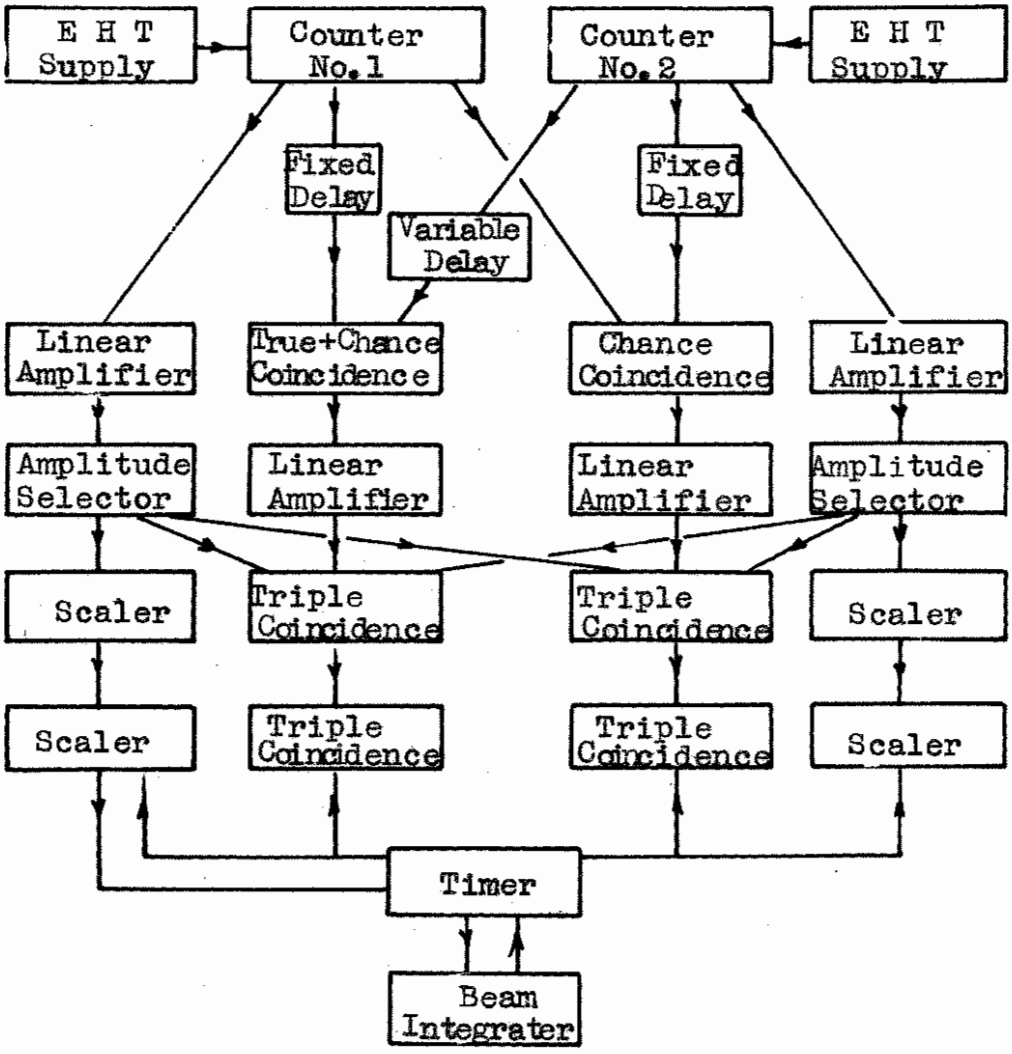

FIGURE 16. BLOCK DIAGRAM OF THE RECORDING UNITS.

on the target is shown in Figure 17. as a function of proton beam energy. Also shown is the variation of the coincidence rate with beam energy. Both curves show the expected resonance at 441 KeV. A proton energy of 450 KeV was used in all the runs with thick targets.

In early runs with thin, 20 KeV targets on copper backing and with protons of 440 KeV, the α-particle detector blocked with beam currents greater than a few microamps. This was attributed to the L X-rays and scattered protons from the target backing. Even with the thick targets, a minimum absorber of 1.4 mgm/cm^2 was required between the target and crystal to prevent excessive currents in the photomultiplier tube. The number of small pulses was still considerable as can be seen from Figure 18., which shows the pulse height distribution of pulses in the α-particle counter. The peak at 380 volts is formed by the 9 MeV α-particles from the $Li^7(p,\alpha)He^4$ reaction. The histogram in Figure 18. represents the coincidence counts associated with α-particles of corresponding amplitude. Chance coincidences contributed most of the counts above 300 volts and some of those below 50 volts, but it is evident that the majority of coincidence events were associated with the small number of α-particle pulses between 50 and 250 volts.

For the experiment, the discriminator in the α-counter

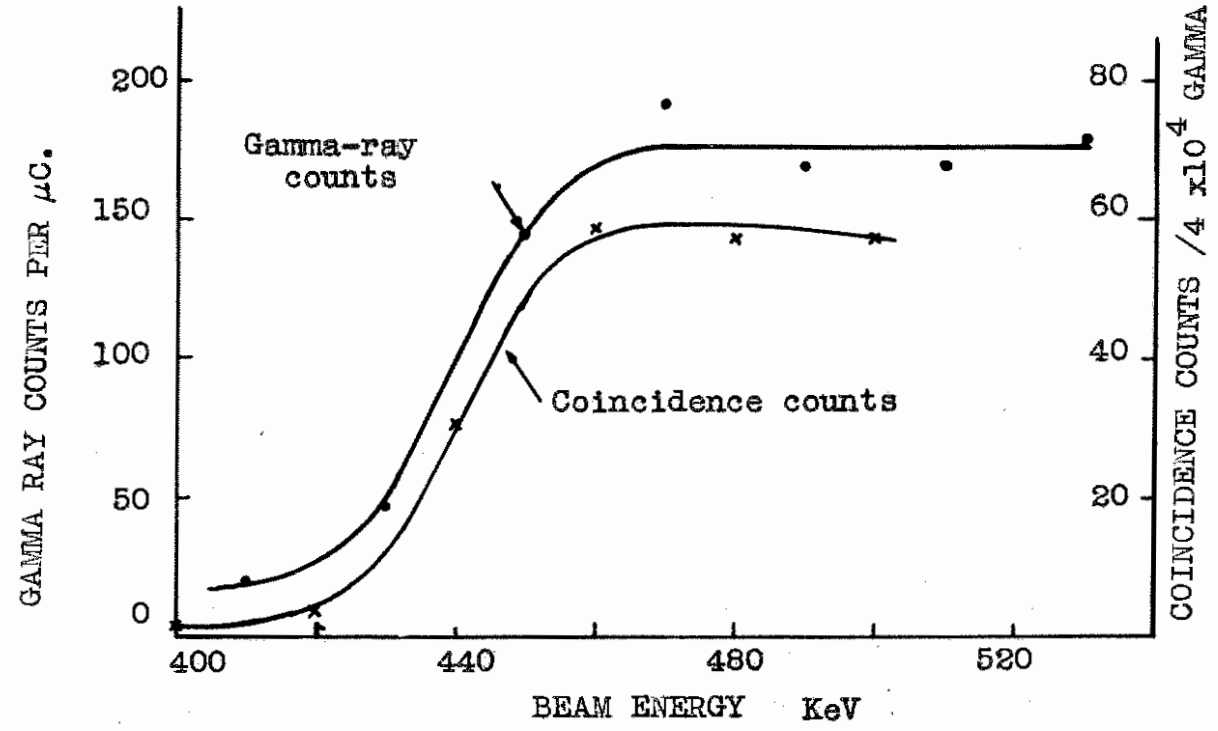

FIGURE 17. VARIATION OF GAMMA-RAY YIELD AND COINCIDENCE RATE WITH BEAM ENERGY.

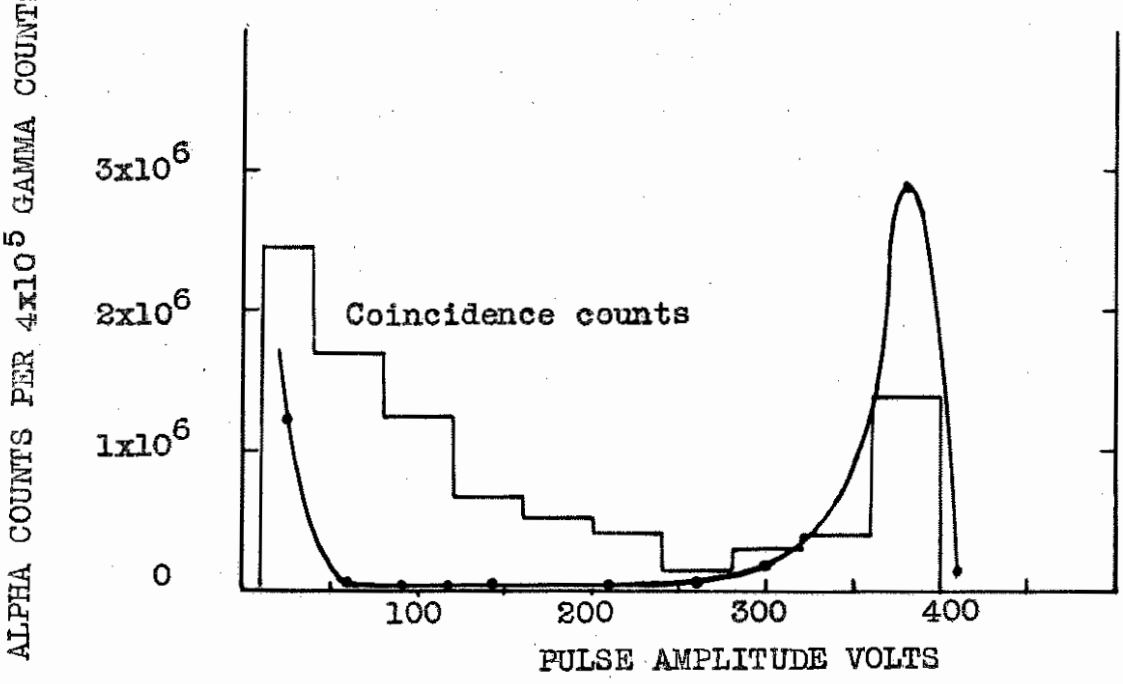

FIGURE 18. ALPHA PARTICLE SPECTRUM AND HISTOGRAM OF THE COINCIDENCE COUNTS.

was set at 25 volts so as to reject these small pulses and the timing unit was arranged to stop the scaling circuits after 10^5 gamma-ray counts had been recorded. The coincidence counts recorded in this interval are plotted in Figure 19. against a value for the equivalent range which includes the range in the crystal required to produce a pulse of sufficient amplitude to be detected. The calibration of this scale is described below.

It was necessary to check the balance of the fast coincidence circuit frequently, since a slight misbalance gave an output from a single large background pulse. In spite of the checks, however, there was a spread in the coincidence counts for any particular absorber. Counts were therefore taken for a sequence of absorbers and this was reversed and repeated several times. Each point on the curve is the average of four observations of 100 seconds duration, during which time 10^5 gamma-rays and some 1.5×10^6 α-particles were counted. Since the large majority of α-particles arise from the $Li^7(p,\alpha)He^4$ reaction and have a range of about 9 cm., the chance coincidence rate changed but little over the range of Figure 19. A slight rise at small ranges was due to the large numbers of low energy pulses.

The errors indicated on the points in Figure 19. represent the quantity $\frac{C}{\sqrt{N}}$ where C is the value plotted

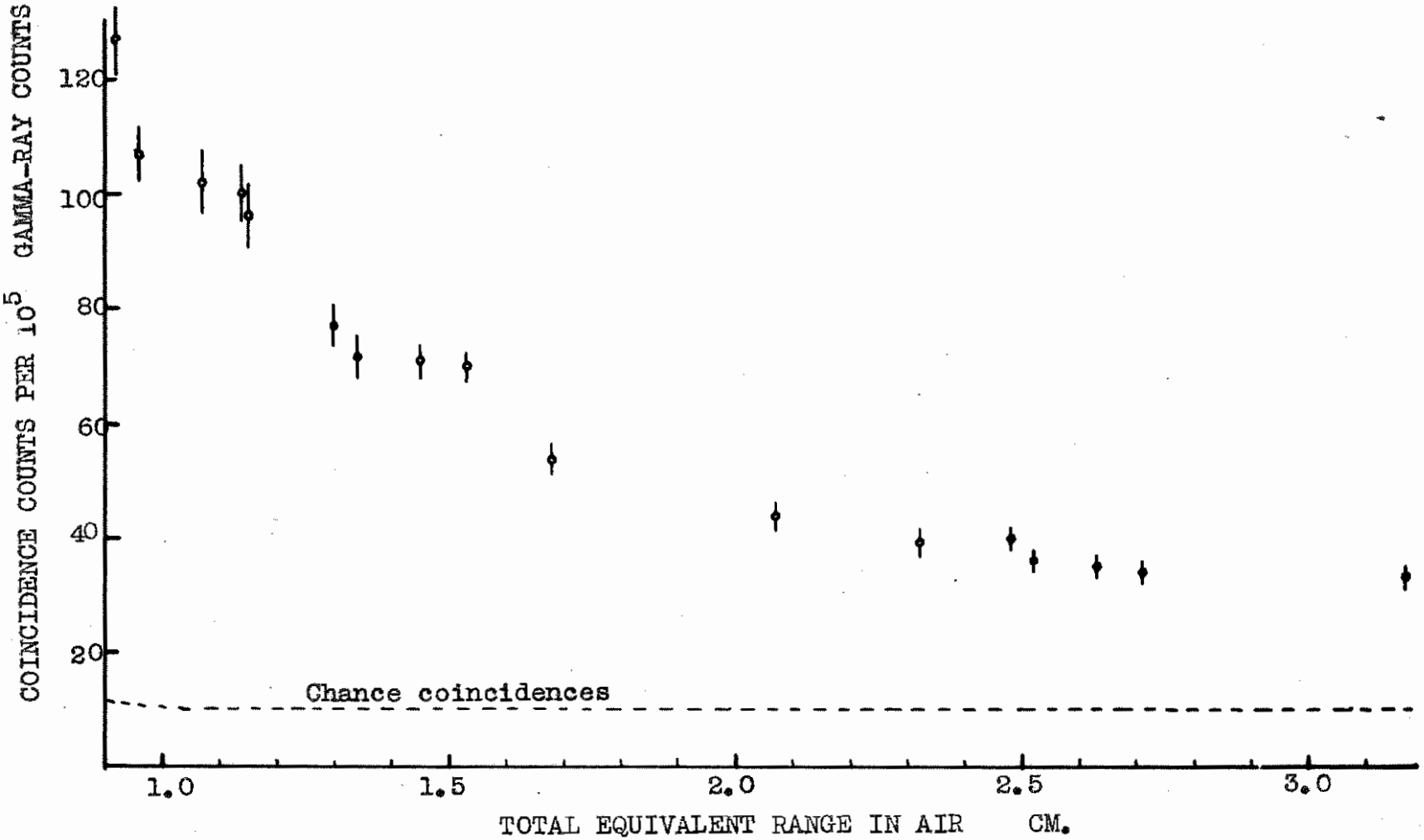

FIGURE 19. SHOWING THE RANGE OF THE α-PARTICLES DETECTED IN COINCIDENCE WITH A GAMMA RAY.

and N the total number of counts recorded. Snedecor's F test applied to the readings taken at each point showed that this standard deviation of the readings was slightly greater than that expected from a Poisson distribution. Further runs with slightly changed values of the bias levels showed the same general trend as that of Figure 19. but suggested that the uncertainty in the count at each point was greater than is indicated there.

4.4 Calibration of Absorbers.

The counter was set up on the bench as shown in Figure 20. and operated under the same conditions of high tension supply, amplifier gain and discriminator bias as had been used in the determination of the absorption curves.

The stopping power of the absorber foils was simply determined by the reduction in air range of the 5.3 MeV polonium α-particles caused by the insertion of the foils in the position shown. This could be measured to an accuracy of 0.01 cm.

The sum, R, of the equivalent range of the foil covering the stilbene crystal plus the residual range in the crystal necessary for detection, was also measured with this arrangement. The position of the polonium source was found for which detection of the

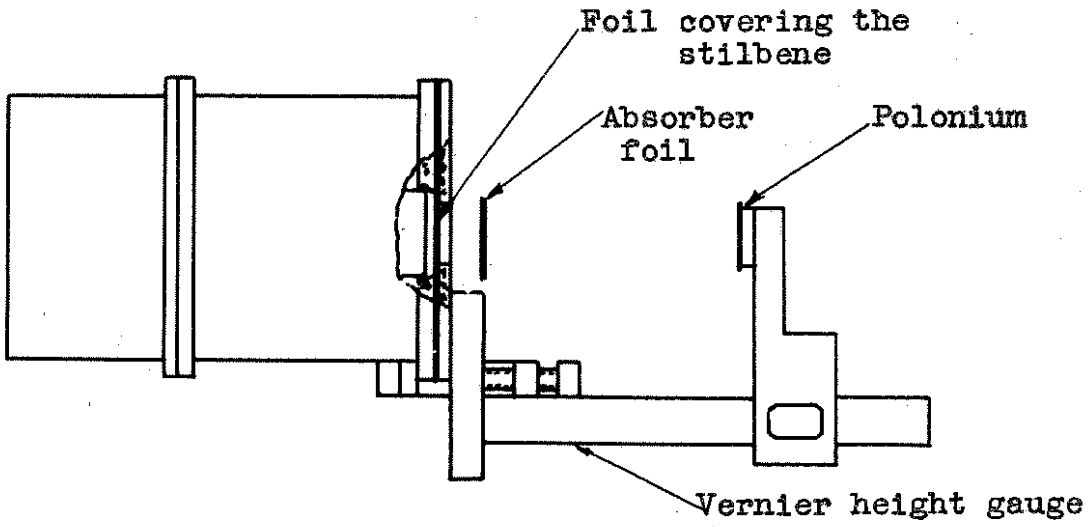

FIGURE 20. EXPERIMENTAL ARRANGEMENT FOR CALIBRATION OF FOILS.

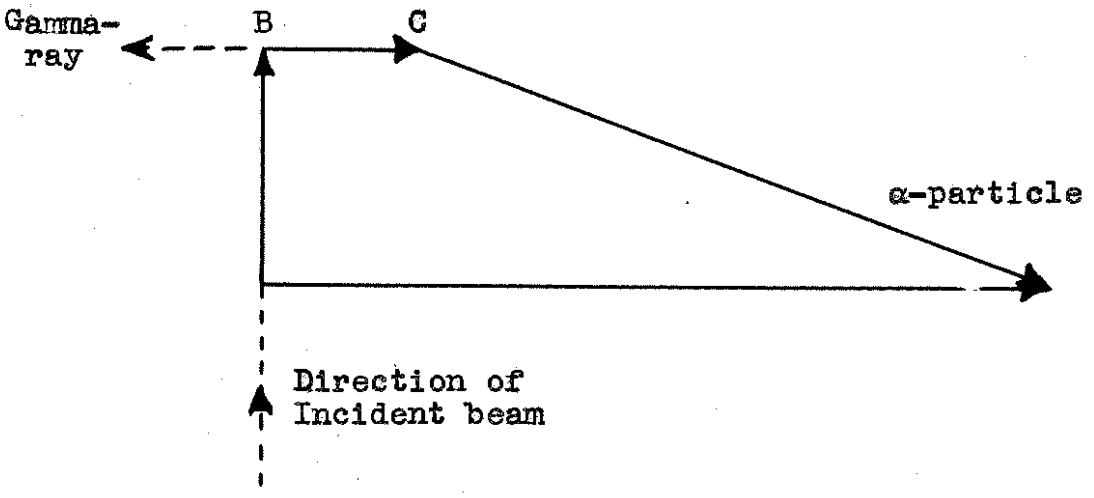

FIGURE 21. VELOCITY DIAGRAM.

α-particles just ceased. The difference between the length of the air path (corrected for temperature and pressure) from the source to the crystal and the known range, 3.8 cm., of the polonium α-particles, gave a value of R=0.8 ± 0.1 cm.

R could be determined more accurately from the energy of protons which were just detected after being scattered through the foils from a molybdenum target. Birks[57] has shown that the scintillation intensity produced by particles in stilbene depends only on the residual range of the particle in the phosphor. Thus, from the data of Warshaw[58] and Aron et al[59], R was found to be 0.76 ± 0.02 cm. This was an average value obtained by measuring the proton energies with several of the absorber foils.

4.5 Relation between the excitation energy of Be^8 and the energy of the disintegration α-particle.

The reaction investigated in these experiments was the following -

$$Li^7 + p \rightarrow Be^{8xx} \rightarrow Be^{8x} + \quad + Q_1 \quad \ldots\ldots\ldots\ldots (1)$$

$$Be^{8x} \rightarrow He^4 + He^4 + Q_2 \quad \ldots\ldots\ldots\ldots\ldots\ldots (2)$$

---

57. Birks, J.B., Proc. Phys. Soc. 64A: 874, 1951.

58. Warshaw, S.D., Phys. Rev. 76: 1759, 1949.

59. Aron, W.A., Hoffman, B.G. and Williams, F.C., A.E.C.U. 663, 1951.

When the excitation energy of the Be^8 nucleus above the ground state is E MeV,

$$Q_1 = (17.25 - E) \text{ MeV}$$

and $$Q_2 = (E + 0.10) \text{ MeV}$$

These Q values were obtained from data given by Ajzenberg and Lauritsen[60].

Since the lifetime of the 17.63 MeV level of Be^8, is about 10^{-19} sec.[61], the Be^8 nucleus is in motion when it disintegrates as shown in (2). This motion is due to the combined effect of the momentum of the incident proton, plus the recoil from the emitted gamma-ray. Since in this experiment the gamma-ray was detected in the opposite direction to the α-particle, the resultant motion of the nuclei which produced coincidence counts was uniquely determined.

Figure 21. is the velocity diagram of the reactions (1) and (2) when the α-particle is detected at 90° to the direction of the beam and at 180° to the direction of emission of the associated gamma-ray. AB represents the velocity of the centre of mass of the system and, since the energy of the bombarding protons was 450 KeV, is proportional to $\frac{1}{8}\sqrt{0.90}$. The recoil velocity of the Be^{8x} nucleus resulting from the

---

60. Ajzenberg,F., and Lauritsen,T., Rev.Mod. Phys. 27: 77, 1955.

61. Devons,S. and Hine,M.G.N., Proc.Phys.Soc. A199: 56, 1949.

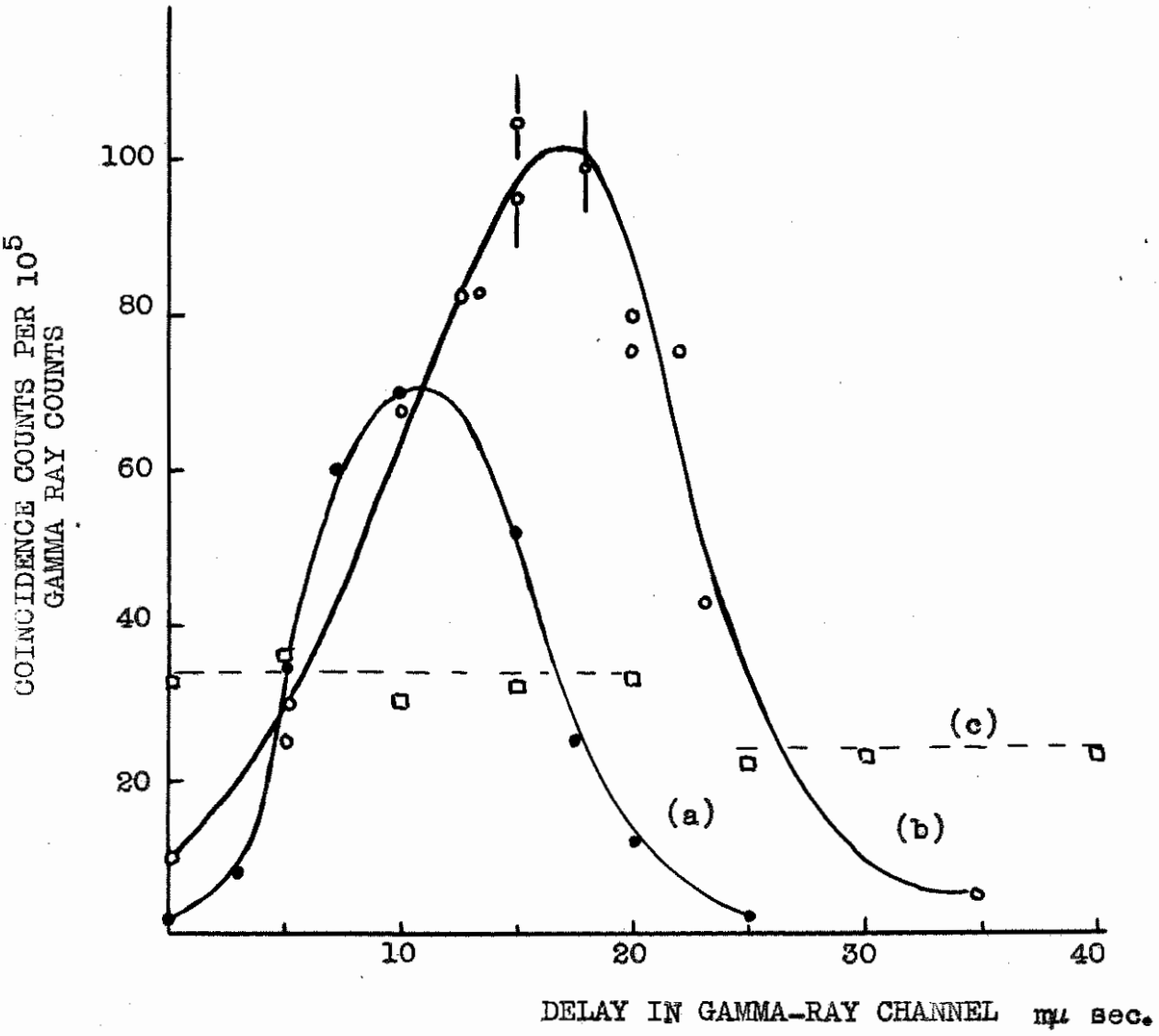

FIGURE 22. VARIATION OF COINCIDENCE COUNTING RATE WITH DELAY BETWEEN CHANNELS.

emission of the gamma-ray is represented by BC. Since the energy of the emitted gamma-ray is (17.64-E) MeV, then BC is proportional to $\frac{1}{8} \cdot \frac{1}{\sqrt{931}} (17.64-E)$.

CD is the velocity of the α-particle in the centre of mass system of Be^{8x} and is given by $\frac{1}{2}(E+0.10)^{1/2}$. The velocity of the α-particle in the laboratory system is therefore given by AD which corresponds to an energy of

$$2\left\{\left(\frac{E+0.10}{4} - \frac{0.90}{64}\right)^{1/2} + \frac{1}{8\sqrt{931}}(17.64-E)\right\}^2 \text{ MeV.}$$

The scale of the abscissa in Figure 19. can now be converted to give the excitation energy of the Be^8 nucleus. This has been done in Figure 23. where also only true coincidences are plotted, the chance coincidences having been subtracted. The range-energy relations of Aron et al were used to give the energy of the α-particle leaving the target and a correction was applied for loss of energy in the target. For a bombarding energy of 450 KeV most of the Be^8 nuclei were formed during the first 20 KeV loss in the target, which was placed at 45° to the beam. Since the energy loss of α-particles at these energies is approximately three times that of protons in the same distance, the average energy loss of the α-particles in passing through the target was 30 KeV.

4.6 Operation of the fast coincidence circuit.

Because such a small fraction of the counts in each

of the detectors was registered as coincident events, it was necessary to ensure that these could not have been produced by faulty operation of the coincidence circuits.

Figure 22. shows the results of three tests which were applied. The coincidence rate is plotted against the delay produced by extra cables inserted in the gamma-counter channel.

Curve (a) was obtained with a Co^{60} source placed between the counters and gives a value for the delay caused by the cable used in the α-channel being longer than that used in the gamma-channel, namely 11 mμs.

Curve (b) was obtained for the gamma-rays and α-particles from the reaction under study. The 5 mμs. displacement of the peak of (b) with respect to (a) compares well with the value 4.4 mμs calculated as the time required by a 2.5 MeV α-particle to travel to the crystal. The assymentry of the curve, would be due to the shorter time of flight of the more energetic α-particles.

With a α-counter in place, the gamma-counter was removed from its position near the target chamber and a Co^{60} source was placed near to it to make the Co^{60} gamma-counting rate equal to that produced by the gamma-rays from the $Li^{7}(p,\gamma)Be^{8}$ reaction. The E.H.T. supply to the photomultiplier was then increased until the output pulses were of the same amplitude as those produced by the gamma-rays from Be^{8}. The

amplitude of the pulses and the number entering the coincidence circuit were then substantially the same as for the main experiment. In this case no more than the expected chance coincidences were observed, (curve (c) Figure 22.), although there was a small reduction in the rate for delays greater than 25 mμs, probably due to unexplained losses introduced by the 25 mμs delay cable.

These experiments taken together confirm that the coincidences observed from Be^8 were due to α-particles and gamma-rays from the target and not to some spurious effect in the circuits.

4.7 Interpretation of the results.

The degree of uncertainty attached to the points in Figure 23. has been discussed in section 4.3. The only definite conclusion that can be drawn concerning the form of the curve through these points is that it must lie between the limits indicated by the lines (a) and (b).

For comparison with later work it is convenient to convert (a) and (b) to their differential forms. The results of this differentiation are shown in the lower diagram where the ordinate is now the percentage of gamma-ray transitions which proceed through a range of energy in Be^8 of 0.1 MeV. This is obtained from the

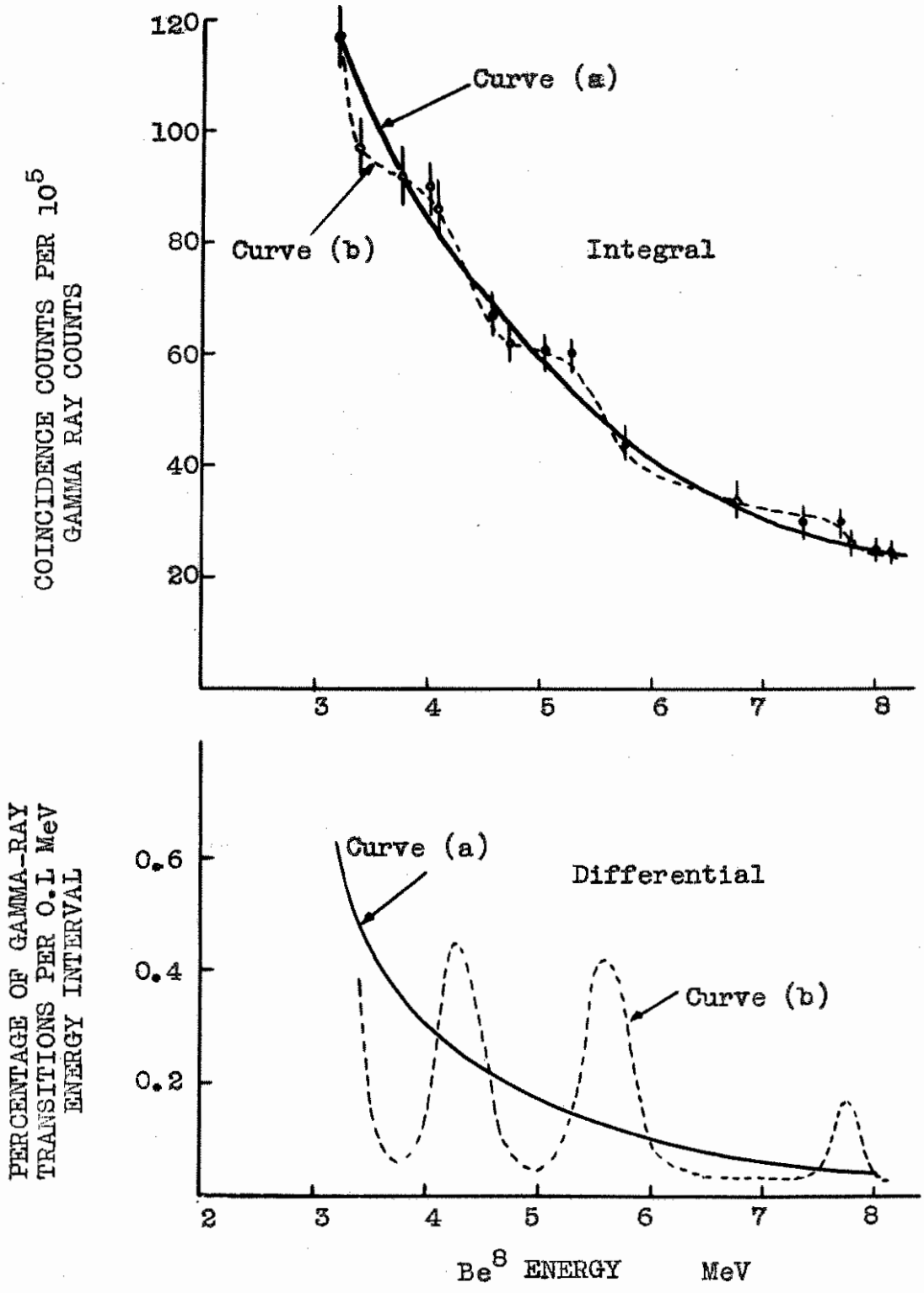

FIGURE 23. TRANSITION PROBABILITY

coincidence counts, and from the known absolute efficiency of the α-counter, e_α, which is $\frac{1}{138}$. The absolute efficiency, e_γ, of the gamma-counter is not required, provided it is assumed that it is constant for gamma-rays in the energy range 10 to 18 MeV (c.f. Figure 1.). The number of coincidence counts C detected from n transitions, each one of which produces a gamma-ray and two α-particles, would be

$$C = e_\gamma \times 2\, e_\alpha \times n.$$

If the n transitions were accompanied by N gamma-radiating events, the number of counts N_γ in the gamma-ray counter would be

$$N_\gamma = (N+n)e_\gamma.$$

The fraction $n/(N+n) = C/(2e_\alpha N_\gamma)$ then gives the required percentage. C is the number of coincident events recorded involving excitations in Be^8 in a range of 0.1 MeV for 10^5 ($=N_\gamma$) gamma-rays detected. The validity of this expression depends on the assumption that all the transitions which emitted products into the cone of acceptance of the counters were detected as coincidence events. Although this is likely to be true it is not possible to be sure of it and consequently the quoted percentages may be too small.

Curve (a) implies that the 3 MeV level plays no part in the transitions in the region above 3.7 MeV and that the breadth previously attributed to this level, was due entirely to a number of unresolved low

intensity levels at 4.3 MeV, 5.5 MeV and 7.7 MeV. The percentage of the total number of gamma-ray transitions which would then proceed through these states is 2%, 2% and 1% respectively. These values are approximate only since they assume that the angular correlation between the α-particles and gamma-radiation is isotropic (c.f. Chapter 6).

Curve (b) suggests that the transitions involving excitation energies in this region arise solely from the broad level known to exist at 2.9 MeV and any curve between these limits would indicate low intensity levels present on a background from the 3 MeV level.

The uncertainties in this experiment arise through instability of the circuits over the period required to record the complete spectrum. These could be eliminated if the whole spectrum was recorded simultaneously. It was for this purpose that the technique of preparation of thin crystals of sodium iodide was developed.

PART B. DIFFERENTIAL SPECTRUM WITH SODIUM IODIDE. I.

4.8 Apparatus.

In the previous experiment the energy of the disintegration α-particles was determined from their range in aluminium absorbers. The stilbene crystal acted almost solely as a simple detector requiring small powers of energy discrimination. In this experiment, the energy of the α-particles was determined from the pulse height spectrum recorded by the same scintillation counter with the stilbene crystal replaced with a thin (.002") crystal of sodium iodide. This crystal was 0.5" in diameter situated 5 cm. from the target and subtended a solid angle of $4\pi/250$ sterad. Details of the preparation and mounting of the crystals is contained in Chapter 2.

Few changes were made in the apparatus that has been described in Part A. The crystal used in the gamma-ray counter was replaced by a larger one 1.1/4" x 2", which was mounted in a perspex case with magnesium oxide to reflect the light onto the photocathode. The efficiency of this counter was about 60%. A layer of lead 0.6 cm. thick was placed across the front of this counter to eliminate coincidences produced by annihilation radiation originating from the metal

around the target chamber.

A block diagram of the new arrangements of the recording equipment is shown in Figure 24. The output from the coincidence unit was used to gate the proportional pulses from the α-counter, so that only the spectrum of α-particles in coincidence with a gamma-ray was recorded in the multichannel pulse analyser.

4.9 Experiment

Separated Li^7 targets were prepared by electrolytic deposition onto copper backings from a Li Cl solution in Pyridene. These thin targets, 20 $\mu gm/cm^2$, were bombarded with 445 KeV protons. The beam currents used were normally in the region of 5 μ amps. As in Part A, a $1mg/cm^2$ aluminium foil was placed over the crystal to prevent the excessive photomultiplier currents which would otherwise arise from scattered protons and soft X-rays. This foil also served to increase the amount of light collected from the crystal and thus helped to improve the pulse height resolution.

The bias of the discriminator in the output of the coincidence circuit was set to exclude the small pulses due to large single pulses in either channel. With the discriminator of the gamma-counter set at an arbitrary value the gated α-particle spectrum was recorded for a fixed number of gamma-ray counts. The

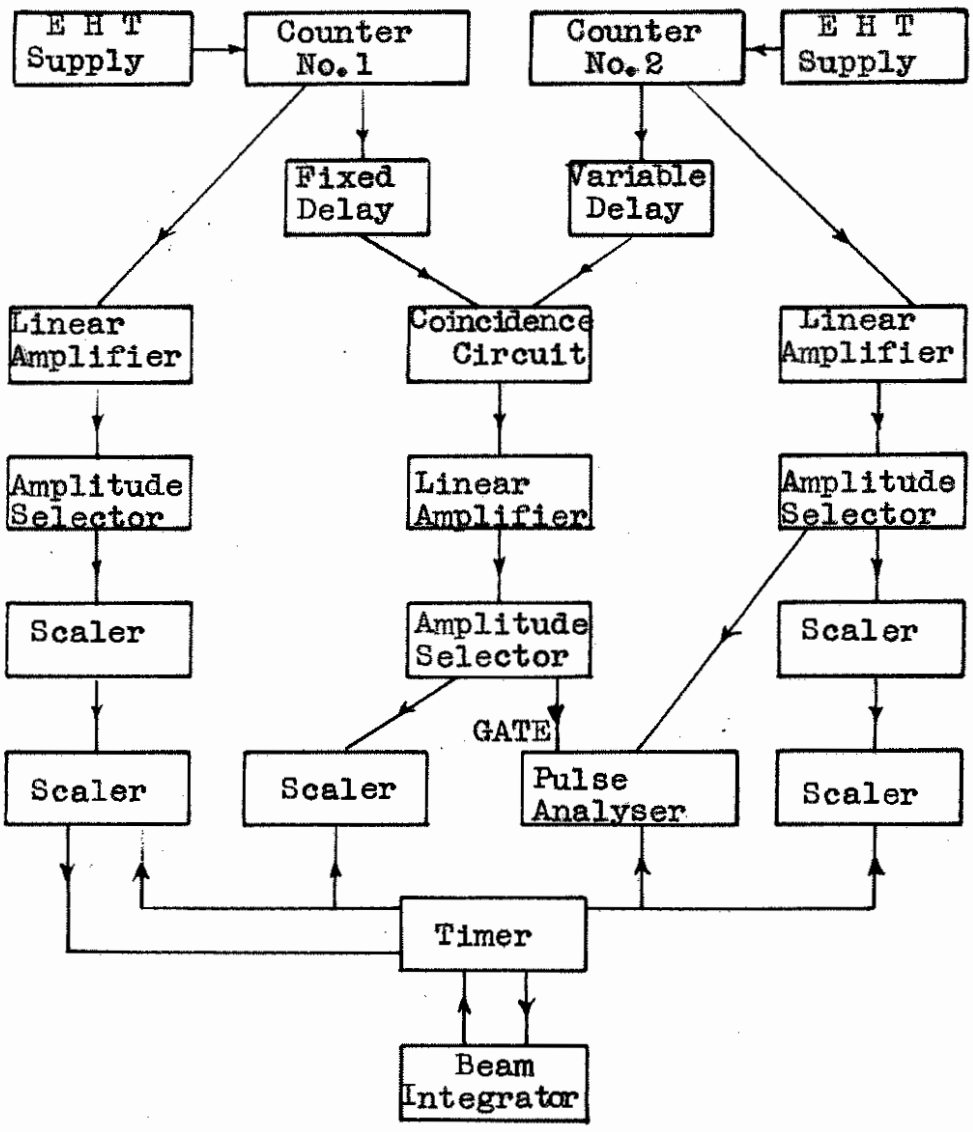

FIGURE 24. BLOCK DIAGRAM OF RECORDING UNITS.

result is shown as the upper curve in Figure 25. This represents the sum of a number of runs for which the total number of gamma-rays recorded was 1.2×10^7. The lower curve is the chance coincidence spectrum obtained by adding an artificial delay in the coincidence output of the gamma-counter. This was recorded for the same number of gamma-rays and under the same conditions of beam current as the true plus chance spectrum. The results below 8 volts are not shown because of the large uncertainty in this region introduced by the coincidences between stray annihilation quanta. The contribution from this effect was found by recording the gated spectrum when all α-particles are prevented from entering the crystal by a thick foil placed before it. It was found to be negligible above 8 volts.

The target was replaced by a thin source of ThC + C' which emits α-particles with energies of 6.08 MeV and 8.78 MeV. Dry air was let into the target chamber and the position of the peak in the pulse height distribution for each component was recorded for a range of air pressures. Using the range-energy relations given by Aron et al[59] and the known distance of the crystal from the target, the scale of the pulse height distribution was calibrated in terms of α-particle energy. Since this calibration was practically linear, the α-particle spectrum of Figure 25, with the chance

coincidences subtracted, was replotted on a scale giving the corresponding excitation of the Be^8 nucleus.

To enable a comparison of this result to be made with those in Figure 23, and with those of later experiments, the ordinate of Figure 26. was expressed in terms of the percentage of the total transitions which proceed through a range of excitation energy of Be^8 of 0.1 MeV. The absolute values given in Figure 26. are approximate only since the fraction of the total number of gamma-ray pulses which was recorded above the discriminator bias was not known accurately.

4.10 Discussion

Since the actual energies of the α-particles when they reach the crystal range only from about 1 to 4 MeV between 8 and 55 volts, the pulse height resolution is very poor, being about 30% and 17% at pulse heights of 8 and 55 volts respectively. Even with this poor resolution, however, peaks would still be observed if the spectrum was similar to that shown in curve (a) of Figure 23.

Figures 25 and 26 definitely indicate that the majority of transitions occurring in this region arise from a broad level whose maximum occurs at a lower energy than is observable in this experiment. The upper limit to the intensity of transitions through the proposed levels at 5.5 and 7.6 MeV can be judged from

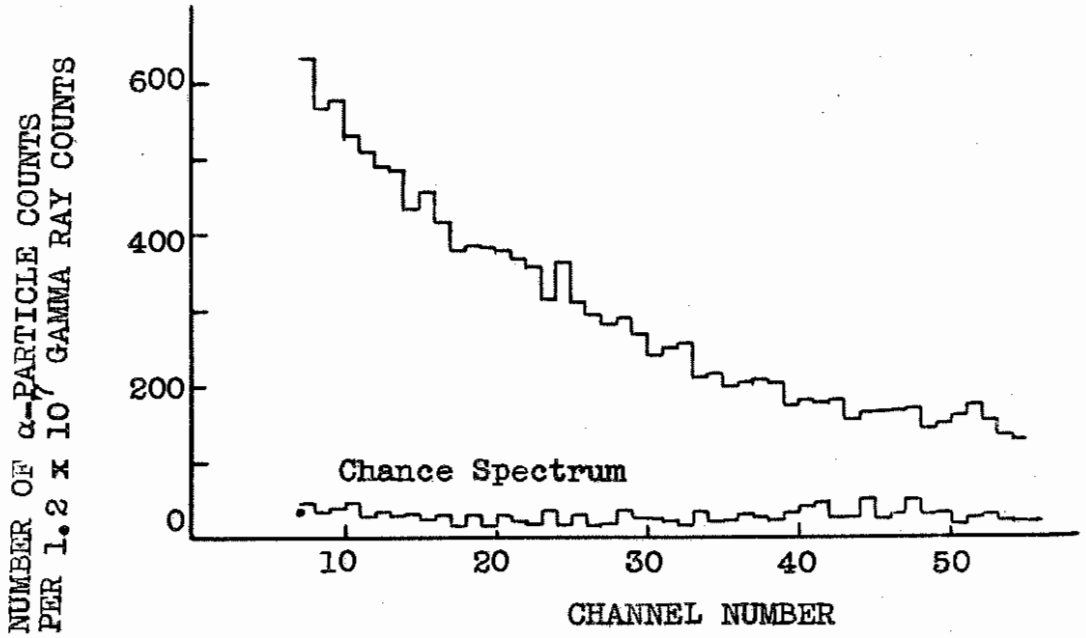

FIGURE 25. GATED α-PARTICLE SPECTRUM.

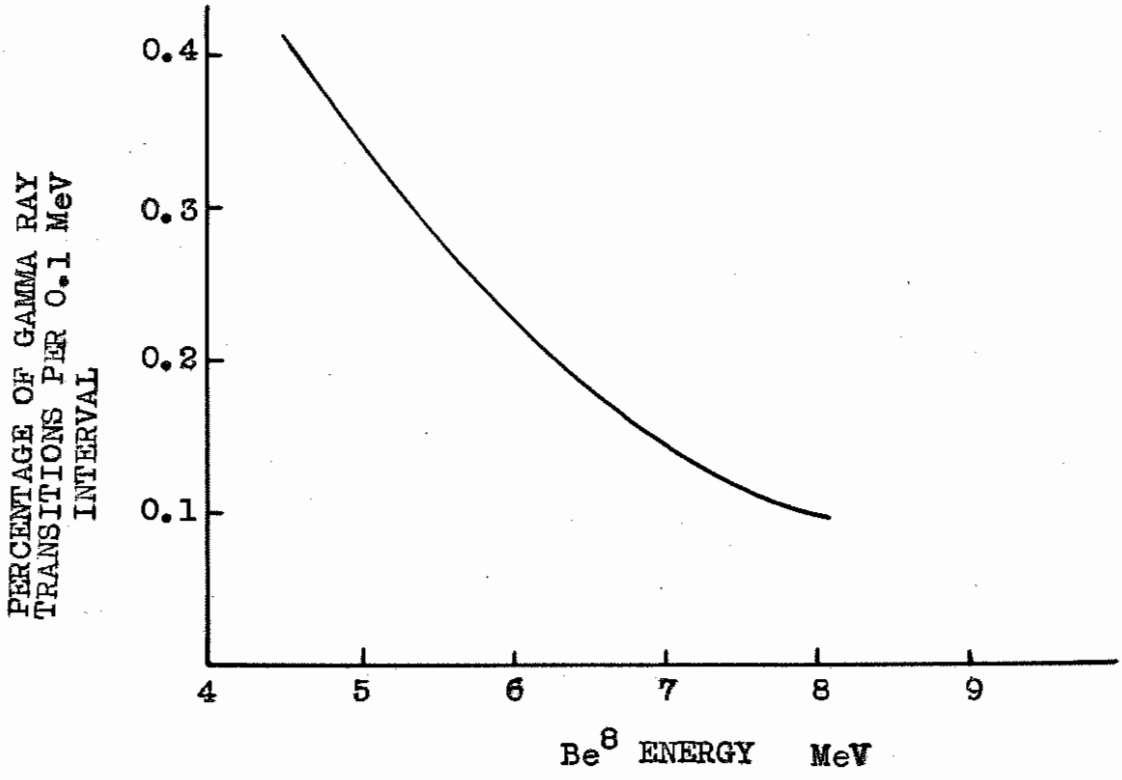

FIGURE 26. TRANSITION PROBABILITY.

proposed levels at 5.5 and 7.6 MeV can be judged from

these figures. Levels at these energies would be observed in this experiment if their intensity was greater than about 1% of the total transitions from the 17.63 MeV level.

4.11 The resonance behaviour of the gated α-particle spectrum.

It has already been shown in Figure 17. that the coincidence events in this region follow the proton resonance at 441 KeV, indicating that the gamma-radiation involved originates from the 17.63 MeV level. This was checked again with the present apparatus. The gated pulse height distribution was recorded for three values of proton energy; 400 KeV, 450 KeV, and 510 KeV, each for the same value of integrated beam current. All three distributions were found to have the same shape and the ordinates of the curves were in the ratio 4 : 100 : 24. The corresponding ratio for the total gamma-ray counts recorded for each of the beam energies was 7 : 100 : 41. These figures clearly show that the gamma-rays involved in the observed coincidence events originate from the 17.63 MeV level of Be^8, and also suggest that the percentage of gamma-ray transitions which proceed to the energy region between 5 and 8 MeV of Be^8 is lower for values of the proton energy above or below the resonance at 440 KeV.

4.12 The gated gamma-ray spectrum.

It was possible to obtain a little more information regarding the gamma-rays participating in these coincidence events in addition to the fact that they originate from the 17.63 MeV level. This was done by observing the pulse height distribution of only those gamma-rays that were in coincidence with an α-particle detected in the α-counter. The full gamma-ray spectrum is shown in Figure 27 and closely resembles that derived in chapter I, Figure 9. On this basis the positions of the upper limits of the pulses from the 17.6 and 14.8 MeV components are marked on Figure 27.

The gated gamma-ray spectrum obtained for a fixed number of counts in the gamma-ray counter is shown in Figure 28. (curve (a) together with the chance spectrum curve (b) obtained for the same number of counts. Curve (c) in this Figure is the result of subtraction of the chance spectrum from the true + chance spectrum. Since the α-counter can detect only those α-particles which result from the disintegration of Be^8 nuclei with greater energy than about 4 MeV excitation energy, gamma-rays with greater energy than 13.6 MeV should not be detected in coincidence. This conclusion is justified by the evidence in Figure 28.

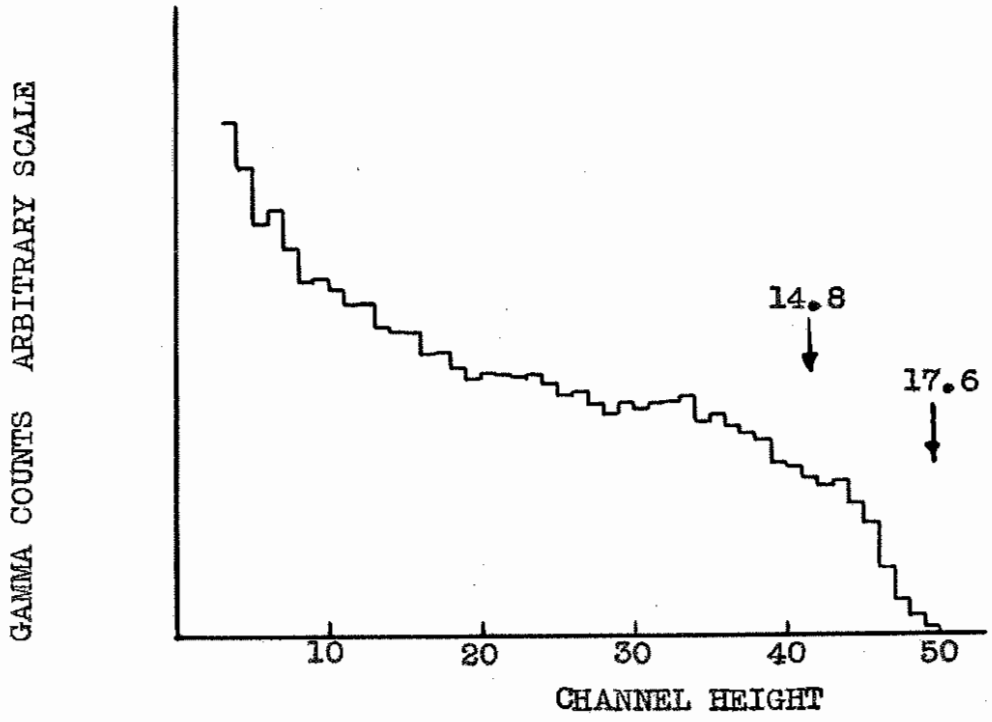

FIGURE 27. GAMMA RAY SPECTRUM.

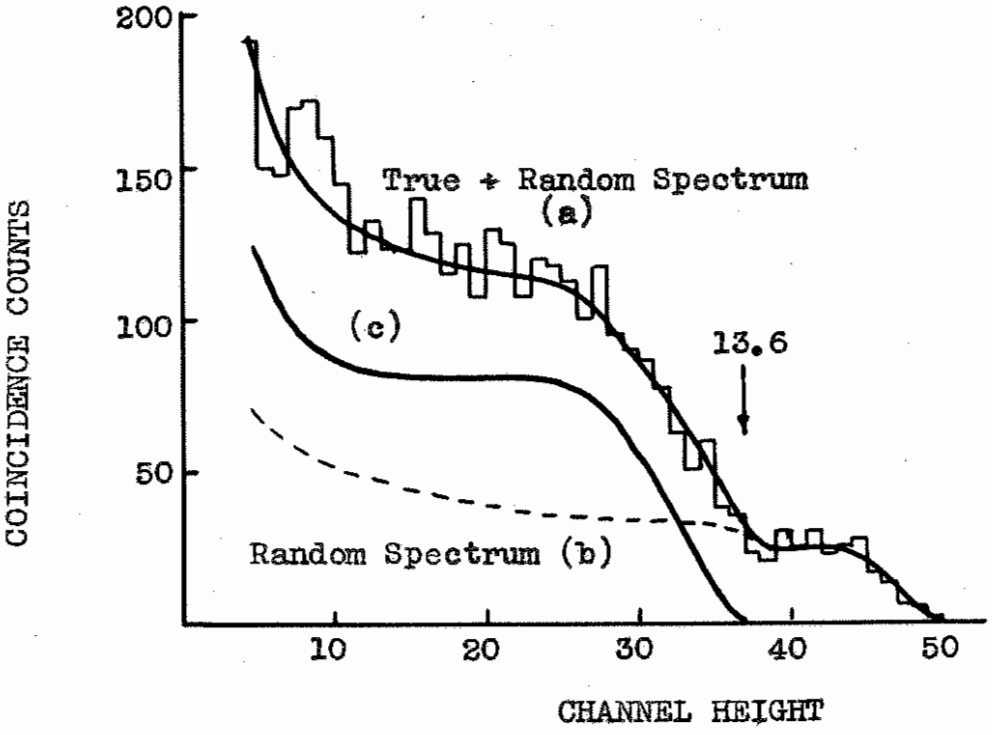

FIGURE 28. GATED COINCIDENCE GAMMA RAY SPECTRUM.

PART C. DIFFERENTIAL SPECTRUM WITH SODIUM IODIDE. II.

In both the preceding experiments it was not possible to examine the level structure of Be^8 below 4 MeV since the absorber necessary to prevent light, soft x-rays and scattered protons from reaching the detector was also thick enough to stop the disintegration α-particles from levels in this region. The removal of this absorber would not only permit detection of these α-particles but would also increase the energy of the α-particles from the energy region observed in Part B. and therefore result in improved pulse height resolution.

4.13 Apparatus.

The aluminium foil between the target and the crystal was eliminated and the exclusion of light and scattered protons, achieved by a system of collimators situated in a magnetic field. The experimental arrangement is shown to scale in Figure 29. where the diameter of the target tube is 2". The magnet was of conventional design and produced a field of 7000 gauss over the area shown. The collimating system is shown in more detail in Figure 30. where the paths of some of the target radiation are drawn. Light, scattered protons and the 9 MeV α-particles from the

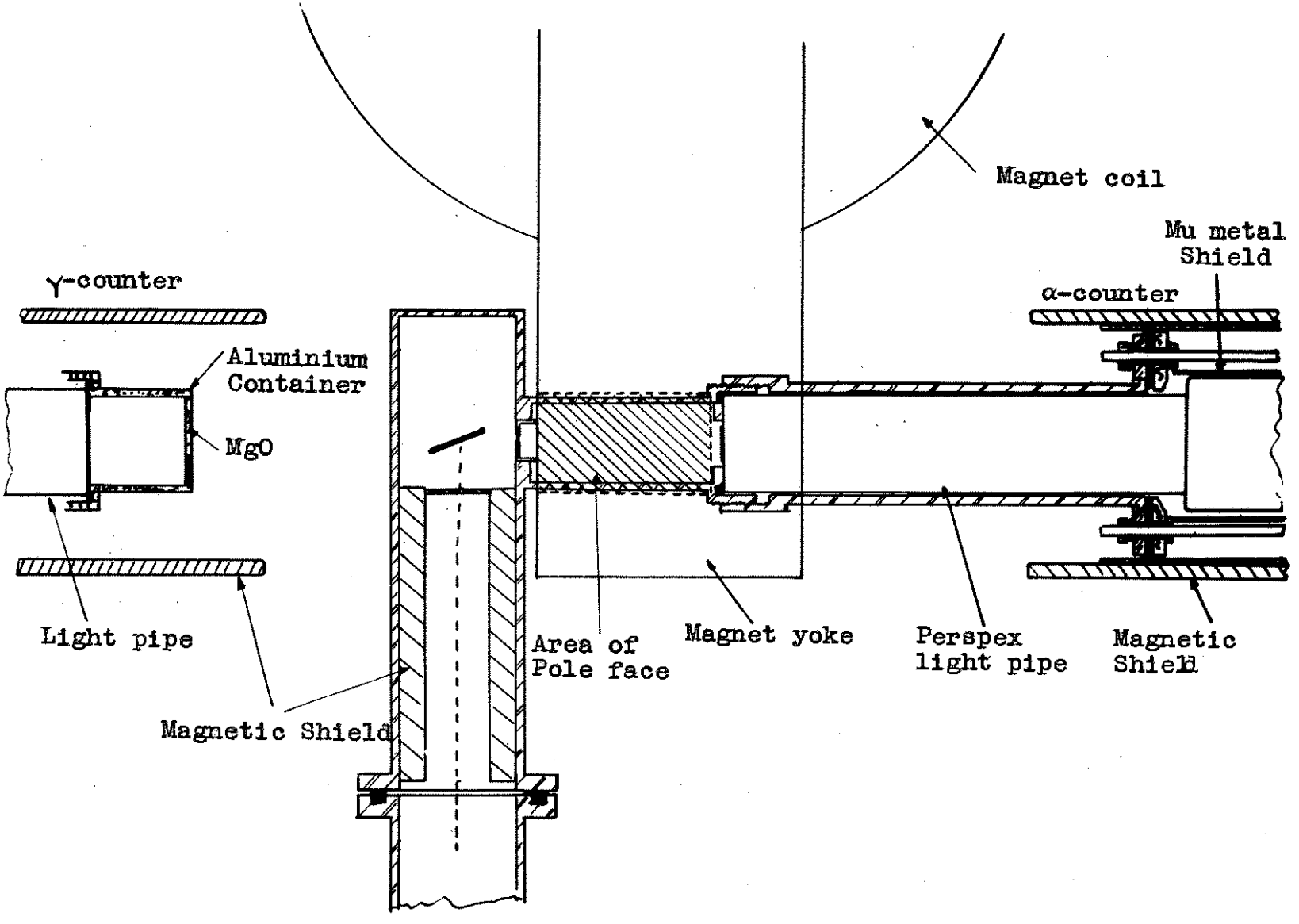

FIGURE 29. ARRANGEMENT OF TARGET CHAMBER, MAGNET AND COUNTERS.

$Li^7(p,\alpha)He^4$ reaction did not reach the detector.

The counting rate in the α-particle detector was very considerably reduced when these 9 MeV α-particles were excluded and the resolving time of the coincidence circuit could be increased without increasing the chance coincidence rate above its former level. The length of the output pulses which were used to operate the coincidence circuit was therefore increased to 45 mμs, with 300 cm. of shorted transmission time. The coincidence circuit was more stable when working with these longer pulses.

The effects of the magnetic field on the operation of the photomultipliers were reduced by surrounding each multiplier with a sheet of mu metal and by enclosing each complete counter in an iron cylinder. The photomultiplier used in the α-counter was removed from the close vicinity of the pole pieces by using a 7" long perspex light pipe to optically couple the crystal to the photocathode. With this protection there was no significant change in the performance of the counters when they were operated with the magnetic field switched on or off. However as this experimental arrangement was to be used later to measure the angular correlation between the directions of emission of the α-particles and gamma-rays, which would involve movement of the gamma-ray counter in the magnetic field, it was considered desirable to use as a monitor a second gamma-ray counter fixed in position at

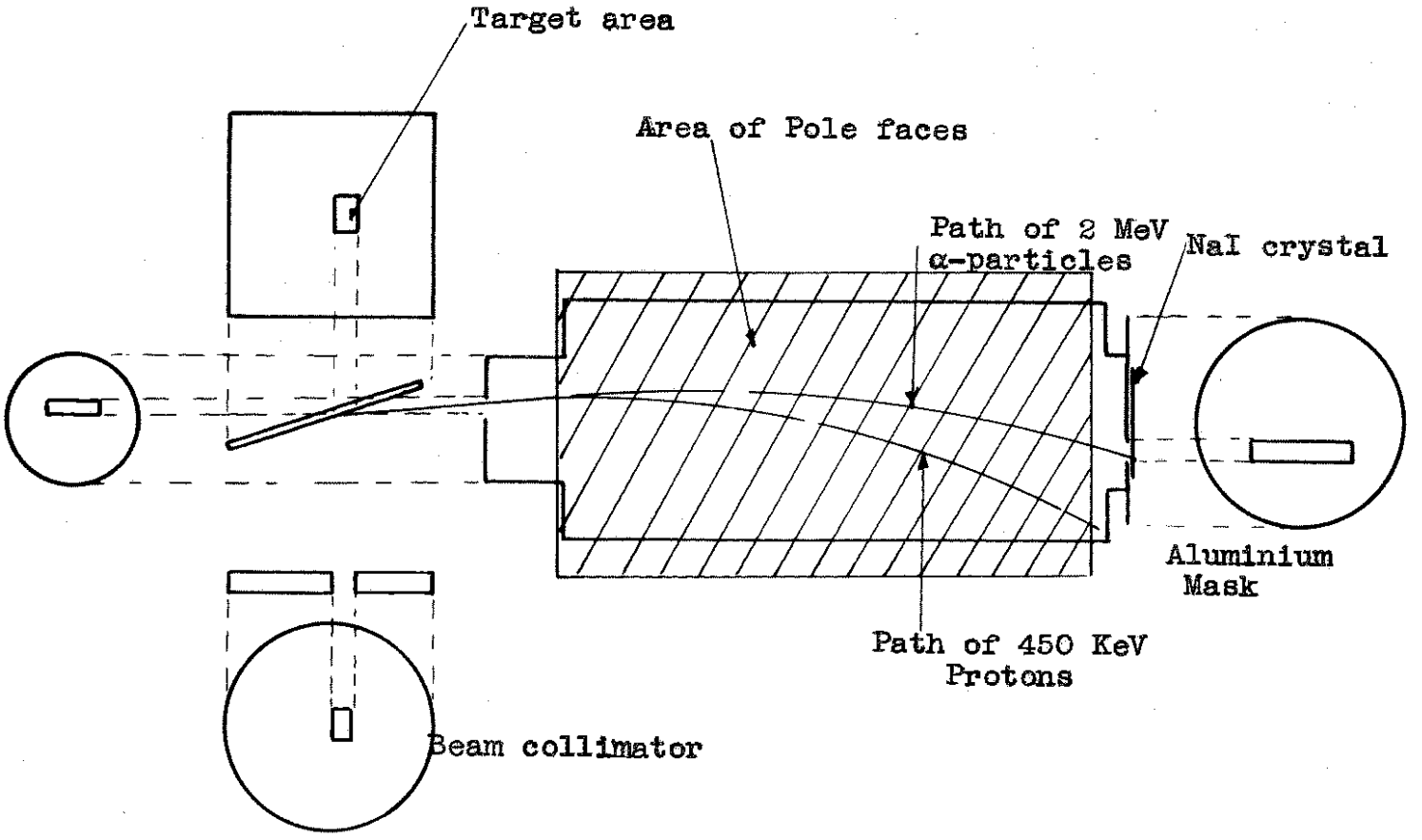

FIGURE 30. COLLIMATION SYSTEM.

some distance from the magnet. Thus the electronic equipment was arranged as shown in Figure 24. apart from this added counter.

4.14 Experiment.

The gated α-particle pulse height distribution is shown in Figure 31. as the sum of a large number of runs taken under the same conditions as have been described in Part B. The stability of the recording apparatus was checked between each run by noting the position of the peaks in the distribution of the α-particles from the ThC+C' source which was fixed to the back of the rotating target. The lower curve is the chance coincidence spectrum taken for the same total number of monitor counts. The large number of low energy pulses is again attributed to protons from the target being scattered into the crystal from the walls of the vacuum chamber.

Upon completion of these spectra the target was removed and replaced by a source of ThC+C'. This was marked so that both its position and area were identical with those of the irradiated section of the Li^7 target which is indicated in Figure 30. The α-particle spectrum from this source was recorded with the multi channel analyser for a fixed time interval and for a range of air pressures. The path length between the source and the crystal was calculated from Figure 30.

and the value of 9.8 cm., so obtained, was assumed to be constant for all α-particle energies between 1 MeV and 5 MeV, (this introduces an error of only 0.02 cm.). The calculated energies of the α-particle were those shown plotted in Figure 10. against the position of the corresponding peak in the pulse height distribution. It was also found that for α-particle energies between 1 MeV and 5 MeV, the total number of counts in the fixed time interval was constant to at least 1%, indicating a constant detection efficiency in this range.

The data obtained with the thorium source also provided the approximate values for the pulse height resolution (full width at half height) for α-particles in this energy range which were used in Figure 13.

4.15 Interpretation.

The positions at which levels at 4.1, 5.3 and 7.6 MeV would occur are marked on Figure 31. Despite the poor resolution, (about 15% at 20 volts), a group 0.5 MeV wide, would be observed at 4.1 MeV if its intensity was greater than 5% that of main group at 3 MeV. Groups at 5.3 MeV and 7.6 MeV would be observed if their intensities were greater than 3% that of the 3 MeV group.

To obtain an estimate of the true shape of the spectrum the distribution of true coincidence events,

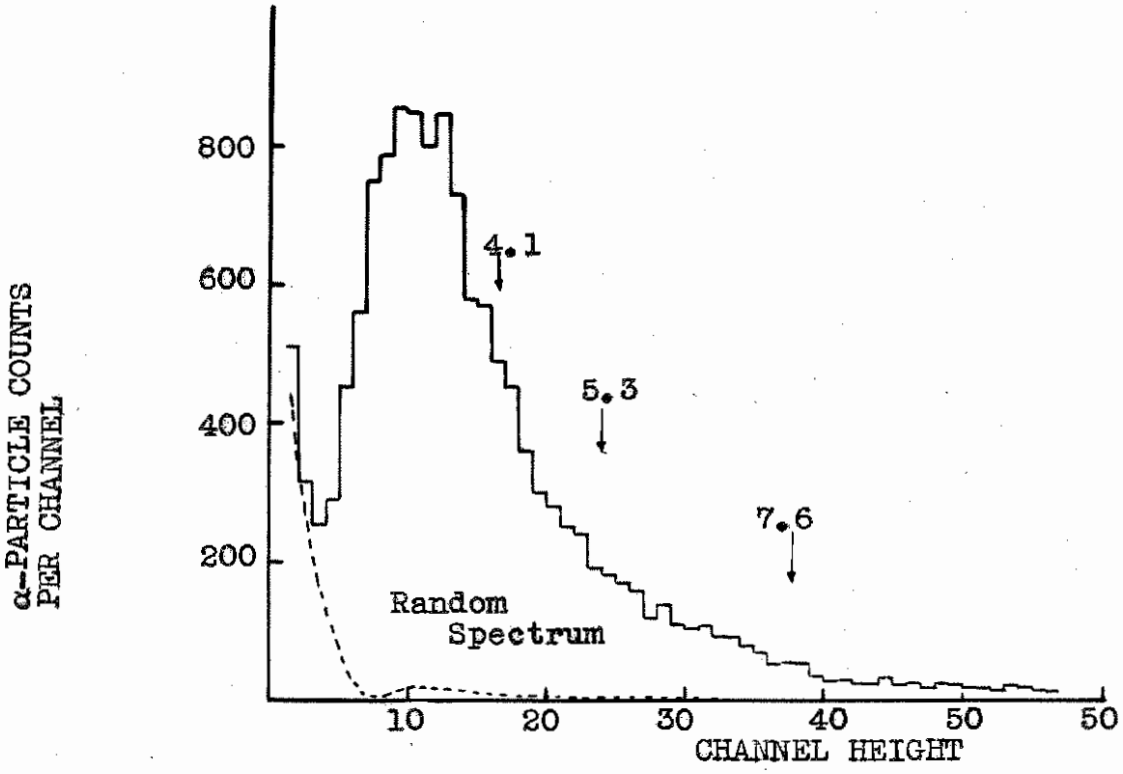

FIGURE 31. GATED α-PARTICLE SPECTRUM

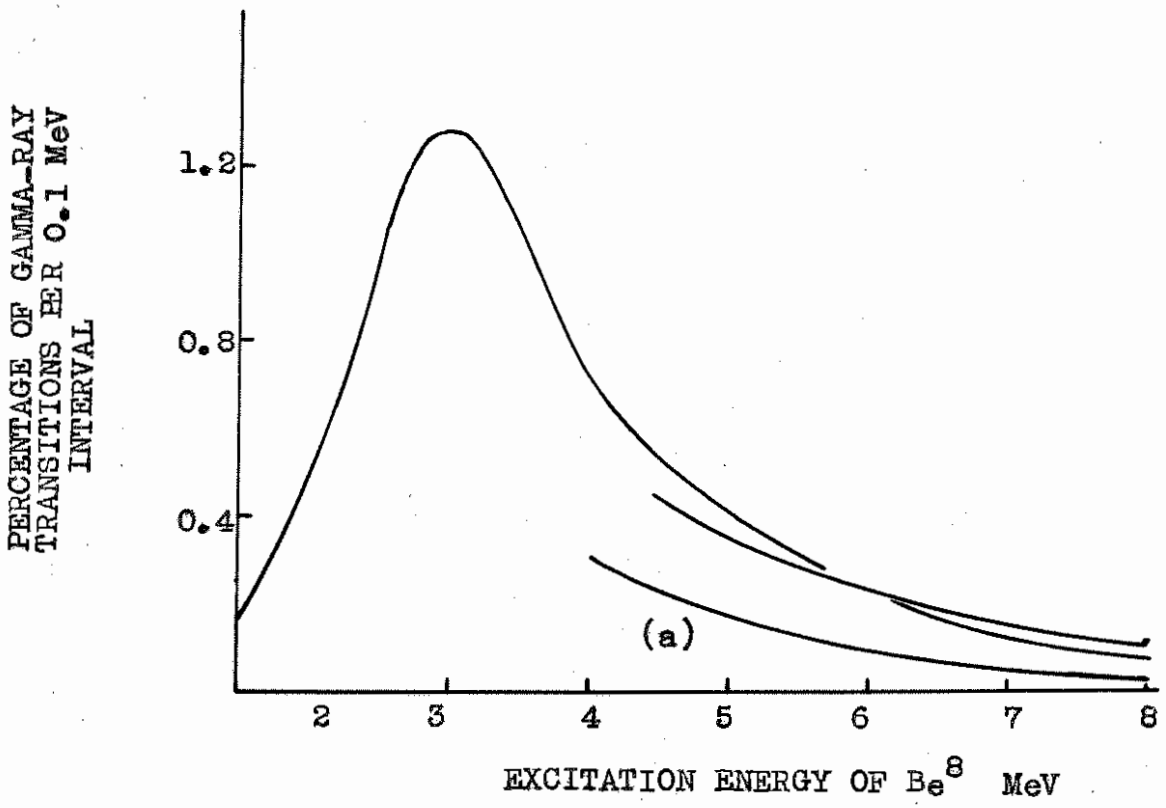

FIGURE 32. TRANSITION PROBABILITY.

found by subtracting the chance coincidence distribution (dotted line) from the histogram in Figure 31., was corrected for the broadening introduced by statistical effects in the photomultiplier. This was done by guessing the final distribution and broadening it with the aid of Figure 13 until a fit was obtained with the experimental spectrum. The calibration curve of Figure 10. was then used to give the distribution in terms of the energy of the disintegration α-particles. Since the calibration of energy against pulse height was not linear this involved a correction for the changing width of interval over the energy range. The relation between the energy of the disintegration α-particles and the energy of excitation of the Be^8 nucleus was slightly changed from that derived in Part A. since in this experiment the α-particles were observed at 100° to the beam. The final distribution obtained for the variation of transition probability with energy is shown as curve (c) in Figure 32.

In order to compare this result with those obtained in Parts A and B the ordinate of Figure 32. is expressed as the percentage transition probability per 0.1 MeV interval. The scale is approximate only since it is based on the assumption that the area under the curve of Figure 32. represented 33% of the total number of gamma-ray transitions from the 17.63 MeV level, as suggested by Walker and McDaniel. The results obtained in Part A,

Figure 23., and Part B, Figure 26. are shown as curves (a) and (b) respectively in Figure 32. The agreement is satisfactory since the absolute value of the ordinates in all three results was not known with any accuracy. The flattening of curve (b) is attributed to the large spreading introduced by the statistical effects in the photomultiplier which in this case, has not been removed.

4.16 The ungated α-particle spectrum.

When the α-particle spectrum is observed without defining the direction of emission of the associated gamma-ray the Doppler broadening introduced is about 0.4 MeV over most of the energy range. As mentioned above this would tend to obscure any low intensity lines that may be present in the spectrum. However, with the present α-particle detector, for which the broadening introduced by statistical effects in the photomultiplier was slightly more than the Doppler broadening, there would be no great advantage in defining the direction of the gamma-ray by a coincidence experiment. The resultant loss of efficiency would be justified only if other effects were also eliminated.

Since the percentage of gamma-ray transitions which proceed through regions of high excitation in Be^8 is very small it is essential to eliminate all possibility

that the α-particles in this energy region are not the result of some reaction involving target or beam contaminants. This can only be done (in the absence of a high resolution magnetic spectrometer) by selecting only those α-particles in coincidence with a gamma-ray. The only possible contaminant reaction would then be $F^{19}(p,\alpha\gamma)O^{16}$ which, although not observed, could also be eliminated by suitably biasing the discriminator in the gamma-counter channel of the triple coincidence circuit.

The magnitude of the effects of these contaminant reactions can be seen from Figure 33. This shows the ungated α-particle pulse height distributions obtained with the thin Li^7 target for the same total integrated beam current, at bombarding energies of 440 KeV and 380 KeV. At 380 KeV the measured gamma-ray yield was 2% relative to that at 440 KeV. A similar distribution was obtained at 520 KeV where the relative yield was 4%. Thus almost the entire distribution obtained at these voltages is contributed by other than the $Li^7(p,\gamma\alpha)He^4$ reaction. The large number of low energy pulses is, as mentioned previously, the result of scattered protons. The peak at an energy of 1.7 MeV is formed by the α-particles from the $Li^7(p,\alpha)He^3$ reaction and the small number of pulses at an energy of approximately 2.8 MeV is probably due to the $O^{16}(d,\alpha)N^{14}$ reaction.

The points shown in Figure 34. were obtained as the result of subtraction of the average of the distributions obtained at 380 KeV and 520 KeV from that of 440 KeV.

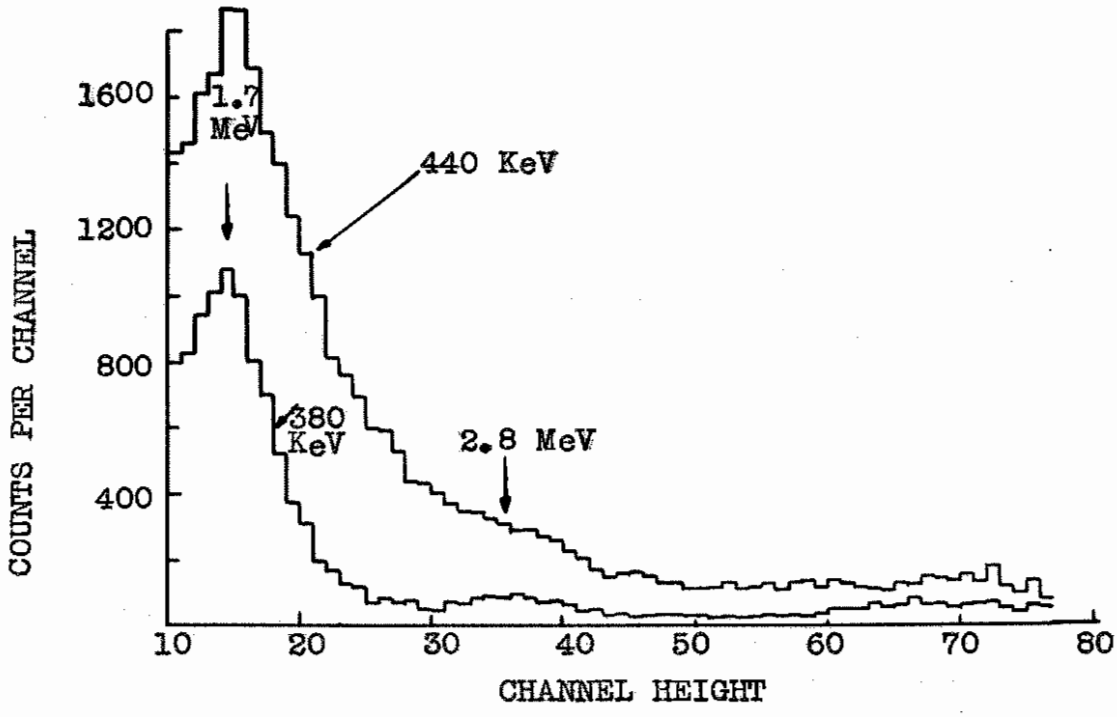

FIGURE 33. UNGATED α-PARTICLE SPECTRA

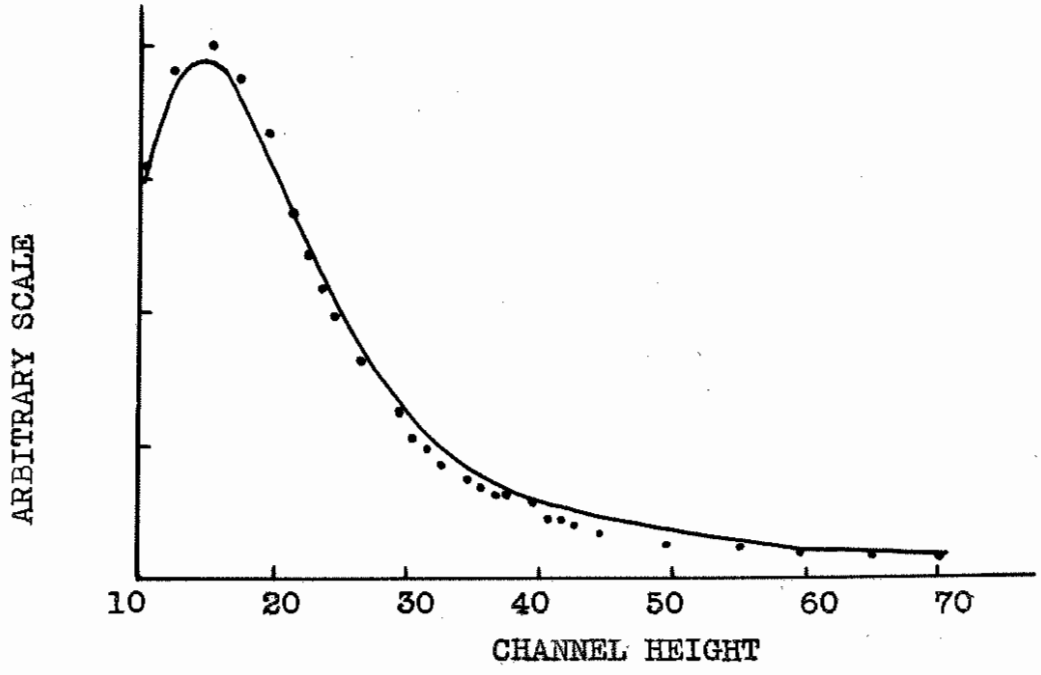

FIGURE 34. COMPARISON OF GATED AND UNGATED SPECTRA.

The solid curve shown in the figure was obtained from Figure 32 and shows good agreement between the gated and ungated distributions.

4.17. Conclusions.

The results of the experiments described in this Chapter are in general agreement with the previous work on the $Li^7(p,\gamma)Be^8$ reaction. They confirm that approximately 10% of the transitions from the 17.63 MeV level involve excitations of Be^8 greater than 5 MeV. However, the previous interpretation of these transitions in terms of levels in this energy region appears, from the present work, to be unjustified.

The results of previous experiments mentioned in the introduction, in which Be^8 is excited by other reactions, have not been confirmed. Levels in Be^8 at 2.2 and 3.4 MeV would be difficult to resolve in the present experiment and it is possible that selection rules invoked in the $Li^7(p,\gamma)Be^8$ reaction prevent the excitation of levels at 4.1 MeV and 7.6 MeV reported from other reactions.

The work described in the following chapter was undertaken in an attempt to resolve these points.

CHAPTER 5

THE ALPHA PARTICLE SPECTRUM FROM THE REACTION $B^{10}(d,\alpha)Be^{8}(2\alpha)$

5.1 Introduction.

The experiments that have been described in Chapter 4 involved measurements of α-particle energies of only 1 or 2 MeV. Since the energy resolution that was obtainable in this region with sodium iodide crystals was quite poor, the conclusions that could be drawn were limited.

For the reaction $B^{10}(d,\alpha)Be^{8}$ the Q value is 17.8 MeV [60], and hence the energy of the α-particles proceeding to the 3 MeV state of Be^{8} have an energy of about 11 MeV. The energy resolution of such α-particles should be approximately 5% and so the measurement of the energy spectrum of these α-particles should provide better information concerning the states of the Be^{8} nucleus.

This reaction had been studied previously by several workers, and although Whitehead[62] found evidence for a level at 4.9 MeV this was not confirmed by Treacy[63]. In these experiments the α-particle spectrum was measured by a single detector, in which case, the α-particles from the break-up of Be^{8} were also recorded. This

---

62. Whitehead, W.D., Phys.Rev. 82: 553, 1951.

63. Treacy, P.B., Phil.Mag. 44: 325, 1953.

background extended over most of the primary α-particle spectrum and would have obscured any low intensity groups that may have been present.

This chapter describes an attempt to remove this background of break up α-particles and so examine the primary α-particle spectrum alone.

5.2 Mechanics of the reaction.

The reaction to be studied can be written -

$$B^{10} + d \rightarrow C^{12x} \rightarrow \alpha_1 + Be^{8x} + Q$$

If E MeV is the excitation energy of the Be^8 nucleus, then Q = (17.81 -E) MeV. The Be^{8x} nucleus subsequently breaks up into two α-parts, thus

$$Be^{8x} \rightarrow \alpha_2 + \alpha_3 + (E + .01)$$

This disintegration scheme assumes that the compound nucleus C^{12} decays by emission of an α-particle to a definite state of Be^8. The possibility of three body break up, i.e. the disintegration of the C^{12} nucleus into three α-particles, which does not proceed through the intermediate Be^8 nucleus will be discussed later in Chapter 7.

Consider an arrangement of two counters in which one, Counter 1, is placed at 0^o to the deuteron beam and the other, counter 2, is situated such that the angle between the counters is Ø. When the pulse height spectrum of the α-particles detected in counter 1 is recorded, results

similar to those of other workers are obtained. In addition to the primary α-particle spectrum, the distribution also contains the spectrum of the secondary α-particles resulting from the breakup of the Be^8 nucleus.

If, now, the spectrum of α-particles in counter 1 is only recorded when there is a coincident event between counters 1 and 2, the contribution from secondary α-particle will be considerably reduced and modified; at the same time however, the shape of the primary α-particle spectrum is altered.

A coincidence event can arise from one of three modes of detection.

i) The primary α-particle incident on counter 1 and one of the secondaries on counter 2.

ii) The primary incident on counter 2 and one of the secondaries on counter 1.

iii) Both secondaries incident on counters 1 and 2.

In designing the apparatus we wished if possible to allow only events of mode i), and we shall discuss now the general considerations involved. The detailed calculations, which depend on the dimensions of the apparatus, are made later.

When the primary α-particle travels in the forward direction, the secondary α-particles appear within a cone, the angle of which depends on the primary α-particle energy. As this energy increases the cone becomes narrower. Thus for a particular value of Ø there will be a certain value of the primary α-particle energy above which no

secondary α-particles are detected by counter 2. As Ø decreases this cut-off energy also decreases.

The effective solid angle of counter 2 also depends on the primary α-particle energy, i.e. the angle of the cone. It is zero when the primary α-particle energy is above its cut-off value and as the primary energy decreases, it increases sharply to a maximum (depending on the dimensions of the counter 2), then decreases gradually with further decrease in the primary α-particle energy, c.f. Figure 40.

To simplify the interpretation of the results it would obviously be desirable to choose a large value of Ø so that the whole of the energy spectrum lay within the region of gradually changing solid angle. However, the effects of the second mode of detection must now be considered.

The primary α-particle which is incident on counter 2 leaves the Be^8 nucleus with an energy E, and the secondary α-particle which reaches counter 1 has an energy E', which depends on E and on the angle Ø. For a fixed value of E, this energy E' decreases with decreasing Ø. Thus in the recorded spectrum of counter 1, the total counts at any particular energy will include a contribution from events involving Be^8 in a state E, giving a secondary of the particular energy. As Ø decreases, the energy E of the state contributing counts at this particular energy will thus increase.

Consideration of mode iii) shows that the energy E of the state contributing counts at a particular energy

decreases as $\emptyset$ decreases, although in this case, the energies of the secondary α-particles from a given excitation energy of Be^8 are spread over a wide range. It is apparent from the foregoing that one value of $\emptyset$ is suitable for examining only a portion of the primary α-particle spectrum and that several values must be used to provide precise knowledge of the complete spectrum.

5.3 Apparatus.

The target chamber and the counter arrangement used for this experiment are shown to scale in Figure 35. The targets of separated B^{10} were evaporated to a thickness of 0.5 mgm/cm^2 onto nickel foil of approximately 3 mm. air equivalent. This was held with a spring clip in a copper frame, which could be water cooled.

The α-particles were detected by 1/16" thick sodium iodide crystals mounted as described in Chapter 2. Aluminium masks were used to define the crystal area and to provide some measure of reflectivity at the end of the light guide. The areas so defined were a circle 11/16" diameter, for the end crystal, and a rectangle 1/2" wide by 5/8" long for the side crystal.

As mentioned in Chapter 2, it is necessary for the crystal surfaces to be perfect in order to obtain the best resolution in the detection of the α-particles. This was achieved by cleaving and mounting the crystals in a dry box. The side flanges and the end assembly of

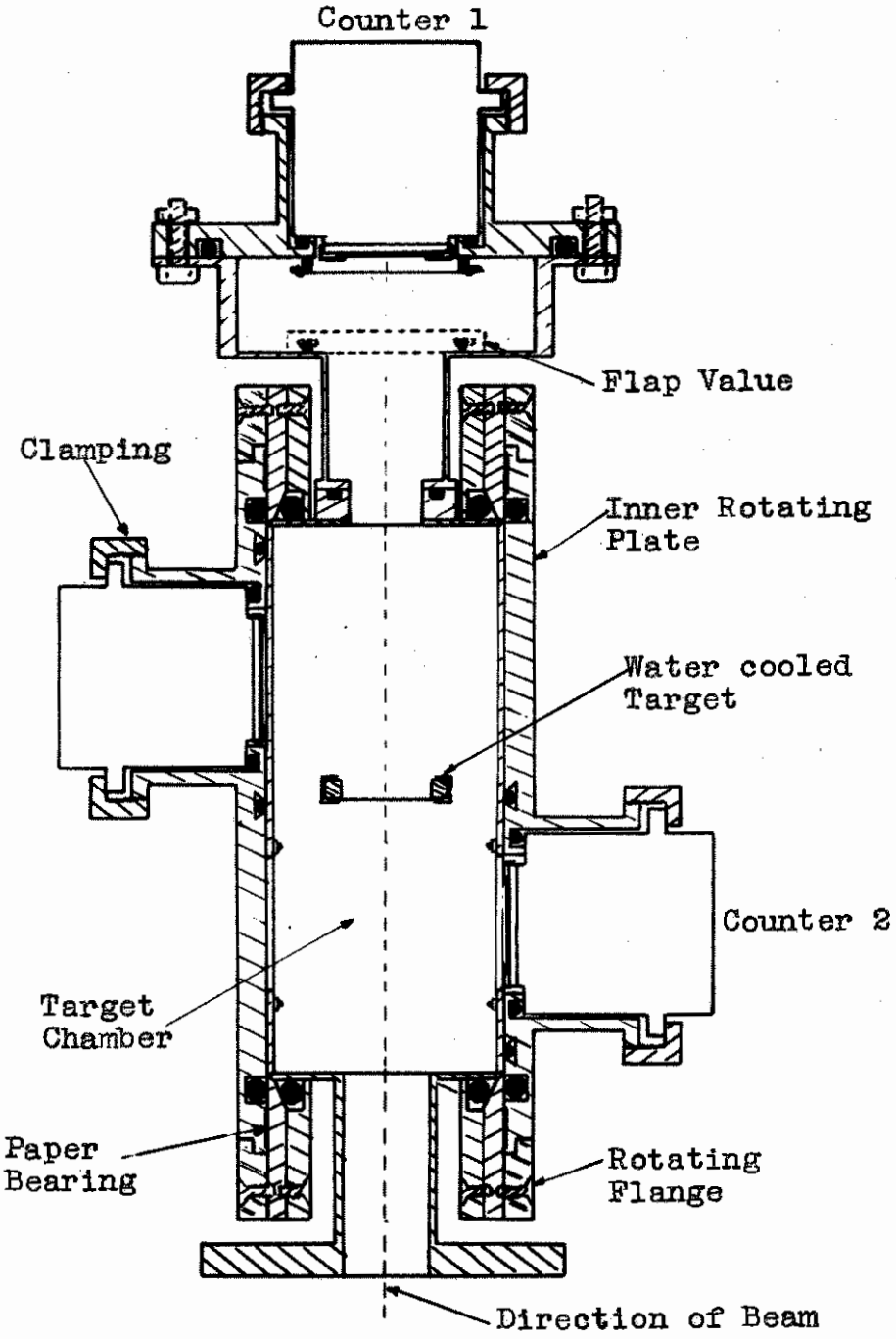

FIGURE 35. TARGET CHAMBER AND CRYSTAL MOUNTINGS.

counter 1 were removeable from the main target chamber, and the light guides could be fixed in position inside the dry box by means of the clamp rings shown in the figure. The crystals could then be sealed off by means of a rotating flange in the case of the side counter and by a sliding flap valve in the end assembly. These were reattached to the main assembly which was then evacuated. After pumping for sufficient time to ensure that no water vapour remained in the system, the valves were opened and the crystals exposed to the vacuum. In Figure 36, counter 2 is shown in the open position and the other side counter in the closed position. These valves also permitted a change of target without causing any deterioration of the crystal surface. When the whole system was evacuated the clamp rings holding the light guides in place were removed and the photomultiplier mounted as shown in Figure 11. A crystal mounted in this way maintained its characteristics for three or four days, after which time it had to be replaced. The resolution (full width at half height) usually obtained for the spectrum of the 8.8 MeV α-particles from ThC' was 6%.

To prevent excessive currents in the counters caused by deuterons scattered from the target, it was necessary to interpose thicknesses of nickel foil between the target and the crystals. Since the resolution for α-particle detection decreases with α-particle energy it was desirable to keep this thickness to a minimum. The yield from the $B^{10}(d,\alpha)$ reaction increases steadily to a maximum at a deuteron

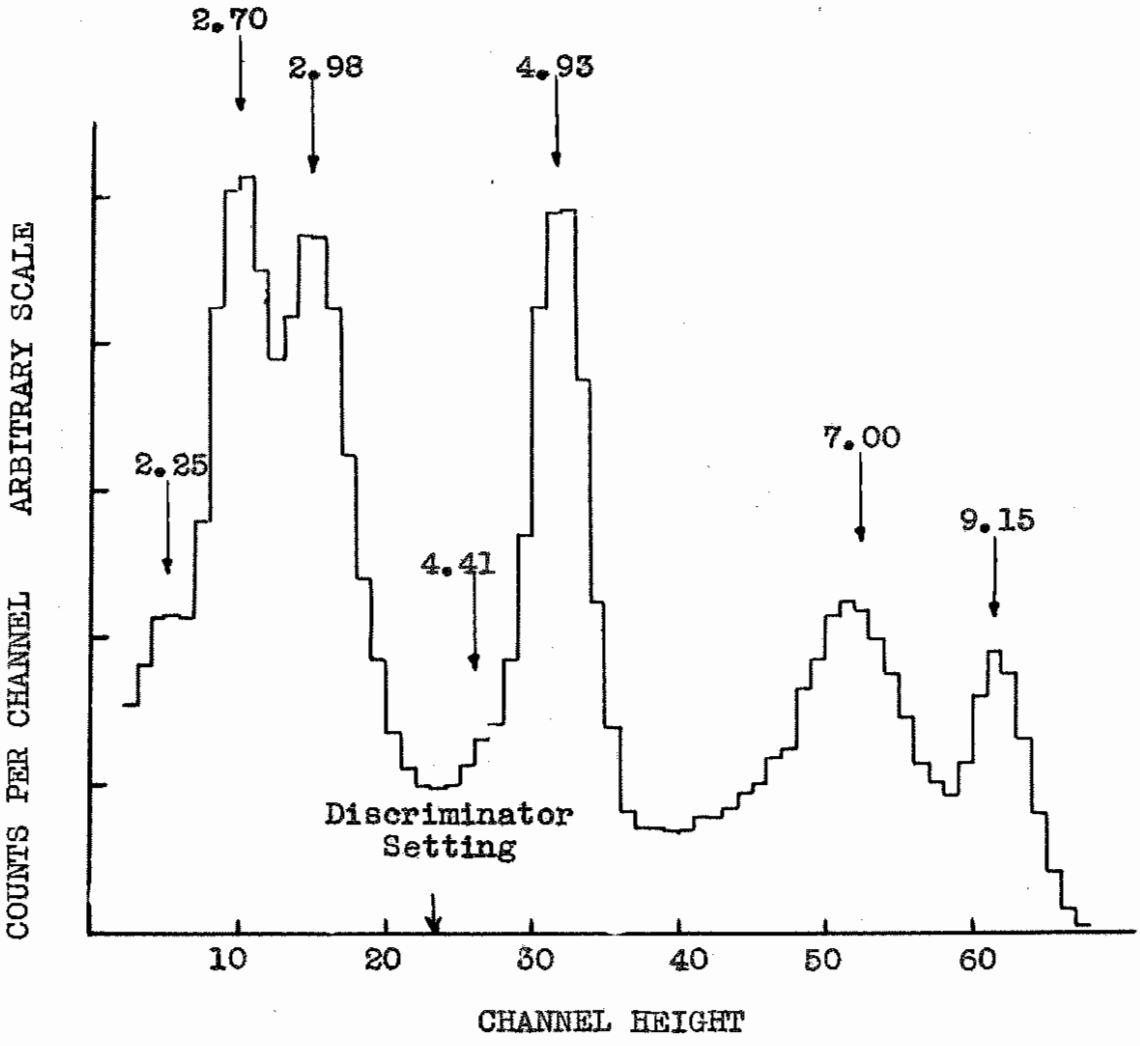

FIGURE 36. UNGATED SPECTRUM.

energy of 1 MeV[62], thus a bombarding energy of 350 KeV was chosen so that the yield was reasonable, and the thickness of foil not too great - 1.2 cm. air equivalent.

In order to vary $\emptyset$, the angle between counters 1 and 2 the side flange holding counter 2 could be rotated on its O ring seal in a plane parallel to the beam. Variation of $\emptyset$ between 51° and 140° could thus be achieved. Provision was also made for rotating the perspex light guide, so that the edge of the detector could be maintained parallel to the beam. Both these operations could be performed when the system was under vacuum.

The recording equipment was arranged as shown in Figure 24. As in the previous experiments proportional pulses were taken from the ninth dynode of the multiplier and the pulses from the last dynode used to operate the coincidence circuit. Since the counting rates in this experiment were quite low (300/sec. for beam currents of 2μa), it was not necessary to use the fast coincidence circuit that was essential for the work on the $Li^7(p, \gamma\alpha)\alpha$ reaction. The partially limited pulses from the multiplier triggered simple flip flops with delay line clipping and the negative output pulses, 20 volt and 0.15 μsec. wide, were fed directly to a coincidence circuit which had a resolving time of 0.3 μsec. The minimum α-particle energy required to trigger the flip flops was 2.0 MeV. This was determined using the α-particles from ThC'.

5.4 Experiment.

The spectrum of pulses from counter 1 was displayed on the 80 channel kicksorter. A typical ungated spectrum is shown in Figure 36. This shows the well known distribution of α-particles from the $B^{10}(d,\alpha)Be^{8}$ reaction with the narrow ground state group and the broad group corresponding to the 3 MeV state of Be^{8}. Superimposed on the background of the secondary α-particles from the breakup of Be^{8}, are peaks corresponding to proton groups from the $B^{10}(d,p)B^{11}$ and $C^{12}(d,p)C^{13}$ reactions. The energies of these groups are marked on the figure. The proton groups corresponding to transitions to the ground and first excited level of B^{11} are not resolved from the α-particle spectrum. The group at 2.98 MeV is contributed by the $C^{12}(d,p)C^{13}$ reaction which arises through deposition on the target of carbon originating from the oil diffusion pumps of the vacuum system. This could be reduced with a liquid air trap in the beam tube and with hot water in the "cooling" tubes to the target. However, the height of this proton peak increased steadily with running time and after about 6 hours was roughly equal to the height of the peak at 2.70 MeV.

The proportional pulses from counter 1 were used as a monitor and the discriminator setting which is marked on Figure 36. was chosen to eliminate the large variations in counting rate which would otherwise arise from the increasing yield from the $C^{12}(d,p)C^{13}$ reaction.

The gated spectrum from counter 1 was recorded for a fixed number of monitor counts for each of three values of ϕ; 140°, 128° and 104°. The results are shown in Figure 37. Each of these distributions was the sum of four runs each of about 50 minutes duration. Between each of the runs the ungated spectrum was recorded and the positions of the proton peaks used as a check on the stability of the recording equipment.

The low intensity peaks evident in these spectra were again proton peaks. The proton pulses from counter 1 were gated by coincidence events occurring between these protons, in counter 1, and the corresponding de-excitation gamma-rays in counter 2. This was checked with an aluminium foil over the side crystal thick enough to stop all α-particles. The gated spectra recorded under these conditions showed clearly that p γ coincidences were being detected.

Since the proton group at 4.93 MeV obscured an important section of the α-particle spectrum, an extra thickness of aluminium foil, 3.6 mgm/cm^2, was placed between the target and the end crystal and the gated spectrum recorded again for the case of $\phi = 128^{\circ}$. The effect of the foil is to leave almost unchanged the pulse height of the proton peaks, but to reduce the α-particle energies sufficiently to bring the pulse heights of those α-particles previously obscured into a region free from proton pulses. This spectrum is shown in Figure 37. (c)

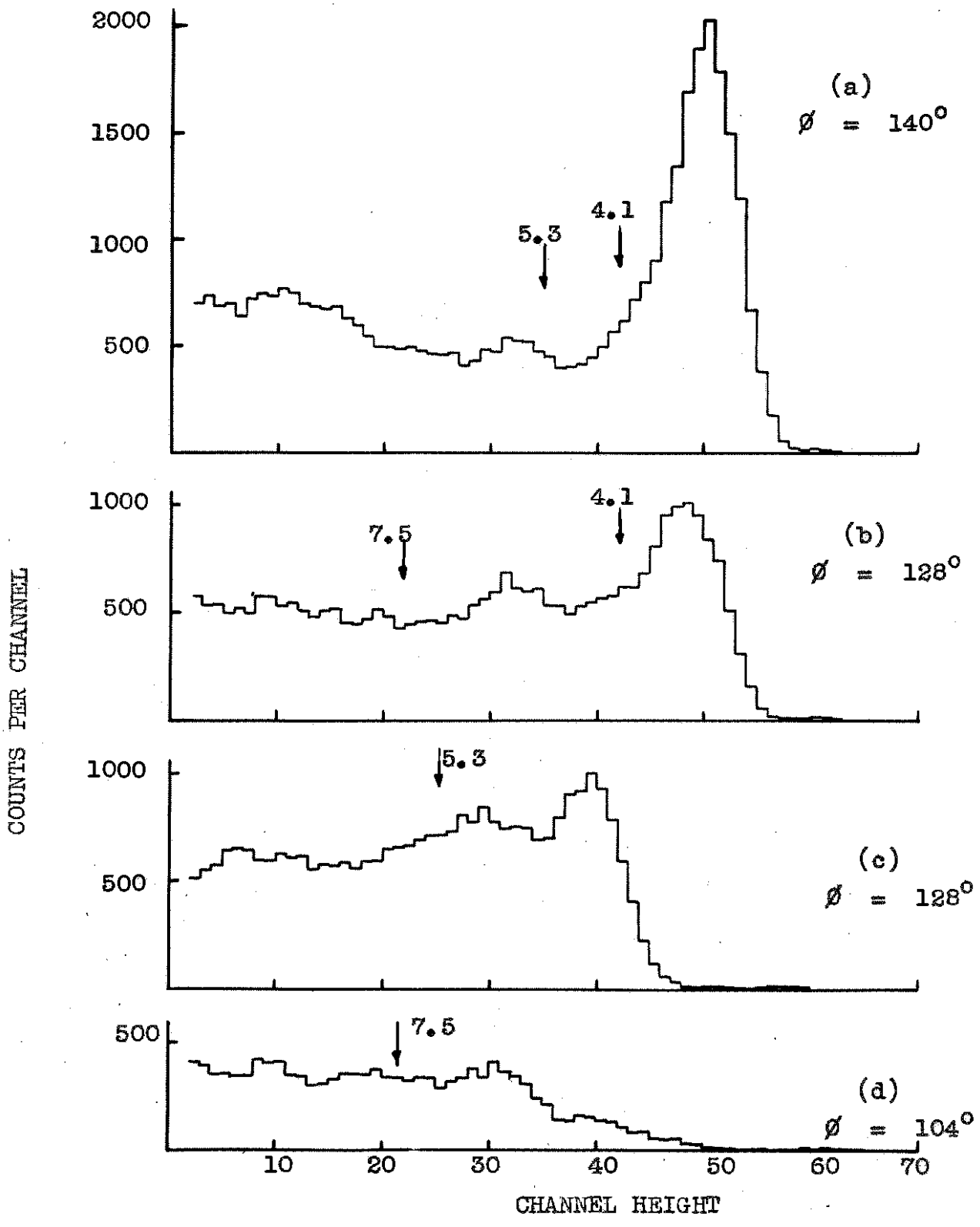

FIGURE 37. GATED α-PARTICLE SPECTRA.

5.5 Interpretation of the Gated Spectra.

The calibration of the pulse height scale in terms of α-particle energy could be done independently up to 8.8 MeV using the α-particles from ThC and C'. Beyond this energy only two calibration points were available - the positions of the peaks corresponding to the α-particle transitions to the ground and first excited state of Be^8 which occur at energies of 13.1 MeV and 11.0 MeV respectively. The width of the 11.0 MeV group, and the fact that there is an unresolved proton group in this region, introduces an uncertainty of about 300 KeV in the position of this point. In this way the calibration of energy against channel voltage was obtained for both foil thicknesses used in the experiment.

As was mentioned in section 5.2, each curve of Figure 37. is the combination of the distributions resulting from each of three modes of detection, i.e. the ordinate at each α-particle energy is built up from contributions from each mode, each of which involves a different excitation energy of Be^8. We shall derive here the relation between α-particle energy as measured in counter 1, and the corresponding excitation energy of Be^8 for each of the three modes.

For mode i), there was a unique value of the primary α-particle energy, E_α, corresponding to each value of the Be^8 energy, E. The finite solid angle of the end counter

introduced a spread of less than 10 KeV in the primary α-particle energy. In the present experiment, for a deutron bombarding energy of 360 KeV, $E_\alpha = 2(\sqrt{\frac{18.11-E}{3}} + .10)^2$ This relation is shown plotted as the solid curve in Figure 38.

For mode ii), the energy of the secondary α-particles resulting from the break-up of the Be^8 nucleus with energy E was not uniquely determined. The finite solid angles of the two counters introduced a spread in energy of about 3 MeV. For any value of E, the mean value of the energy of the secondary α-particles also depended on ∅. The relation between E and E_α for this case was found graphically and is shown in Figure 38. for the three values of ∅. Since the minimum α-particle energy required to operate the coincidence circuit was 2 MeV, levels in Be^8 above 15 MeV would not contribute any events from i) or ii). For mode iii), the α-particle energies were spread over a very wide range and events of this type were recorded only for values of E within certain limits. These limits depended on the angle ∅. The relations in this case were also found graphically, and are shown for two values of ∅. For $\emptyset = 140^\circ$, only values of E greater than 12 MeV contribute events and the relation for this case has not been shown.

With the information contained in Figure 38. some conclusions can now be drawn from the gated spectra shown in Figure 37. Figure 37 (a) shows the spectrum recorded for $\emptyset = 140^\circ$, and the position is marked at which primary

α-particles leading to Be^8 with energies of 4.1 and 5.3 MeV would appear. For E = 4.1, E_α = 10.2, and Figure 38. indicates that only levels above 8 MeV would contribute secondary α-particles above this energy. Since no sharp levels have been observed in this region it is reasonable to assume that the spectrum above about 10 MeV was almost entirely contributed by primary α-particles. Thus, since the pulse height resolution in this region was about 5%, failure to observe any fine stucture in this region of the distribution is significant.

For Figure 37 (b), a similar argument suggests that only levels above 10 MeV will contribute to the counts above the position marked for E = 4.1 MeV. However, in this case, the solid angle effect makes the interpretation of the distribution in this region uncertain.

In Figure 37 (c), the only levels contributing to the counts at E = 5.3 MeV lie above 8 MeV and any group occurring in this region should not be obscured by the presence of secondary α-particles.

At the position indicated for E = 7.6 MeV in Figure 37 (d), there will be a small contribution from levels between 6 and 9 MeV and above 11 MeV, but, since this would be very broad, any group appearing in this region should be observed.

Upper limits to the intensity of unobserved groups are difficult to assess because of the variation in effective solid angle with energy. However, it can be stated approximately that groups 1 MeV wide would have been

observed if their intensity were greater than 5% the intensity of the group at 3 MeV. For sharper groups, this limit is lower.

5.6 Further analysis of the Gated Spectra.

It was possible to draw some further conclusions from the results of Figure 37, but before this could be done the background due to chance and p-γ coincidences must be subtracted from the distributions.

The random spectrum was obtained as the gated spectrum recorded with a delay of 2 μsec. inserted in one or other of the channels. Ideally the random spectrum should be recorded simultaneously with the recording of the true plus random gated spectrum, but as this was not possible, the random spectrum was recorded directly after the other for the same number of monitor counts. This would correspond to the required spectrum provided that the counting rate, i.e. the beam current, was maintained at the same level in both cases.

Since the shape of the random spectrum is identical with the shape of the ungated spectrum, it was necessary, in fact more accurate because of the small numbers involved, to record the random spectrum only once to ascertain the total number of random events for a given number of monitor counts. The ungated spectrum which had been recorded between each run was then

scaled suitably to give the random spectrum in each case. Since the time to record each gated spectrum was 50 minutes, this procedure also greatly reduced the total time involved in the experiment.

The contribution to each gated spectrum from the p-γ coincidences was constant throughout the experiment since it did not depend on the counting rate and did not include the variable group resulting from the $C^{12}(d,p)C^{13}$ reaction, as the protons in this case leave C^{13} in its ground state. Thus p-γ coincidence spectrum was only recorded once. As mentioned above, it was obtained simply as the gated spectrum with an α-particle stopping foil placed over the side crystal.

In Figure 39. the distributions (a), (b) and (d) of Figure 37. are shown with the random and p-γ backgrounds subtracted. The scale of the abscisson has been converted to an energy scale with the aid of the calibration obtained above. Since this calibration was not linear, the ordinates of the figure have been corrected as described in section 2.2.

These three distributions each contain contributions from the three modes of detection and it should be possible to obtain a consistent interpretation of the primary α-particle spectrum with the aid of Figure 38. Before this could be done, however, it was necessary to calculate the variation of the effective solid angle with energy and angle for each of the three modes. This

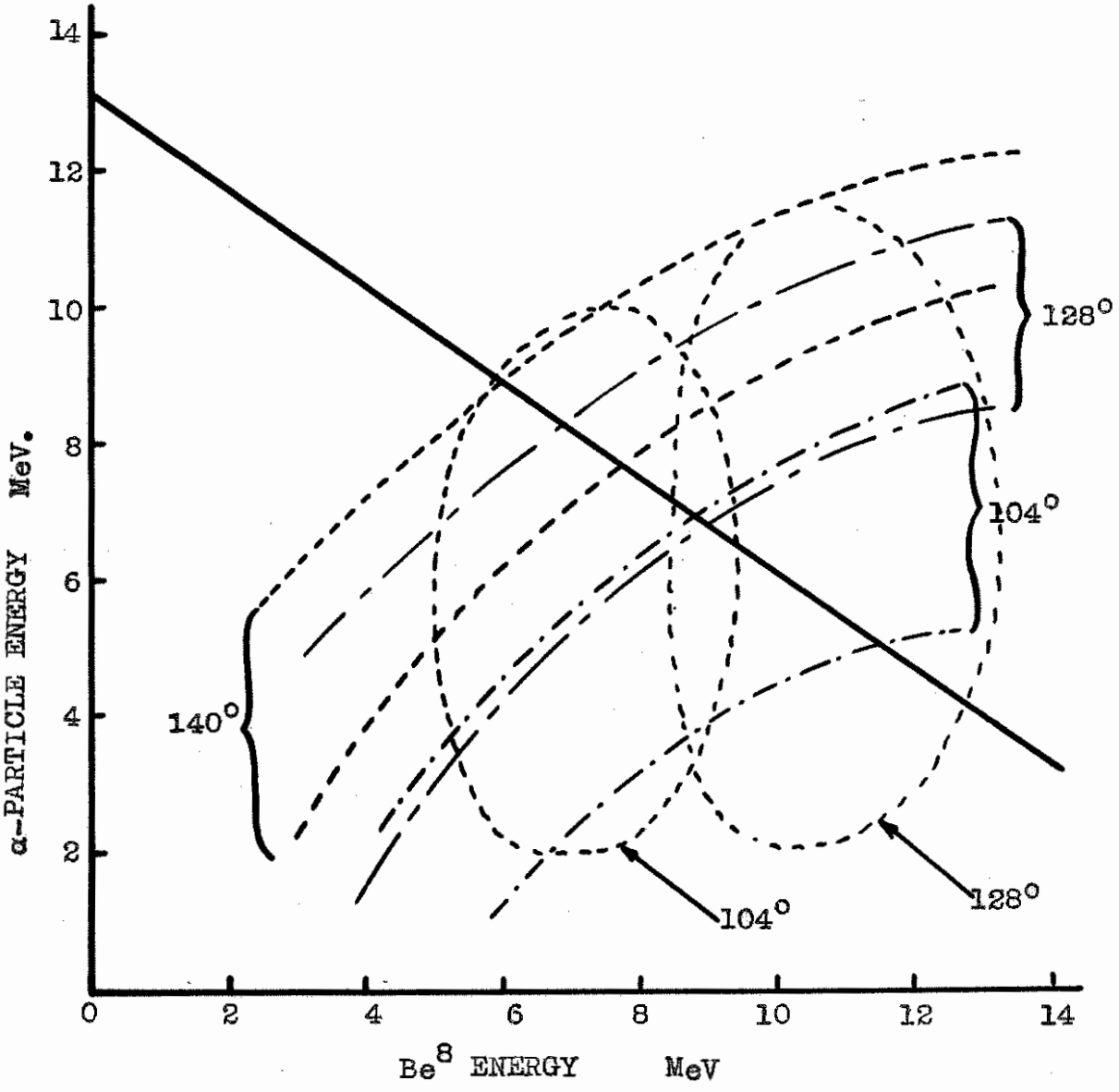

FIGURE 38. RELATION BETWEEN α-PARTICLE ENERGY AND EXCITATION ENERGY OF Be^8.

wasdone graphically for mode i) and the results for the three values of ϕ are shown in Figure 40. This result was also assumed to apply to mode ii), since the two modes were symmetrical if the small effect of the centre of mass motion was neglected. The variation of effective solid angle for mode iii) could not be derived explicity, but is implied in the curves of Figure 38.

In all these calculations it has been assumed that both the angular distribution of the primary α-particles and the angular correlation between the primary and secondary α-particles is isotropic. There is no evidence in the literature regarding the spin of the level in C^{12} which is formed by the capture of deuterons by B^{10}. This level can have a spin of 2, 3 or 4 and it is by no means certain that the distributions are isotropic, since only the value 2 would require such isotropy.

The fact that the values of the effective solid angle were the same for each value of ϕ over part of the energy range, simplified the interpretation of Figure 39. The dotted curves in this figure are the results of a trial and error process continued until consistency was obtained between the three ϕ values and with Figures 38. and 40. The areas above the dotted curves for $\phi = 140^{\circ}$ and 128° represent the contribution from mode ii) and the area below the dotted curve for $\phi = 104^{\circ}$, the

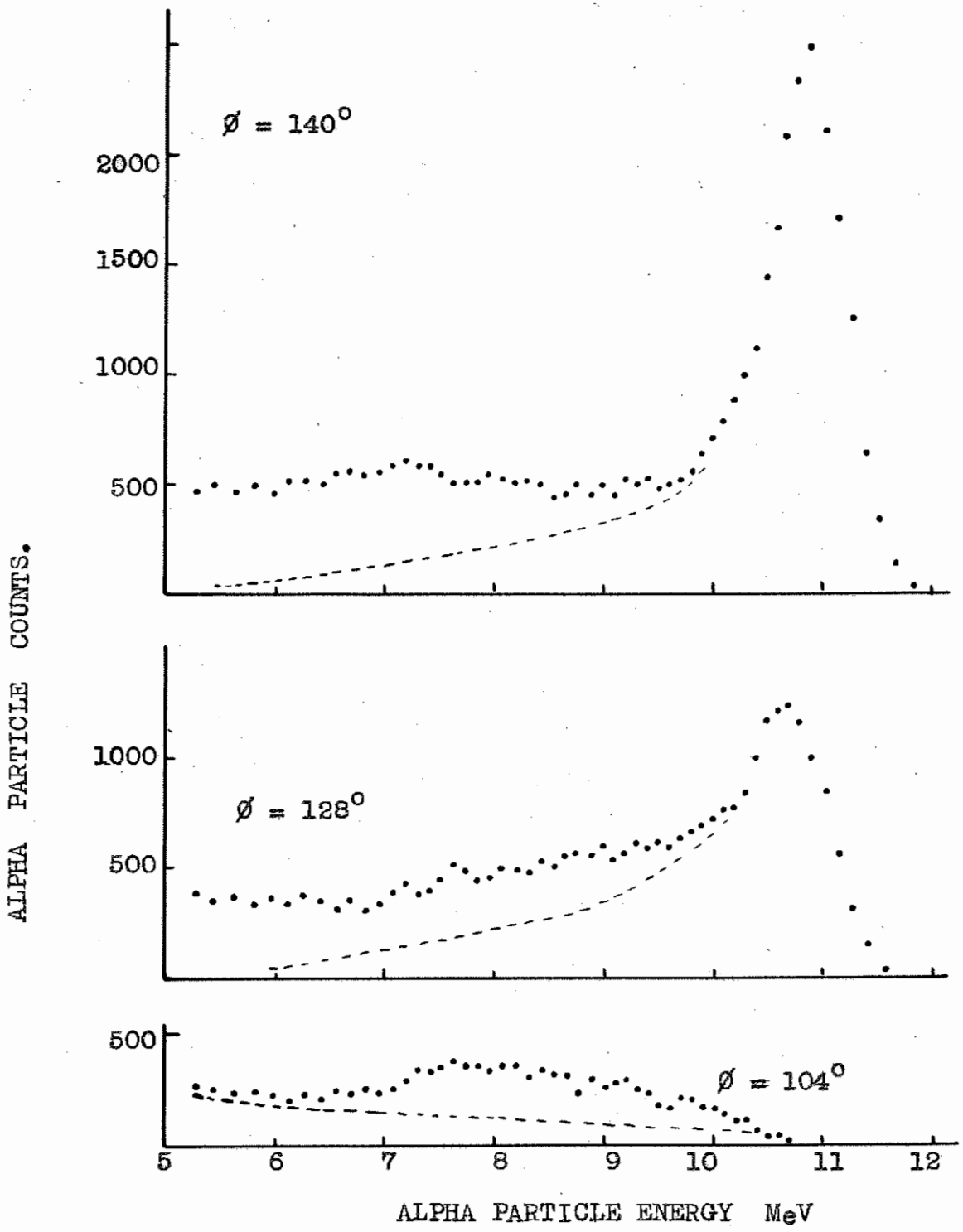

FIGURE 39. CORRECTED ALPHA PARTICLE SPECTRA.

contribution from mode iii). The remaining areas represent the contribution from mode i) alone.

Each of these primary α-particle distributions was corrected for the variation of effective solid angle and the results are shown combined in Figure 41. The vertical lines through the curve indicate the probable errors in the ordinate of the curve at each point relative to that at 3 MeV. Below 3 MeV the shape of the curve is very uncertain as this covers the energy range over which the effective solid angle varies rapidly with energy.

5.7 Conclusions and Subsequent Experimental Evidence.

The general conclusions to be drawn from the work described in this chapter and the preceeding one are the same. In both the experiments, the energy region in Be^8 from 2 to 9 MeV has been examined and no evidence found for levels other than that at 3 MeV. This level has a width in these experiments of approximately 1.5 MeV, and extends throughout the energy range examined. This is in general agreement with the theoretical predictions discussed in Chapter 3.

The experiments mentioned in Chapter 3, which have been interpreted to suggest other levels in Be^8 can all be explained in terms of this one very broad level when allowance is made for the statistical

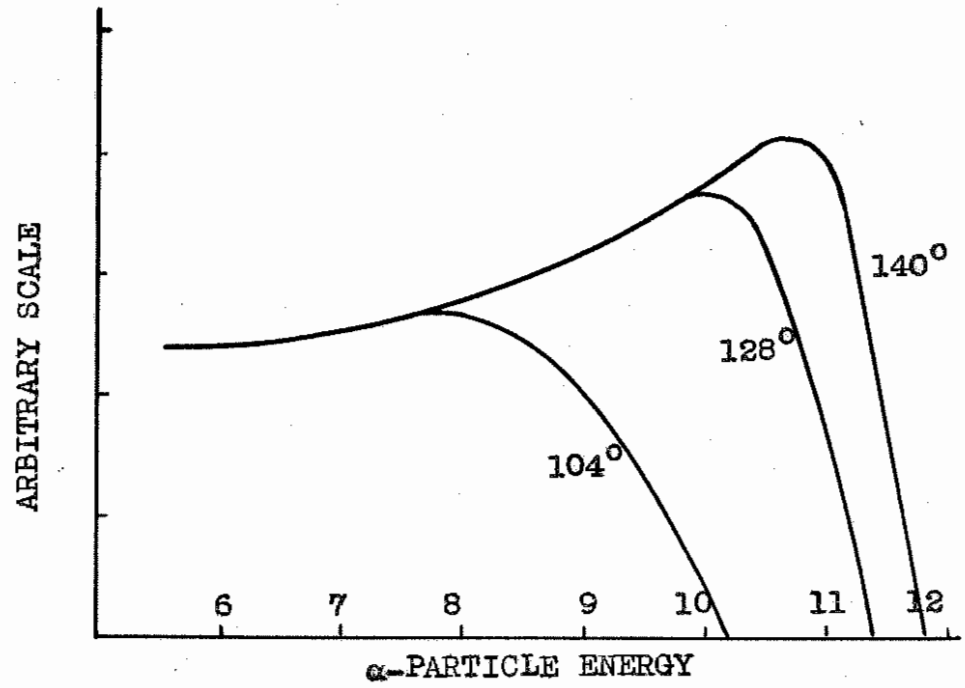

FIGURE 40. VARIATION OF EFFECTIVE SOLID ANGLE WITH ENERGY.

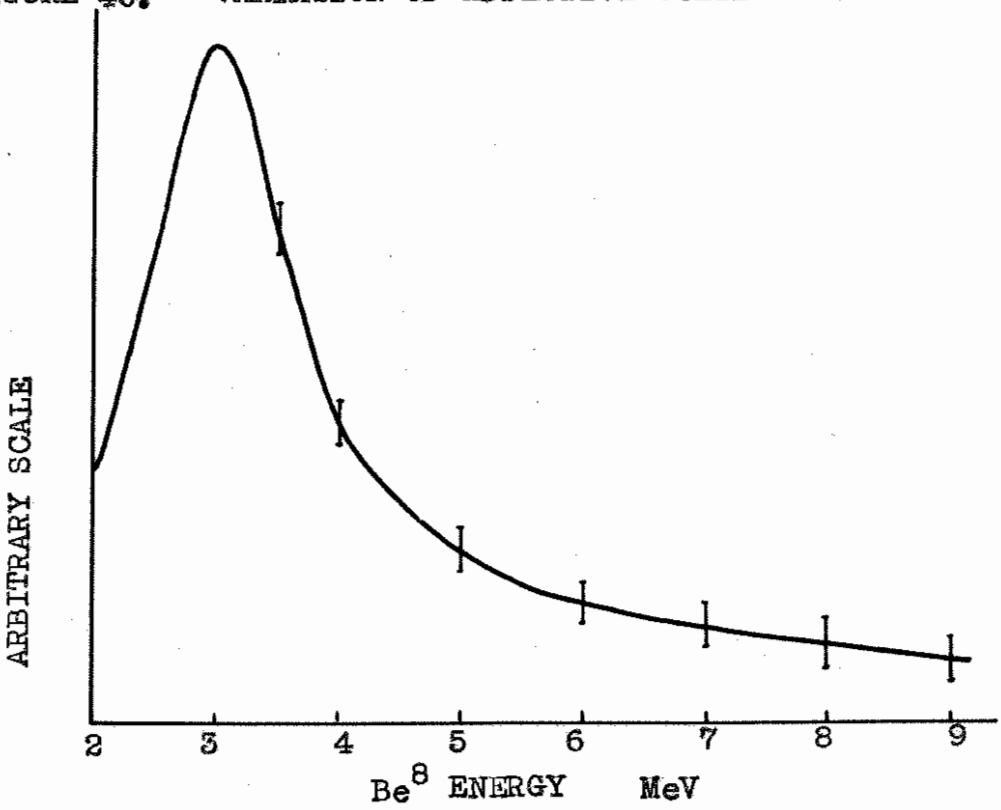

FIGURE 41. TRANSITION PROBABILITY.

uncertainties introduced by the small number of counts recorded in each case. The one exception to this conclusion is the result obtained in the α-α scattering experiment performed by Steigert and Sampson[55]. However, this experiment has since been repeated by Nilson[64], who finds no evidence for an S level at 7.5 MeV, but confirms the existence of the D and G levels at 2.9 and 10.8 MeV respectively.

Many experiments have recently been performed employing a varity of reactions to excite the Be^8 nucleus and some of these will be discussed in Chapter 7. Most of the experiments involved the observation of very large numbers of events and, in general, confirmed the results of the present work. Two of the experiments[65,66] also suggested evidence of a very broad level at approximately 12 MeV, thus confirming the results of the α-α scattering work[64].

Two groups of workers, however, report results which indicate other levels in Be^8. Cüer et al[67] have examined the α-particle spectrum from the

---

64. Nilson, R., Ph.D. Thesis. Illinois, 1956.

65. Moak, C.D., and Wisseman, W.R., Phys.Rev. 101: 1326, 1956.

66. Frost, R.T., and Hanna, S.S., Phys.Rev. 99: 8, 1955.

67. Cuer, Jung and Bilwest, Compt.rend. 238: 1405, 1955.

$B^{10}(d,\alpha)be^{8}$ reaction with photographic plates at four angles with a deuteron bombarding energy of 1 MeV. Groups are shown in their distributions at 4.0, 4.9 and 7.2 MeV. The most prominent of these is the 7.2 MeV group observed at 0^{o}, which is made up of five high points, 12% above the continium. Cüer et al also suggests that the intensity of the groups varies with the angle of detection. However, Holland et al[68], have examined the same spectrum with a magnetic spectrometer for a range of angles and deuteron energies. The number of counts recorded at the 2.9 MeV peak in these experiments was over 5,000 compared to 500 events in the experiment of Cüer et al. No evidence was found for any low intensity groups. It is interesting to note that a group observed by Treacy[63] at 7 MeV was attributed by him to carbon contamination.

Gilson and Prowse[69] report levels at 2.1, 4.0 and 5.3 MeV, observed in the neutron spectrum from the $Li^{7}(d,n)Be^{8}$ reaction. Photographic plates were employed and 170 events were observed at the

---

68. Holland, Inglis, Malm and Mooring, Phys.Rev. 99: 92, 1955.

69. Gibson, W.M., and Prowse, D.J., Phil.Mag. 46: 807, 1955.

2.9 MeV peak. Trial and Johnson[70, 71] however, did not observe any groups when they examined the same neutron spectrum with a scintillation spectrometer which had a resolution of about 8%. They observed 400 counts at the 2.9 MeV peak.

Thus the overwhelming evidence is in support of the conclusions drawn above.

---

70. Trail, C.C., and Johnson, C.H., Phys.Rev. 95: 1363, 1954.

71. Trail, C.C., and Johnson, C.H., private communication.

SECTION C

THE SPIN AND SHAPE OF THE FIRST EXCITED LEVEL OF Be^8.

CHAPTER 6

THE ANGULAR CORRELATION BETWEEN THE DIRECTIONS OF EMISSION OF THE α-PARTICLE AND THE GAMMA-RAYS FROM THE $Li^7(p,\gamma)Be^8(\alpha)He^4$ REACTION.

6.1 Introduction.

All the general theoretical models of the Be^8 nucleus suggest that the level at 3 MeV is a D state, but until recently there has been very little evidence to confirm this.

Studies of the shape of the α-particle spectra observed in the photodisintegration[72] of C^{12} and in the reaction $B^{10}(d,\alpha)Be^8$ [63], are consistent with a spin 2 for this level. Geer et al[73] also make this assignment on the evidence of the α-α angular correlations in the $B^{11}(p,\alpha)Be^8(\alpha)He^4$ reaction. This chapter describes a direct determination of the spin from the measurement of the correlation between the directions of emission of α-particles and gamma-radiation at the 440 KeV resonance in the reaction $Li^7(p,\gamma)Be^8\alpha(He^4)$.

The level in Be^8 at 17.63 MeV is formed by p-wave protons with channel spins 1 and 2 in a ratio

---

72. Telegdi, V.L. Phys. Rev. 84: 600, 1951.

73. Geer, E.H., Nelson, E.B., and Wolick, E.A. Phys. Rev. 100: 215, 1955.

of 1 to 5[74]. This establishes that the level has $J = 1^+$ and accounts for the observed isotropy of the capture gamma-radiation[75] since this mixture of channel spins results in equal population of the magnetic substates.

The measurement of the angular distribution of the radiation off the 441 KeV resonance[61] indicated individual anisotropy of the two components leading to the ground and 3 MeV levels respectively. This implies that the spins of these levels are different, and since the levels are known to disintegrate into two α-particles, the spins must be even.

Values of the spin greater than 2 would imply that the radiation from the $J = 1$ level was octupole or higher order radiation. The intensity of such radiation would be less than magnetic dipole or electric quadrupole radiation by a factor of approximately 10^6 [76]. Since the intensity of the transitions to the ground and 3 MeV level are of the same order of magnitude the spins of these levels must be either 0 or 2.

For $J = 0$, the radiation is pure magnetic dipole and the angular correlation between the gamma radiation and the disintegration

---

74. Warters, Fowler and Lauritsen, Phys.Rev. 91: 917, 1953.

75. Devons,S., and Lindsay,G.R., Proc.Phys.Soc. 63A: 1202 1950.

76. Blatt,J.M., and Weisskopf,V.F. "Theoretical Nuclear Physics". John Wiley and Sons, 1952.

α-particle is isotropic. For J = 2, the radiation can be a mixture of both magnetic dipole and electric quadrupole and the angular correlation function has the general form

$$W(\theta) = 1 + A_2P_2(\cos\theta) + A_4P_4(\cos\theta)$$

where θ is the angle between the axes of the detectors, A_2 and A_4 are constants and $P_2(\cos\theta)$ and $P_4(\cos\theta)$ are the second and fourth order Legendre polynomials respectively.

In Chapter 4, three experiments were described in which the spectrum was obtained from those α-particles in coincidence with a gamma-ray. In these three cases the angle θ between the detectors was 180°. This chapter describes the extension of these experiments to cover a range of values of θ.

The angular correlation between α-particles and gamma-rays is easily determined in a simple case that involves only a single narrow level of the intermediate nucleus. It is only necessary to record the number of coincidences for a fixed number of particles detected in one counter, as a function of the angle between the counters. The $F^{19}(p,\alpha,\gamma)O^{16}$ reaction is an example of this kind. At the 340 KeV proton resonance, 98% of the transitions involve the narrow 6.1 MeV level of O^{16}. In the $Li^7(p,\gamma,\alpha)He^4$ reaction, however, there is no narrow level in Be^8 through which all the transitions proceed. In this case it is

necessary to record the gated α-particle spectrum for several values of θ, each for a fixed number of gamma-ray events. From the results, the correlation between the gamma-radiation and α-particles can be found for transitions through different regions of excitation of Be^8.

6.2 Experiment I.

With the apparatus described in Part C of Chapter 4, the α-particle spectrum was recorded for four angles between the counters: 120°, 140°, 160° and 180°. The α-counter was fixed at 90° to the beam and the gamma-counter could be rotated in the plane perpendicular to the beam. The four distributions are shown in Figure 42. Each spectrum is the sum of a number of separate runs of about 20 minutes duration, each recorded for the same number of monitor counts. The beam current was about 7 μA. Four times as many runs were made at 120° and 180°, than at the two intermediate angles. The shift in α-particle energy with changing direction of gamma-ray emission is apparent from the curves, and gamma-particle energies at the maxima of the four distributions correspond to an excitation energy in Be^8 of 2.95 ± 0.03 MeV.

The angular correlation associated with this energy of Be^8 is plotted in Figure 43. and was obtained from

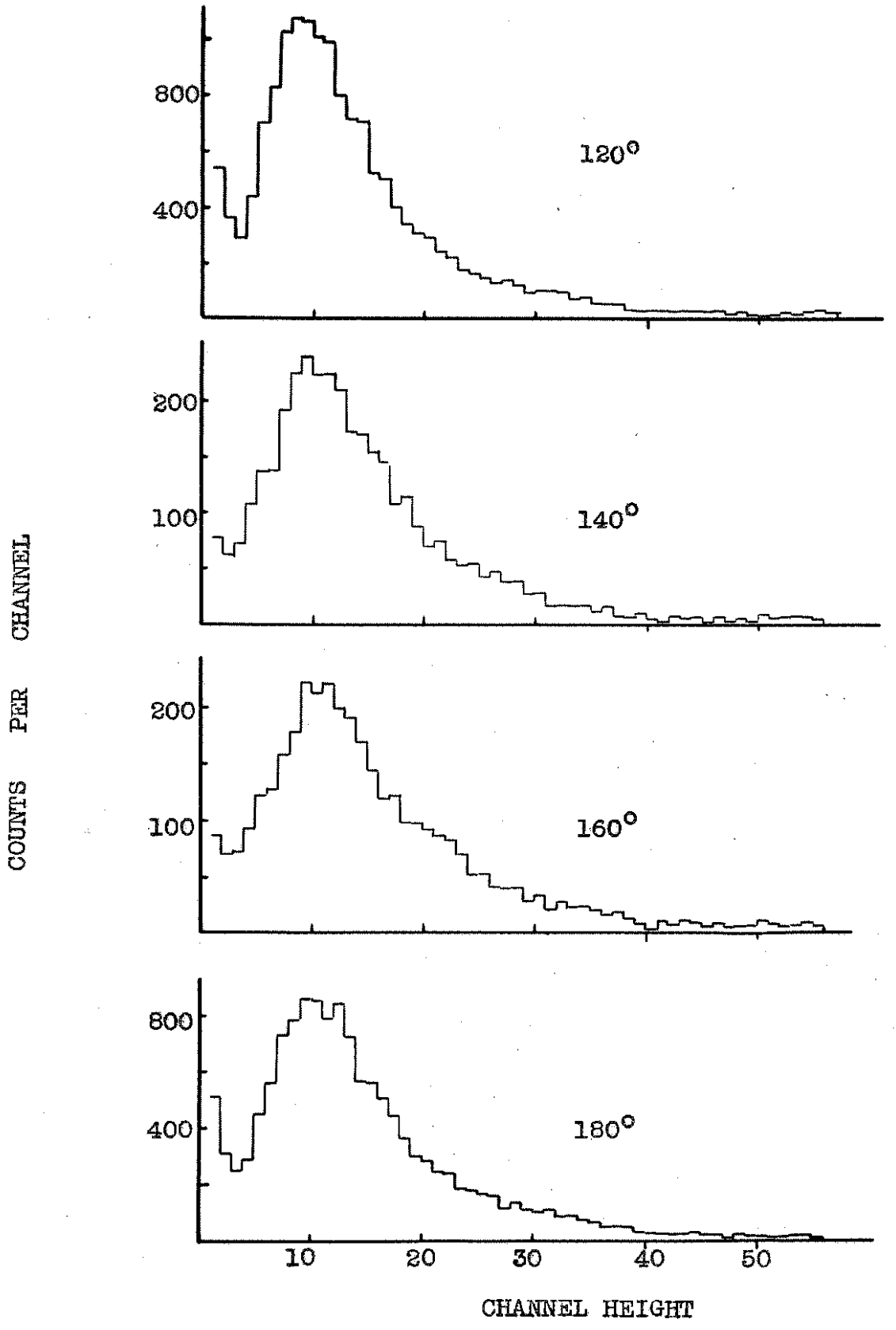

FIGURE 42. GATED SPECTRA.

the ordinates of the maxima of the four spectra of Figure 42. The small contribution from random coincidences, amounting to twenty counts at the peak energy, was subtracted before the ratios were taken. Since the actual α-particle energy at the maximum varies, there is also a small correction of 2%, arising from the non-linearity of the calibration of pulse height against α-particle energy.

The errors shown on the points were calculated from the results of the many runs which made up each of the spectra. The variation of the peak height of the spectra taken at any one angle for a fixed monitor count was not purely statistical. Because of the collimation that was necessary between the target and the crystal detector, (see Figure 30), the solid angle subtended by this detector at the target depended very much on the position of the irradiated area. Thus variations in the beam direction produced changes in the efficiency of the α-particle detector. The monitoring of the disintegration rate should be done with the α-particle detector, but this was not possible because of the large proportion of events in this counter which arose from reactions other than the one under study. Use of the gamma-ray counter as the monitor gave a measure of the actual disintegration rate, but not the effective disintegration rate that was required. Thus coincidence spectra recorded for the

same number of gamma-ray monitor counts may differ because the average of the effective solid angle over the period of each run may be different in each case. This variation was kept to a minimum by collimating the beam and recording spectra only when the accelerating machine was operating as steadily as possible.

It is immediately apparent from the anisotropy indicated in Figure 43. that the spin of the level in Be^8 at 2.95 MeV must be 2. The true correlation can therefore be expressed in the form

$$1 + A_2 P_2(\cos\theta) + A_4 P_4(\cos\theta) \ldots\ldots\ldots\ldots (1)$$

where A_2 and A_4 are constants.

The experimental correlation, as represented by the curve drawn through the points of Figure 43, will have the same form as (1) but because of the finite solid angle of each the detectors, the constants A_2 and A_4 will be changed. The experimental correlation can be written as

$$1 + a_2 A_2 P_2(\cos\theta) + a_4 A_4 P_4(\cos\theta).$$

The constants a_2A_2 and a_4A_4 can be determined from the curve in Figure 43. and have the values $a_2 A_2 = -0.18 \pm 0.01$ and $a_4 A_4 = 0.016 \pm 0.008$.

The solid angle correction factors, a, have been given by Devons and Goldfarb[77]

---

77. Devons, S., and Goldfarb, Handbuch der Physik (in press).

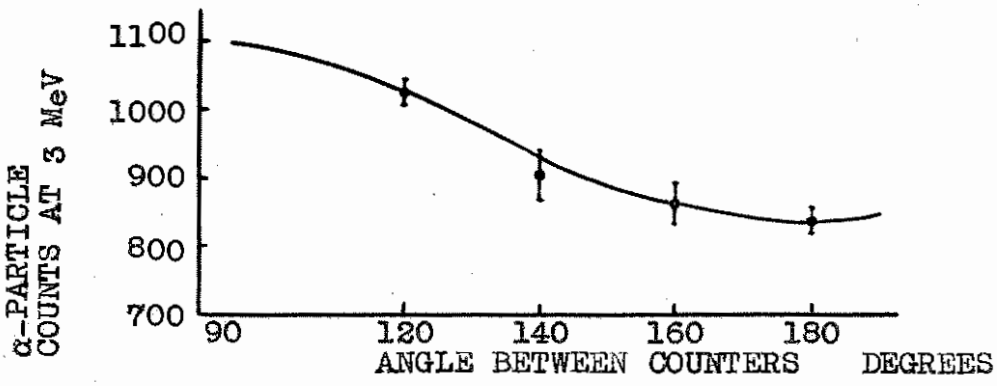

FIGURE 43. ANGULAR CORRELATION AT 3 MeV

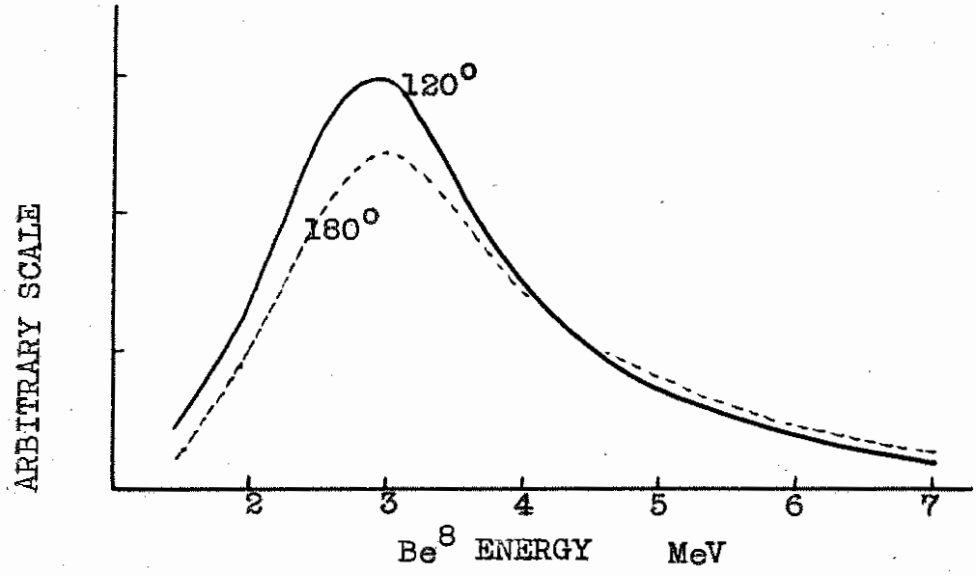

FIGURE 44. TRANSITION PROBABILITY.

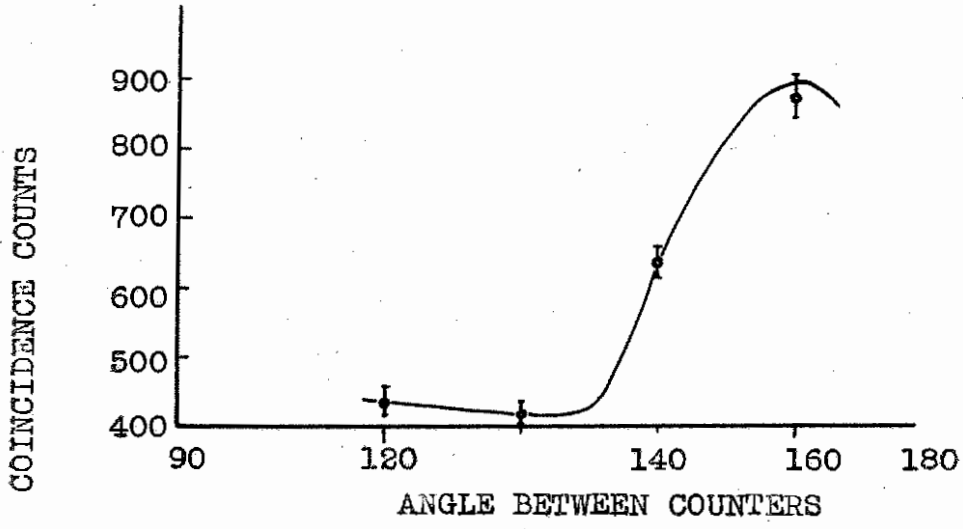

FIGURE 45. ANGULAR CORRELATION WITH FLUORINE.

as $a_k = a_k^{\alpha} \cdot a_k^{\gamma} < 1$

where $$a_k^{\alpha} = \frac{\int_o^{\phi_\alpha} P_k(\cos\phi) e_\alpha(\phi) d(\cos\phi)}{\int_o^{\phi_\alpha} e_\alpha(\phi) d(\cos\phi)}$$

A similar expression holds for a_k^{γ}. ϕ_α is the half-angle of the α-particle detector, and $e_\alpha(\phi)$ the efficiency of this detector for radiation incident at an angle ϕ to the central vector. Here, both $e_\alpha(\phi)$ and $e_\gamma(\phi)$ are assumed to be constant. This is strictly true for $e_\alpha(\phi)$ and holds approximately for $e_\gamma(\phi)$.

The values of a_k can be calculated approximately from the geometry of the experimental arrangement where $\phi_\alpha = 3^\circ$ and $\phi_\gamma = 8^\circ$. This leads to the following values.

$$a_2 = 1 \text{ and } a_4 = 0.95.$$

However, the values of a_2 and a_4 can be obtained with more certainty from the results of an experiment performed under exactly the same conditions using the reaction $F^{19}(P,\alpha\gamma)O^{16}$ for which the theoretical angular correlation is known. With this reaction it was possible to monitor with the α-particle counts and so eliminate the effects of any variation in the effective solid angle. The experimental points shown in Figure 45. are fitted best by the curve

$$1 + 0.67P_2(\cos\theta) + 0.032P_4(\cos\theta) + 0.61P_6(\cos\theta)$$

Since the theoretical distribution is given by

$$1 + 0.76P_2(\cos\theta) + 0.051P_4(\cos\theta) + 1.70P_6(\cos\theta)$$

the values of the constants are then found to be

$$a_2 = 0.89 \pm 0.01,\ a_4 = 0.64 \pm 0.02 \text{ and } a_6 = 0.36 \pm 0.04$$

The values of a_2 and a_4 found in this way are seen to be smaller than the values determined above from the geometrical calculations. This is due to the fact that the effective solid angle of the gamma-counter is not given entirely by its actual dimensions. It is increased by the presence of large masses in the neighbourhood of the target, particularly the magnet, which scatter into the counter, gamma-rays which have been emitted at angles other than those subtended by the counter itself. The values of a_2 and a_4 found above imply that the effective value of ϕ_γ is 23°.

Using these values for a_2 and a_4 and the values given above for $a_2 A_2$ and $a_4 A_4$ we obtain

$$A_2 = -0.202 \pm 0.014 \text{ and } A_4 = 0.025 \pm 0.013$$

Examination of the distributions shown in Figure 42. indicate that the angular correlation tends to become more isotropic as the excitation energy of Be^8 increases. If any such effect is present it would be obscured in these results by the broadening introduced by statistical effects in the multiplier. An approximate picture of the actual situation can be obtained by removing this broadening. This was done as described in Part C. of Chapter 3, and the results for 120° and 180° are shown in Figure 44. where the scale of the abcissa is now the

energy of excitation of Be^8. It is apparent from this Figure that the correlation does change markedly with energy E and more information regarding this trend is examined in the following sections.

6.3 Experiment II.

The experiment which was described in Part A of Chapter 4 has been extended by Inall[78] to examine the angular correlation in the Be^8 energy range of 4 - 7.5 MeV.

Inall recorded the number of coincidence counts obtained for a fixed number of gamma-rays with absorber thicknesses of 1.01 and 1.23 cm. air equivalent. Each reading was repeated several times at each of several angles between the counters. The difference between the number of counts obtained for the two absorbers is shown plotted against the angle in Figure 46. The same procedure was repeated for absorber thicknesses of 1.34 and 1.93 cm. air equivalent. It is apparent from these results that, qualifatively, these correlations are significantly different from that obtained in section 6.1 for a Be^8 energy of 3 MeV. However, the final interpretation of these results depends very much on the

---

78. Inall, E.K., Phil.Mag. 45: 768, 1954.

level structure of Be^8 in the region examined.

Since the recorded energy of an α-particle arising from a transition through a particular energy of Be^8 depends on the angle of emission of the corresponding gamma-rays, the range of Be^8 energy involved in each count in Figure 46. is different for each angle. This range can be calculated from the mechanics of the reaction and from the range-energy relations for α-particles. Table 4. gives the results for both absorber ranges.

TABLE 4

RANGE IN Be^8 -E MeV.

Absorber Range	180°	150°	120°	90°
1.01 cm. - 1.23 cm.	3.40-4.20	3.46-4.26	3.63-4.43	3.85-4.65
1.34 cm. - 1.93 cm.	4.56-6.03	4.62-6.09	4.79-6.26	5.01-6.48

If the level structure is as indicated in curve (b) of Figure 23, then each of the absorber ranges covers only a single level, and the angular correlations involving these levels are given by Figure 46. This is the interpretation given by Inall. However, since it has been shown that the level structure is of the form given by curve (a) of Figure 23, the conclusions to be drawn from the results in Figure 46 are considerably modified.

The varying energy range covered at each angle

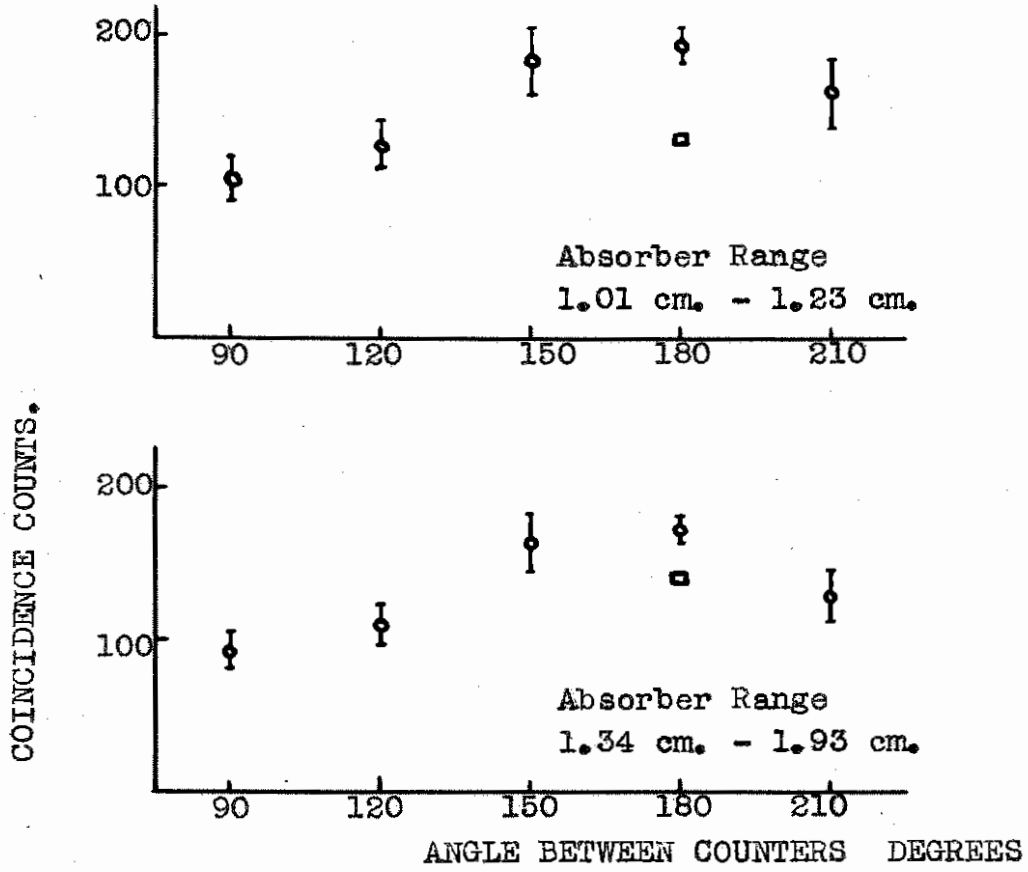

FIGURE 46. ANGULAR VARIATION OF COINCIDENCE COUNTS.

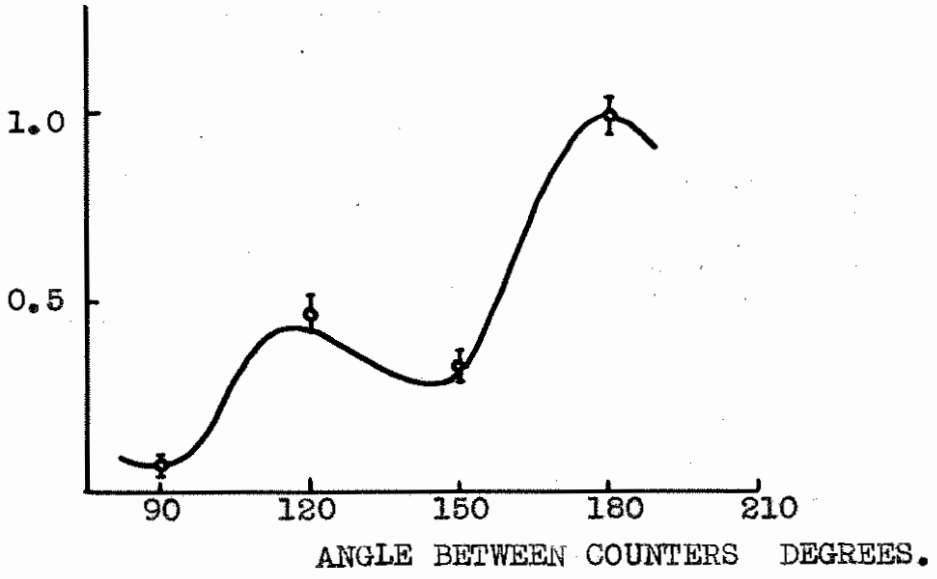

FIGURE 47. ANGULAR CORRELATION WITH FLUORINE.

increases the apparent anisotropy of the observed correlation since the mean value of E involved in each count increases, and hence the transition probability decreases, as the angle between the counters decreases. The count obtained at 180° can be corrected with the aid of Figure 32. to give the count that would be obtained in the same energy range that is involved in the count at 90°. These corrected points are shown in Figure 46.

Thus the ratio of $\frac{W(180^{\circ})}{W(90^{\circ})}$ averaged over a small energy range, can be determined in the two cases with the results

$$\frac{W(180^{\circ})}{W(90^{\circ})} = 1.22 \pm 0.14 \text{ for the mean E} = 4.25 \text{ MeV}$$

and 1.46 ± 0.14 for the mean E = 5.7 MeV

6.4 Experiment III.

The results quoted in the previous section could be checked by extending the method described in Part B, Chapter 4. Also the region of Be^{8} energy around 7 and 8 MeV could be examined.

The gated α-particle spectrum was recorded at 180° and 90° for the same total gamma-ray count. The two distributions are shown in Figure 48. together with the random gated spectrum recorded for the same monitor count. The positions corresponding to some values of the Be^{8} energy are marked on the Figure. These

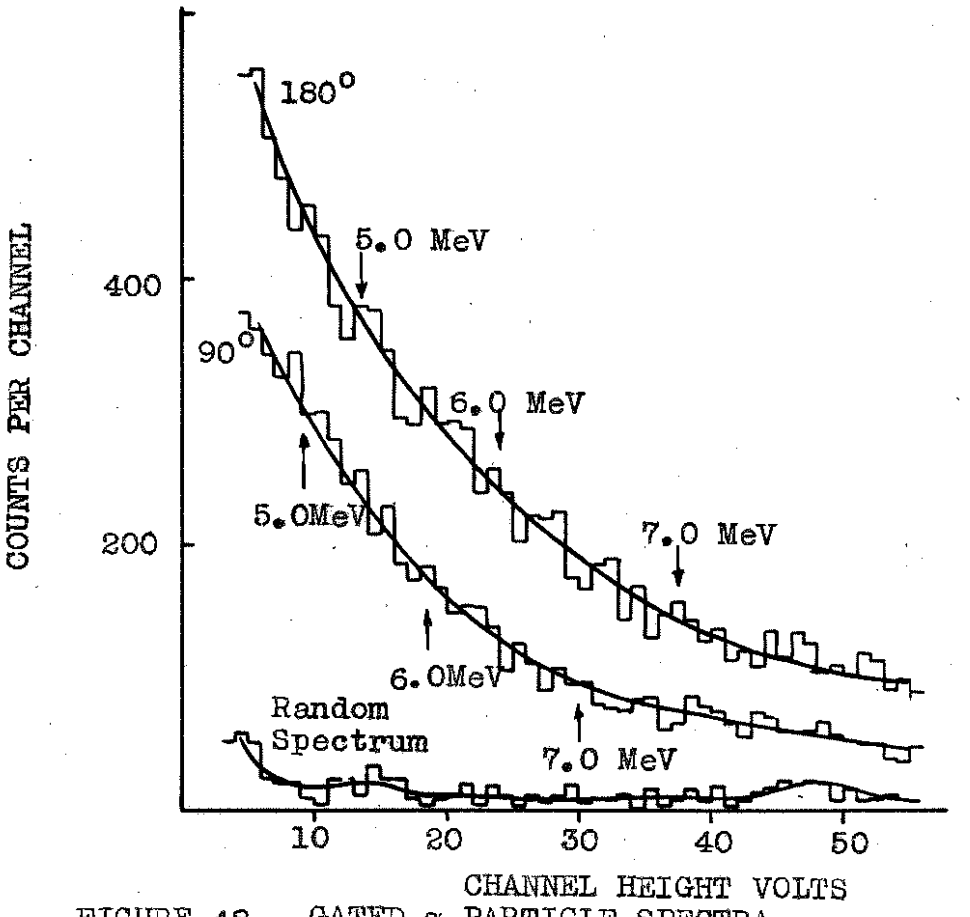

FIGURE 48. GATED α-PARTICLE SPECTRA.

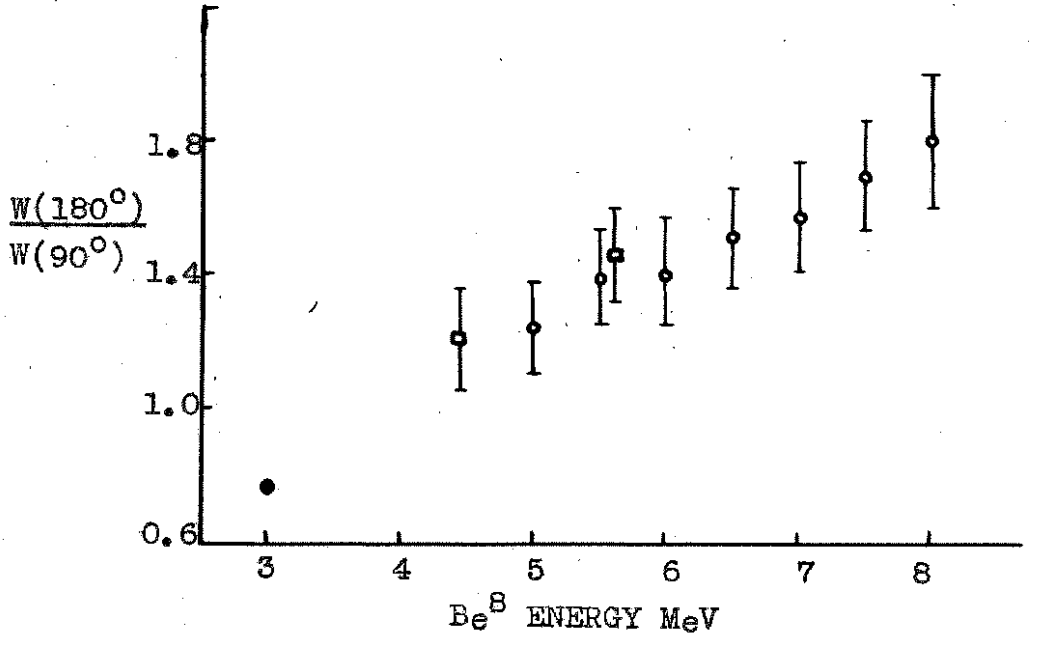

FIGURE 49.

were derived from the energy calibrations described in Part B, Chapter 4.

The ratio of the counts at 180° and 90° for several values of E are plotted in Figure 49. Shown for comparison are the results of sections 6.1 and 6.2 which were obtained for Be^8 energies of 3, 4.3 and 5.7 MeV. Although the errors are quite large, the upward trend of the results is significant.

Any correction for the finite apertures of the counters is unnecessary in this experiment because of the small number of counts involved in each case and the broadening of the distributions introduced by statistical effects in the photomultiplier. However, the angular correlation for the Fluorine reaction was measured with this apparatus and the results are shown in Figure 47. The half angle of each counter was 8.5° and the values for a_k calculated from the relation given in 6.1 were

$$a_2 = 0.97,\ a_4 = 0.92 \text{ and } a_6 = 0.81$$

The experimental Fluorine correlation should then have the form

$$1 + 0.73P_2 + 0.047P_4 + 1.38P_6$$

This is shown by the curve in Figure 47. and agrees well with the experimental points.

6.5 Calculations.

In this reaction, where transitions proceed from a 1^+ state at 17.63 MeV to a level with J = 2, the gamma-radiation can be either magnetic dipole, (l=1), or electric quadrupole, (l=2). Since the spins and parities of all the levels are defined, the angular correlation function can be calculated explicity apart from the parameter, δ, which defines the ratio of the reduced matrix elements[79] for the electric quadrupole and the magnetic dipole interaction.

The result arrived at from relations given by Devons and Goldfarb[77] was

$$W(\theta) + 1 + \frac{0.36\delta^2 + 2.24\delta - 0.5}{1 + \delta^2} P_2(\cos\theta) + \frac{1.14\delta^2}{1+\delta^2} P_4(\cos\theta)$$

and consequently

$$\frac{W(180^\circ)}{W(90^\circ)} = \frac{2\delta^2 + 1.79\delta + 0.40}{\delta^2 - 0.88\delta + 1.00}$$

δ has been shown to be real[79] and can be found from the experimental results obtained in the preceeding sections.

For transitions to Be^8 with an energy of 3 MeV, $\delta = 0.13 \pm 0.01$, whereas at 5 MeV, $\delta = 0.27 \pm 0.03$, and at 8 MeV $\delta = 0.50 \pm 0.05$. These results indicate that the admixture of electric quadrupole radiation increases as the gamma-ray energy decreases.

---

79. Biedenharn, L., Cand Rose, M.E., Rev.Mod.Phys. 25: 729, 1953.

This result is difficult to interpret since the only terms involving the energy of the radiation, which appear explicitly in the matrix elements are of the form $(E_\gamma)^{2l+1}$. E_γ is the energy of the gamma ray and l its orbital angular momentum. Thus the energy variation of the ratio of electric quadrupole to magnetic dipole would be expected to be proportional to $(E_\gamma)^2$. This implies a decreasing value of δ with decreasing E_γ i.e. with increasing Be^8 energy, whereas the experimental results indicate a trend in the opposite direction.

Very simply, δ can be written

$$\frac{\int \phi_b^* |E| \phi_a \, d\tau}{\int \phi_b^* |M| \phi_a \, d\tau}$$

where ϕ_a and ϕ_b are the wave functions for the initial and final states and E and M are the operators describing the electric and magnetic interactions respectively. Since the energy dependent parts of E and M do not account for the observed variation of δ, it is possible that the wave functions themselves may be involved.

In the simple theory ϕ represents the wave function of a stationary state and $|\phi|^2$ is zero beyond the range of the nuclear forces. However, the wave function that describes the broad 3 MeV level can not be of this form and must extend into the sides of the potential well. This penetration would be expected to increase as the energy increased, implying that the wave function ϕ_b is a function of energy. If this were the

case, ϕ_b could be represented as a combination of a stationary state wave function, ϕ_{bS}, and the wave function representing the state of two α-particles, $\phi_{2\alpha}$. Thus

$$|\phi_b|^2 = |\phi_{bS}|^2 + A(E)\ |\phi_{2\alpha}|^2$$

where A(E) is a function of energy. Such an interpretation might explain the increasing probability of electric dipole transitions, signifying that transitions to a D state of two α-particles are electric quadrupole in character. The fact that the radiation to the narrow ground state of Be^8 is pure magnetic dipole is consistent with this interpretation, since, although this is a virtual state, it is sufficiently narrow to be regarded as a stationary state.

If the argument given above is valid, the increasing contribution of $\phi_{2\alpha}$ might be expected to be evident in other reactions since it implies an increasing probability of three body break-up. This point is discussed again in Chapter 7.

CHAPTER 7

THE SHAPE OF THE FIRST EXCITED LEVEL OF Be^8.

The description of a nuclear reaction involving a level in the compound nucleus of definite J, can be made in terms of the single level Breit-Wigner formula provided that the spacing of levels with the same J and parity is large compared to their widths. Since no other 2^+ levels are known to exist below an energy of 20 MeV, this formula should describe the behaviour of the cross sections involving Be^8 in its first excited state.

The Breit-Wigner single-level formula can be written in the form

$$\sigma_a \propto \frac{\Gamma_a \Gamma}{(E_o + \Delta - E)^2 + \Gamma^2/4} \quad \text{.....(20}$$

where σ_a is the cross section for the transition, a, to the level in Be^8 of total width Γ. In this case the partial width for α-particle emission is equal to the total width of the level since no other mode of decay is energetically possible. The cross section is a function of the energy, E, of the Be^8 nucleus.

Γ_a represents the partial width for the transition, a, and since it includes barrier penetrability effects, it is a function of E. Γ includes the effect of the barrier on the disintegration α-particles and can be

expressed in terms of the more fundamental quantity, the reduced width y^2, measured in MeV. cm.

$$\Gamma = \frac{2ky^2}{F_2^2+G_2^2}$$

where k is the wave number of the reduced mass particle and F_2 and G_2 are the regular and irregular Coulomb wave functions for J = 2. E_o is the characteristic energy of the state, and Δ is the level shift defined by

$$\Delta = - \frac{y^2}{a} \left(\frac{kr(F_2F_2' + G_2G_2')}{F_2^2 + G_2^2} \right)_{r = a}$$

where the primes mean differentiation with respect to kr, and, a, is the nuclear radius. The results of Nilson[64] suggest a value for, a, of 4.48×10^{-13} cm. which has been used in the following calculations.

Information concerning the shape of this level is provided by the results of several experiments[65,66,68,80] for which the statistical accuracy and energy resolution was very high. These results are shown in Figure 50. together with those obtained in Chapters 4 and 5. Since all the results agreed with the assignment of 2.94 MeV for the energy of the maximum, the ordinates of the experimental distributions have been fitted at this energy. To avoid confusion in the figure, only representative points are shown for each of the distributions The α-particle spectrum obtained by Holland et al[68] is shown

---

80. LaVier, E.C., Hanna, S.S., and Gelinas, R.W., Phys. Rev. 103: 143, 1956.

only below 4 MeV, since above this energy the background from the break-up α-particles became significant.

The partial widths, Γ_a, for the different processes leading to this level depend on the energy in different ways. So that direct comparisons can be made, each of the experimental distributions should be corrected for this variation.

For the $B^{10}(d,\alpha)$ and $Li^6(He^3,p)$ reactions this variation will be negligible since the energy of the particles is very much greater than the barrier height. No correction has been applied to these points.

For the $Li^7(p,\gamma)$ reaction the transition probability for γ-radiation of energy E_γ, varies as $(E_\gamma)^{2l+1}$. Since magnetic dipole radiation is predominant at 3 MeV a correction for a variation proportional to $(E_\gamma)^3$ has been applied over the complete spectrum. Thus the points for the higher values of E are probably slightly low.

Although the β decay probability varies rapidly with energy, the distribution from this reaction has not been corrected since the rate of variation was not known accurately. Thus the points shown for this distribution are too low by a factor of at least two in the region of 8 MeV.

The constants E_o and y^2 in (2) were chosen so that

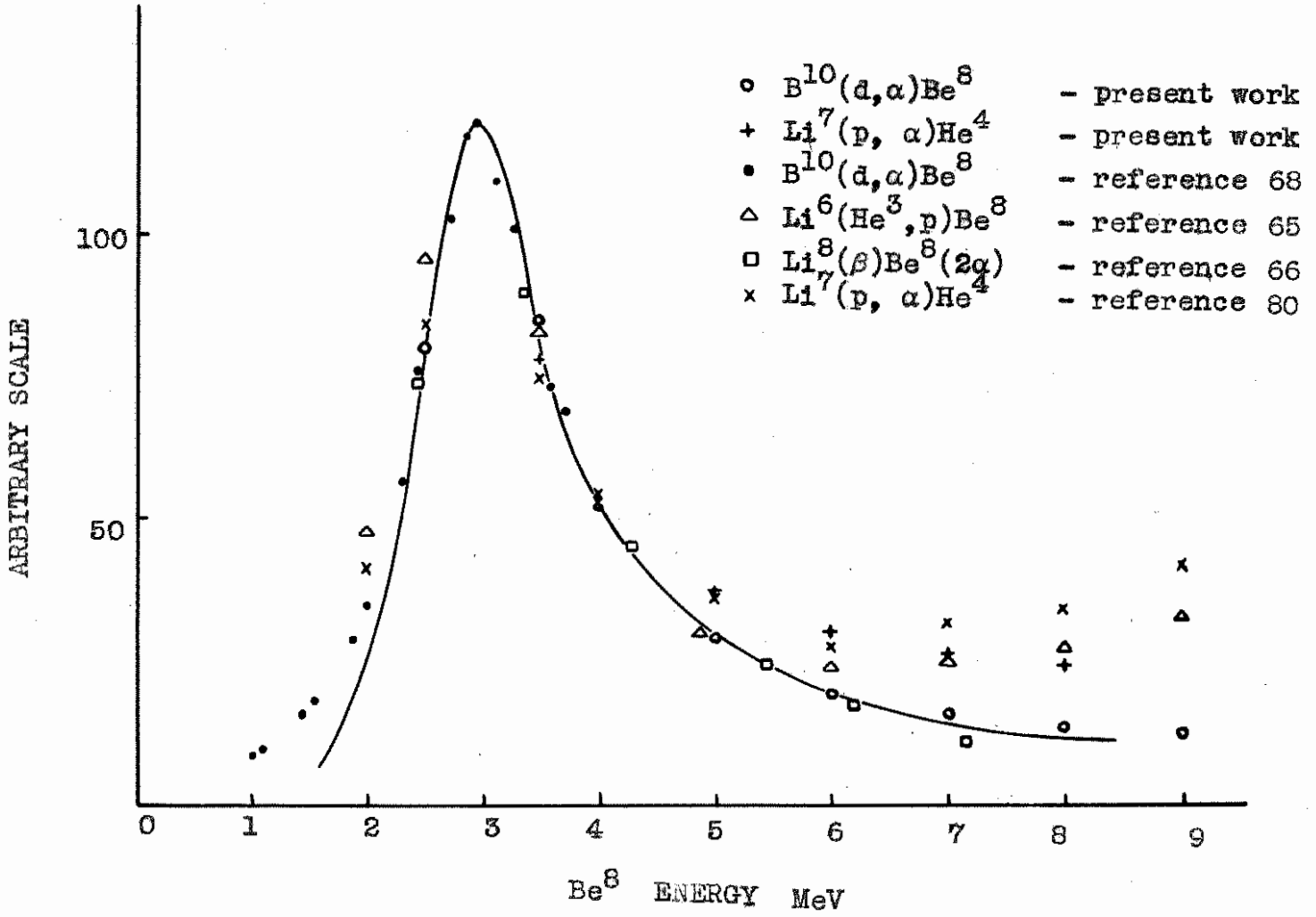
ARBITRARY SCALE
100
50
0
1
2
3
4
5
6
7
8
9
Be8 ENERGY MeV
o B10(d,α)Be8 - present work
+ Li7(p, α)He4 - present work
• B10(d,α)Be8 - reference 68
△ Li6(He3,p)Be8 - reference 65
□ Li8(β)Be8(2α) - reference 66
× Li7(p, α)He4 - reference 80

FIGURE 50.

a fit was obtained with the experimental points at 2.5, 2.94 and 3.5 MeV. Thus values obtained for the constants were $E_o = 4.40$ MeV and $y^2 = 6.2 \times 10^{-13}$ MeV cm. The full distribution derived from these values is shown by the curve in Figure 50.

The upward trend of the experimental points above about 6 MeV cannot be explained by the presence of the 4^+ level at 11 MeV since transitions to such a level are most unlikely to be observed in the $Li^7(p,\gamma)$ reaction for the reasons given in section 6.1.

Since the Breit-Wigner formula only applies to the description of a level with a well-defined wave function, the gradual departure of the experimental points from the Breit-Wigner curve can be explained in terms of the suggestion made in Chapter 6.

An oversimplified picture of the behaviour can be drawn from the $Li^6(He^3,p)Be^8$ reaction. While the emitted proton is still within the region of the nucleus it will perturb the motion of the residual Be^8 nucleus and later the α-particles resulting from its disintegration. This mutual interaction will be very small when the proton has left the region of the nucleus. However, if the proton is still within the nuclear boundary when the Be^8 nucleus disintegrates the interaction may be significant and interpretation of the reaction in terms of a definite compound nucleus state in Be^8

is probably no longer justified. An approximate calculation shows that a proton leaving Be^8 with an excitation energy of 6 MeV is just within the nuclear boundary when the Be^8 nucleus disintegrates into two α-particles. Thus the departure of the proton spectrum from the predictions of the Breit-Wigner formula can be interpreted in terms of the onset of three body break-up i.e., an increasing contribution of the two α-particle wave function describing the Be^8 nucleus at these energies.

If the wave function of the 2^+ state can be written solely as the product of single particle wave functions (in this case the single particles are α-particles), then the upper limit of the reduced width is given approximately by the first sum rule of Teichmann and Wigner[81]

$$y^2 = \frac{3\hbar^2}{2\mu a}$$

where μ is the reduced mass. For $a = 4.48 \times 10^{-13}$ cm. $y^2 = 0.7$ MeV cm. Since this is very close to the experimental value of .62 MeV cm. the possibility of an added term in the wave function expressing the state of two separated α-particles is not excluded.

---

81. Teichman, T. and Wigner, E.P., Phys. Rev. 87: 123, 1952.